

**Block Copolymer Nanofibrillar Micelles  
gelation, manipulation and applications**

Zhang, Kai

**DOI**

[10.4233/uuid:b5fd172c-b0ac-4023-851e-88b7d0ca31c5](https://doi.org/10.4233/uuid:b5fd172c-b0ac-4023-851e-88b7d0ca31c5)

**Publication date**

2018

**Document Version**

Final published version

**Citation (APA)**

Zhang, K. (2018). *Block Copolymer Nanofibrillar Micelles: gelation, manipulation and applications*. [Dissertation (TU Delft), Delft University of Technology]. <https://doi.org/10.4233/uuid:b5fd172c-b0ac-4023-851e-88b7d0ca31c5>

**Important note**

To cite this publication, please use the final published version (if applicable).  
Please check the document version above.

**Copyright**

Other than for strictly personal use, it is not permitted to download, forward or distribute the text or part of it, without the consent of the author(s) and/or copyright holder(s), unless the work is under an open content license such as Creative Commons.

**Takedown policy**

Please contact us and provide details if you believe this document breaches copyrights.  
We will remove access to the work immediately and investigate your claim.

# Block Copolymer Nanofibrillar Micelles: gelation, manipulation and applications

Kai ZHANG



# Block Copolymer Nanofibrillar Micelles: gelation, manipulation and applications

Proefschrift

ter verkrijging van de grad van doctor

aan de Technische Universiteit Delft,

op gezag van de Rector Magnificus prof. dr. ir. T. H. J. J. van der Hagen,

voorzitter van het College voor Promoties,

in het openbaar te verdedigen op

maandag 9 april 2018 om 12:30 uur

door

**Kai ZHANG**

Master of Science in Polymer Science and Engineering,

Sichuan University, China

geboren te Hubei, China



Dit proefschrift is goedgekeurd door de:

promotor: Prof. dr. J. H. van Esch

copromotor: Dr. hab. E. Mendes

Samenstelling promotiecommissie:

Rector Magnificus	Technische Universiteit Delft	voorzitter
Prof. dr. J. H. van Esch	Technische Universiteit Delft	promotor
Dr. hab. E. Mendes	Technische Universiteit Delft	copromotor

Onafhankelijke leden:

Prof. dr. P. Dubruel	Universiteit Gent	
Prof. dr. A. Kros	Universiteit Leiden	
Prof. dr. R. P. Sijbesma	Technische Universiteit Eindhoven	
Prof. dr. S. J. Picken	Technische Universiteit Delft	
Dr. C. Marques	Instituut Charles Sadron, CNRS, France	
Prof. dr. E. J. R. Sudhölter	Technische Universiteit Delft	reservelid

The work described in this thesis was carried out in the Advanced Soft Matter group at Delft University of Technology. This research was financially supported by China Scholarship Council.

Cover design by Kai Zhang

Copyright © 2018 by Kai Zhang

ISBN: 978-94-6186-917-3

Printed by :Gildeprint - Enschede

All rights reserved. The author encourages the communication of scientific contents and explicitly allows reproduction for scientific purposes provided the proper citation of the source. Parts of this thesis have been published in scientific journals and copyright is subject to different terms and conditions.

*To my family*



# Contents

<b>1. Introduction .....</b>	<b>1</b>
1.1. Self-assembly of block copolymers .....	2
1.2. Manipulation of block copolymer micelles .....	5
1.3. Nano-fibril micellar hydrogels .....	7
1.4. Challenges .....	8
1.5. Outline of this thesis.....	8
1.6. References.....	9
 <b>2. Hydrogels from block copolymer nanofibrillar micelles: thermal fusion crosslinking of micellar cores and/or chemical crosslinking of coronas .....</b>	<b>15</b>
2.1. Introduction.....	17
2.2. Results and Discussion .....	18
2.2.1. Formation of wormlike micelles.....	18
2.2.2. Physically crosslinked micellar hydrogels.....	21
2.2.3. Chemically crosslinked micellar hydrogels.....	25
2.3. Conclusion .....	30
2.4. Experimental section .....	30
2.4.1. Materials.....	30
2.4.2. Modification of PS-b-PEO .....	30
2.4.3. Preparation of nano-fibrous micelles and micellar gels.....	31
2.4.4. Characterization .....	31
2.5. References.....	32
2.6. Appendix.....	35
 <b>3. A facile approach for the fabrication of 2D supermicelle networks .....</b>	<b>41</b>
3.1. Introduction.....	43
3.2. Results and Discussion .....	43
3.3. Conclusion .....	49
3.4. Experimental section .....	49
3.4.1. Preparation of Ultralong micelles .....	49
3.4.2. Fabrication of PDMS stamp.....	49

3.4.3. Alignment of ultralong micelles .....	50
3.4.4. Transfer printing of aligned micelles onto receiver substrate .....	50
3.4.5. Characterization .....	51
3.5. References.....	51
3.6. Appendix.....	53
 <b>4. Patterned nano-fibrous micelles of block copolymers for controlled cell alignment.....</b>	<b>61</b>
4.1. Introduction.....	63
4.2. Results and Discussion .....	64
4.2.1. Fabrication of micellar platform.....	64
4.2.2. Unidirectional micelles .....	67
4.2.3. Multidirectional micelles .....	71
4.3. Conclusions.....	73
4.4. Experimental section .....	74
4.4.1. Synthesis and preparation of micelles .....	74
4.4.2. Fabrication of PDMS stamp .....	75
4.4.3. Alignment of micelles .....	75
4.4.4. Printing and crosslinking micelles onto glass slides .....	75
4.4.5. Cell Culture .....	76
4.4.6. Characterization .....	76
4.4.7. Micelle alignment analysis .....	76
4.4.8. Cellular alignment analysis.....	77
4.5. References.....	77
4.6. Appendix.....	79
 <b>5. Soft gel micro-devices from supramolecular assemblies of block copolymers.....</b>	<b>81</b>
5.1. Introduction.....	83
5.2. Results and Discussion .....	83
5.3 Conclusions.....	91
5.4. Experimental section .....	92
5.4.1. Synthesis of methacrylated block copolymers.....	92
5.4.2. Preparation and alignment of functionalized block copolymer micelles.....	92
5.4.3. Synthesis of methacrylated dextran (DexMA) .....	92

5.4.4. Synthesis of photoinitiator LAP .....	93
5.4.5. Lazer-assisted fabrication of hydrogels with supramolecular assemblies .....	93
5.4.6. Fabrication of pH responsive actuators .....	94
5.4.7. Fabrication of fishnet device and investigation of trapping/releasing particles.....	94
5.5. References.....	94
5.6. Appendix.....	97
 <b>Summary.....</b>	 <b>101</b>
<b>Samenvatting .....</b>	<b>103</b>
<b>Acknowledgements .....</b>	<b>105</b>
<b>Curriculum Vitae.....</b>	<b>107</b>



# Introduction

1



## 1.1. Self-assembly of block copolymers

Nowadays, the wide use of functional nano-objects, which have the characteristic sizes ranging from 1 to 100 nm and the unique physical/chemical properties, in many fields has fascinated and motivated researchers to further understand and develop new strategies for constructing these nano-structures. In general, there are two types of approaches, “top-down” and “bottom-up”, established to solve this problem. The first one is mainly based on diverse lithography and etching techniques while the later one is realized by the self-assembly of various building blocks including small molecules, nanoparticles and block copolymers, etc. Contrary to the high cost and low throughput of lithography techniques, self-assembly method offers a powerful toolbox for fabricating novel materials and devices with functional and complex structures. Especially for self-assembly of block copolymers, the developments achieved in polymer synthesis during last decade afford many kinds of block copolymers with designed compositions, molecular weights and architectures of chains. This makes block copolymers as a great candidate for producing the sophisticated and functional nano-objects, like what nature does.

During the past decades, block copolymers, a class of macromolecules formed by covalently linked two or more chemically distinct polymer blocks, have attracted considerable attention, not only from scientific point but also from practical aspect. This is due to their unique properties and potential widespread applications, such as in the fields of drug delivery[1], microelectronics[2], micro-/nano- reactors[3], etc. The recent developments in polymer chemistry have exposed a variety of opportunities for building block copolymers with various architectures, such as linear, branched, dendritic, star-like and cyclic copolymers[4]. The most important and unique property they have is that all types of these block copolymers - regardless of their architectures - can self-assemble into diverse morphologies under certain conditions. Because the thermodynamic incompatibilities between different constituent segments can give rise to phase separation at nano-/micro- scale, resulting in the organization of block copolymer chains to reduce the total free energy.

According to the circumstance, self-assembly of block copolymers can be simply categorized into self-assembly in bulk and self-assembly in solution[5]. Regarding to the former case, long-range ordering or periodic structures are usually formed throughout the bulk material, such as body-centered-cubic spheres, hexagonally packed cylinders, bicontinuous gyroids and lamellae[6]. These resulting structures of self-assembly primarily rely on three critical parameters including the volume fraction of each constituent segments, the total polymerization degree (or molar mass) and the Flory-Huggins parameter[6]. Regulating these parameters permits access to control over the phase separation behaviour of block copolymers, leading to design and generate ordering structures on nanoscale. As such, block

copolymer self-assembly in bulk has been widely utilized as templates in nanolithography to create nano-patterns[2, 7, 8]. Compared with conventional photolithography, block copolymer based lithography offers a cheaper, simpler and higher throughput technology for generating smaller features (less than 10 nm) and is even recognized as a versatile tool for next-generation nanolithography[9].

In comparison with the first case, self-assembly of block copolymers in solution becomes more complex. After introducing the solvents, the interactions between each block of copolymers and different solvents (good or poor solvent for each segment) can also affect the process of self-assembly. For example, when linear diblock copolymers (A-b-B) are dissolved in a selective solvent, the association of insoluble block B of copolymer chains may occur, leading to the formation of copolymer aggregates which show a colloidal stability due to the soluble corona formed by block A. This self-assembly process of block copolymers in solution and corresponding aggregates formed are referred to as block copolymer micellization and block copolymer micelles, respectively[10].

Generally, the micellization mechanism of block copolymers is similar to that of classical small molecular surfactants, consisting of charged (hydrophilic) head and hydrophobic tail. In brief, it stems from the unfavourable solvophobic interactions between solvent and insoluble (or hydrophobic) blocks. To minimise the interfacial energy, hydrophobic segments of copolymer chains associate with each other by attractive forces from their hydrophobic interactions or the ability of crystallization[11, 12], leading to the formation of micellar aggregates, which compose of the solvophobic core and hydrophilic corona surrounding the core. The micellization is governed by several factors, such as concentration of block copolymers, temperature, copolymer composition and chain architecture. For instance, micellization of certain block copolymers with fixed molecular weights can only occur when the concentration of block copolymers is above a specific value, called critical micellization concentration (CMC)[13], at a fixed temperature. In contrast, block copolymer chains disperse molecularly in the solution when the concentration is lower than the CMC. Similarly, a critical micelle temperature (CMT) can also be defined. Taken block copolymers of poly(ethylene oxide)-b-poly(propylene oxide)-b-poly(ethylene oxide) (PEO-PPO-PEO) as an example, CMC decreases with increasing total molecular weight of PEO-PPO-PEO at a fixed PPO/PEO ratio[14]. Increasing temperature makes a decline of the CMC for PEO-PPO-PEO. Compared with triblock and cyclic copolymers, diblock architecture has shown much lower value of CMC in copolymers of poly(butylene oxide)-b-poly(ethylene oxide) (PBO-PEO) and PBO-PEO-PBO[15].

Analogous to self-assembly of small molecular surfactants, the morphology of block copolymer micelles can also be coarsely estimated by the packing parameter,  $p$ , which is defined as:

$$p = \frac{v}{a_0 l_c} \quad (1)$$

where  $v$  is the volume of the hydrophobic block,  $a_0$  is the contact area between hydrophilic and hydrophobic blocks and  $l_c$  is the length of hydrophobic segment. As shown in Figure 1.1, spherical micelles are formed in the cases of  $p \leq 1/3$ , while cylinder structures are formed under medium curvature, namely,  $1/3 < p \leq 1/2$ . With further increasing  $p$  to  $1/2 < p \leq 1$ , lamellae or polymersomes are formed.

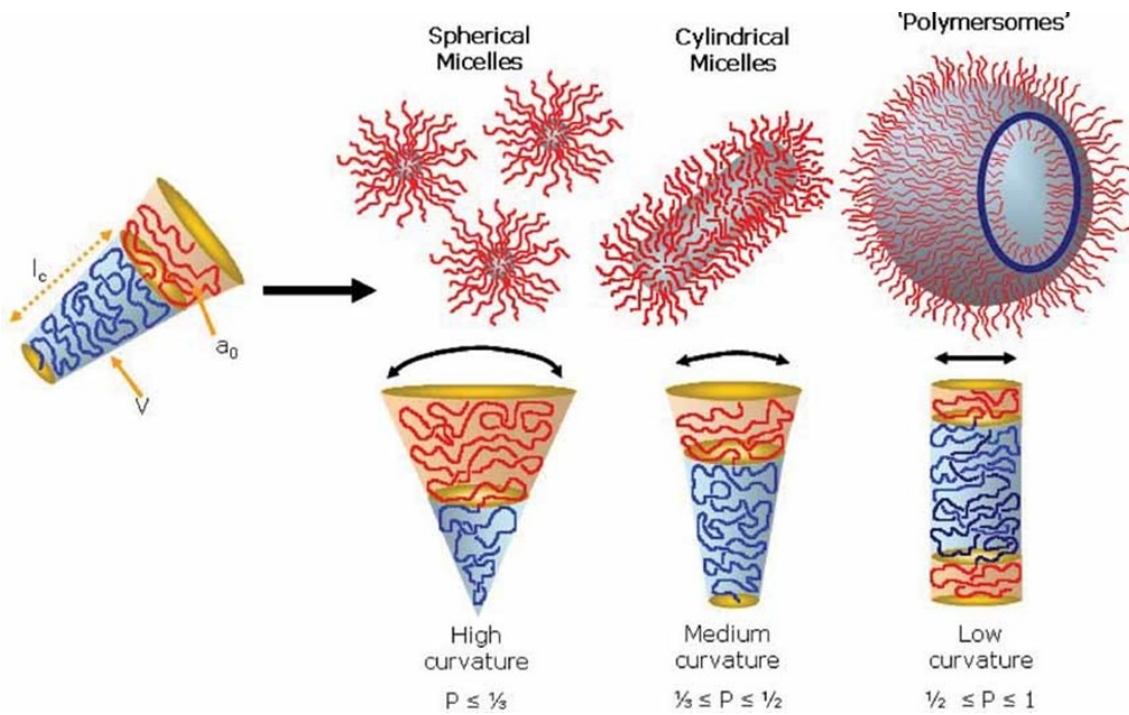


**Figure 1.1.** Schematic illustration of the relationship between self-assembled structures and packing parameter of block copolymers. The assembled structures can be estimated by calculating the dimensionless packing parameter,  $p$ , of the molecular chain[16].

The micellization processes mentioned above are mainly under thermodynamic control. However, Eisenberg et al.[17-20] found that the kinetics of micellization process also determine the final morphologies of micelles or aggregates, which are relevant to the paths of micelle preparation. Except the common morphologies mentioned above, more complex structures including large compound micelles, large compound vesicles, “onions”, “eggshells” etc. are obtained[5]. In such case, the hydrophobic segments are gradually desolvated and frozen (or quenched) with increasing the fraction of poor solvent. The dynamic exchange of copolymer chains between micelles and bulk solution or between micelles and micelles is significantly diminished. In the end, the out-of-equilibrium micelles are formed, typically, for

block copolymers containing a hydrophobic segment with a high glass transition temperature, such as polystyrene-*b*-poly(acrylic acid) (PS-*b*-PAA)[17, 19-22] or polystyrene-*b*-poly(ethylene oxide) (PS-*b*-PEO)[18, 23-27].

To prepare block copolymer micelles, several strategies have been established. Most popular one is the co-solvent (or solvent switch) method[17], in which block copolymers are first dissolved in a common solvent (i.e. good for both blocks) and then a selective solvent is added to induce the association of copolymer chains and form micelles. Unlike co-solvent method, the second one is a solvent-free method[28]. Micelles can be formed directly by dissolving block copolymers in a selective solvent with or without extra thermal, mechanical or ultrasonic treatments. This method is usually suitable for the block copolymers that have a low molecular weight and short insoluble block or have a relatively flexible solvophobic block, such as polybutadiene-*b*-poly(ethylene oxide) (PB-PEO). The third one is called evaporation-induced self-assembly[24, 26]. In brief, block copolymers are dissolved in a volatile and common solvent and dispersed as emulsion in a continuous aqueous phase. During the evaporation process of common solvent, block copolymers have arranged on the interface between oil and water phases and formed micelles through a series of interfacial instabilities. When the crystallisable component is introduced into block copolymer chains, the fourth method “living-crystallization-driven self-assembly” proposed by Manners et al. can be utilized to produce the micelles with precisely controlled size[11, 29, 30] and more complex architectures, such as 2D lamellar platelets[31-33] and multidimensional supermicelles[12, 34-36]. Another recently developed method is polymerization-induced self-assembly[37, 38], namely the micelles are formed during synthesis of block copolymers. Other methods have also been reported for the formation of micelles, especially for vesicles, like microfluidics[39] and electroformation[40].

## **1.2. Manipulation of block copolymer micelles**

Inspired by nature, people always try to build the materials or structures with distinctive hierarchy, which usually plays an important role in determining the final properties[41]. However, exquisite control over the structures on different scales (from nano- to micro- and macro- scales) still represents a big challenge. Since the self-assembly of block copolymers in solution has already permitted to create a wide range of organized structures in one length scale (nanoscale), integrating spatiotemporal manipulation of micelles will offer an intriguing strategy to fabricate novel materials or devices with hierarchical and high order structures. To date, few works have been reported on this aspect. According to the mechanism, the approaches used before can be classified into three main categories. First category is flow-based. As the pioneers, Spatz and Möller et al. used a dip-casting method to form micelle arrays of block copolymers on the flat substrates[42, 43] or pre-structured substrates[44, 45],

which is based on capillary forces generated at the edge of meniscus. The formation mechanism of micelle arrays is similar to that Nagayama et al. investigated for formation of particle arrays[46, 47]. The distance between micelles is affected by molecular weight of block copolymers and topographical structures of the substrates. Higher molecular weights result in larger distance, but less position quality that arises from the increased softness of micellar shell. To improve the arrangement of micelles, Sohn and colleagues used the solvent-annealing method to narrow the size distribution of micelles and create long-range hexagonal order[48]. By incorporating metallic salts with block copolymer micelles and subsequent reduction, such as gold, ordered particle arrays are formed. Based on this mechanism, a new type of lithography approach, named block copolymer micelle nanolithography (BCML)[45], was developed and a series of researches was conducted to pattern or structure various solid surface (including glass, silicon and Teflon) with ordered micelles[43, 49-57]. More recently, through this approach, the soft surface of hydrogels were also successfully structured with binary nanopatterns[58]. Pugin et al. used the ordered micelles as a mask to prepare nanopillars with controlled spacing[59]. Analogous to BCML, Lin et al. demonstrated a simple method called controlled evaporative self-assembly or flow-enabled self-assembly is able to create hierarchical ordered structures of micelles over large areas[60, 61]. Second, lithographic-template was used to guide self-organization of micelles. In this regard, long-range order structures can be obtained[62, 63]. Cohen and co-workers got a patterned micelles by micro-contact printing of the micelles that deposited on a poly(dimethylsiloxane) (PDMS) stamp[64]. Third is based on optical tweezers, which is described more in following part.

Here, we should note that the micelles mentioned above most are the spherical ones that have isotropic structure. However, for anisotropic micelles, such as cylindrical ones, it becomes more complex for manipulation. In 2003, Manners and co-workers attempted to pattern the cylindrical micelles with pre-patterned grooves on the resist film[65]. Despite the aligned nanolines were achieved, the efficiency of this method still needs to be improved. Strikingly, by utilizing holographic optical tweezers, they can efficiently manipulated the cylindrical micelles in three-dimension recently[66]. Some new superstructures of micelles, namely supermicelles, were successfully prepared and precisely positioned. In our group, we developed a flow-based method, guided de-wetting method, for cylindrical micelles, especially ultra-long ones[67, 68]. The capillary forces that generated during de-wetting process of micelle solutions on patterned surface instruct the alignment of cylindrical micelle on micro-pillars.

### 1.3. Nano-fibril micellar hydrogels

Hydrogels are usually regarded as a water-swollen, three-dimensional network of polymer chains. They are either chemically or physically crosslinked polymers or supramolecular aggregates. In the former case, hydrogels are formed by irreversible covalent crosslinks bridging the polymer chains, such as the classical polyacrylamide hydrogels[69]. In contrast, physically crosslinked hydrogels are typically held together by reversible physical cross-linking via hydrogen bonding, hydrophobic forces, electrostatic interactions or other forces of non-covalent nature[70].

Due to their unique characteristics, hydrogels have attracted increasing attention over the last decades[71]. First, owing to the presence of many hydrophilic segments in polymer chains or supramolecular aggregates, hydrogels can usually absorb a large amount of water and swell without dissolving. Second, hydrogels have a highly porous structure that permits a high permeability to small molecules. These abilities allow them to mimic the nature soft tissue and offer numerous potential applications, such as in tissue engineering[72] and drug delivery[73].

Among many kinds of hydrogels, there is a new type of hydrogels, which is formed by self-assembly of cylindrical micelles of block copolymers, so called “nano-fibril micellar hydrogels”. Unlike the conventional hydrogels that are mainly based on covalently cross-linked polymer chains, the networks in this kind of hydrogels are formed by association, branching or entanglement of cylindrical micelles[70]. For instance, the formation of micellar hydrogels of PB-PEO copolymers occurred by entanglement of wormlike micelles[74]. Nanofibrillar thermoreversible micellar microgels can be generated by association of corona chains poly(N-isopropyl acrylamide) between wormlike micelles of poly(N-isopropyl acrylamide)-b-polystyrene at 37°C [75].

Compared with the conventional hydrogels, the self-assembly property of this new type of hydrogel is a unique feature, which offers a stimulus-responsive nature. Changing the external conditions, such as temperature, can control the formation and disintegration of micellar hydrogels. This advantage of micellar hydrogels enables the capability of drug loading (or cell encapsulation) and relative drug releasing (or cell release). Moreover, the self-assembly property offers a simple tool to biologically functionalize the hydrogel network[76]. For example, the assemblies of block copolymers used to form micellar hydrogels can be bound with some specific proteins that can interact with cells to control the cell fate.

Despite nano-fibril micellar hydrogels have a dramatic property that can mimic the filamentous morphology of natural collagen gels, application of this kind of novel hydrogel is

often limited by their poor mechanical properties. For example, as the scaffolds in tissue engineering, hydrogels must be strong enough to support the development of tissue[77]. At the meantime, for the drug delivery system, mechanical properties of hydrogels are also crucial to the drug loading and releasing. If their mechanical strength is too weak, the target drug could be released before arriving the specific location. Therefore, improving the mechanical properties of micellar hydrogels is of great importance.

## **1.4. Challenges**

Block copolymer self-assembly as a diverse toolbox is essential for the generation of complex and novel functional devices. However, the poor mechanical properties of micellar hydrogels and difficulties in manipulation of the micelles, especially cylindrical micelles, for generating sophisticated soft devices have limited their applications.

To improve the mechanical properties of hydrogels, scientists have proposed some strategies for conventional ones. For instance, a tough hydrogel system can be made by using slide-ring polymers to synthesize the hydrogels or by introducing a second network for dissipating energy[78]. However, in case of micellar hydrogels, examples of improving the mechanical properties have been rarely reported. Researchers are mainly focused on the self-assembly of short and flexible cylindrical micelles and used in-situ methods, such as polymerization-induced self-assembly or phase separation induced self-assembly, to study the mechanism of micellar hydrogels formation. For the ultra-long and stiff cylindrical micelles systems, it is still a challenge due to their narrow phase region. Here, we propose to prepare the micellar hydrogels with ultra-long and stiff cylindrical micelles, which may reinforce themselves by their glassy nature and long fibrous structures. The formation mechanism of hydrogel based on ultra-long and glassy micelles might help us understand the micellar hydrogels and design new systems. To address the second challenge, we develop a hybrid method combining “bottom-up” self-assembly and “top-down” lithographic approaches to manipulate the cylindrical micelles. Through controlling the spatial arrangement of micelles, new types of soft devices are designed and constructed.

## **1.5. Outline of this thesis**

This thesis contributes to the micellar hydrogels field by investigating a new system, which is based on ultra-long and stiff cylindrical micelles. Moreover, it proposes a new method to build up superstructures of micelles and investigates their potential applications, such as patterning cells and programming stimuli-responsive hydrogels. The outline of this thesis is listed following:

Chapter 2 presents a new kind of micellar hydrogel systems, which are formed by physically or chemically cross-linked glassy fibril micelles. We investigated the gelation process in both situations and analysed the corresponding evolution of microstructures. The mechanisms of gelation are discussed.

Chapter 3 describes a hybrid approach combining guided de-wetting, transfer-printing and thermal welding techniques for fabrication of two dimensional supermicelle networks.

Chapter 4 demonstrates a new micellar platform is capable of controlling cell alignment and gives an insight to how the area density of fibril micelles affects the elongation and orientation of cells. Furthermore, the cellular response to competitive guidance is briefly studied here.

Chapter 5 represents a novel approach that combines the self-assembly of block copolymers and lithographic methods for construction of some new soft devices, such as “soft concrete” and “fishnet”. We demonstrate that a single layer of supramolecular assemblies is capable of controlling the stimuli-responsive behaviour of hydrogels.

## 1.6. References

- [1] Kataoka K, Harada A, Nagasaki Y. Block copolymer micelles for drug delivery: design, characterization and biological significance. *Adv Drug Deliver Rev.* 2001;47:113-31.
- [2] Bang J, Jeong U, Ryu DY, Russell TP, Hawker CJ. Block Copolymer Nanolithography: Translation of Molecular Level Control to Nanoscale Patterns. *Adv Mater.* 2009;21:4769-92.
- [3] Bakshi MS. Colloidal micelles of block copolymers as nanoreactors, templates for gold nanoparticles, and vehicles for biomedical applications. *Adv Colloid Interfac.* 2014;213:1-20.
- [4] Hadjichristidis N, Pitsikalis M, Iatrou H. Synthesis of block copolymers. *Block Copolymers I.* 2005;189:1-124.
- [5] Mai YY, Eisenberg A. Self-assembly of block copolymers. *Chemical Society Reviews.* 2012;41:5969-85.
- [6] Bates FS, Fredrickson GH. Block copolymers - Designer soft materials. *Phys Today.* 1999;52:32-8.
- [7] Jeong SJ, Kim JY, Kim BH, Moon HS, Kim SO. Directed self-assembly of block copolymers for next generation nanolithography. *Mater Today.* 2013;16:468-76.
- [8] Hamley IW. Nanostructure fabrication using block copolymers. *Nanotechnology.* 2003;14:R39-R54.
- [9] Kwak J, Mishra AK, Lee J, Lee KS, Choi C, Maiti S, et al. Fabrication of Sub-3 nm Feature Size Based on Block Copolymer Self-Assembly for Next-Generation Nanolithography. *Macromolecules.* 2017;50:6813-8.
- [10] Riess G. Micellization of block copolymers. *Prog Polym Sci.* 2003;28:1107-70.
- [11] Wang XS, Guerin G, Wang H, Wang YS, Manners I, Winnik MA. Cylindrical block copolymer micelles and co-micelles of controlled length and architecture. *Science.* 2007;317:644-7.



- [12] Gadt T, leong NS, Cambridge G, Winnik MA, Manners I. Complex and hierarchical micelle architectures from diblock copolymers using living, crystallization-driven polymerizations. *Nat Mater*. 2009;8:144-50.
- [13] Gohy JF. Block copolymer micelles. *Block Copolymers II*. 2005;190:65-136.
- [14] Nace V. *Nonionic Surfactants: Polyoxyalkylene Block Copolymers*: Taylor & Francis; 1996.
- [15] Alexandridis P, Lindman B. *Amphiphilic Block Copolymers: Self-Assembly and Applications*: Elsevier Science; 2000.
- [16] Blanz A, Armes SP, Ryan AJ. Self-Assembled Block Copolymer Aggregates: From Micelles to Vesicles and their Biological Applications. *Macromol Rapid Comm*. 2009;30:267-77.
- [17] Zhang LF, Eisenberg A. Multiple morphologies and characteristics of "crew-cut" micelle-like aggregates of polystyrene-*b*-poly(acrylic acid) diblock copolymers in aqueous solutions. *J Am Chem Soc*. 1996;118:3168-81.
- [18] Yu K, Eisenberg A. Multiple morphologies in aqueous solutions of aggregates of polystyrene-*b*-poly(ethylene oxide) diblock copolymers. *Macromolecules*. 1996;29:6359-61.
- [19] Zhang LF, Eisenberg A. Thermodynamic vs kinetic aspects in the formation and morphological transitions of crew-cut aggregates produced by self-assembly of polystyrene-*b*-poly(acrylic acid) block copolymers in dilute solution. *Macromolecules*. 1999;32:2239-49.
- [20] Shen HW, Eisenberg A. Block length dependence of morphological phase diagrams of the ternary system of PS-*b*-PAA/dioxane/H<sub>2</sub>O. *Macromolecules*. 2000;33:2561-72.
- [21] Yu YS, Zhang LF, Eisenberg A. Morphogenic effect of solvent on crew-cut aggregates of amphiphilic diblock copolymers. *Macromolecules*. 1998;31:1144-54.
- [22] Burke SE, Eisenberg A. Effect of sodium dodecyl sulfate on the morphology of polystyrene-*b*-poly(acrylic acid) aggregates in dioxane-water mixtures. *Langmuir*. 2001;17:8341-7.
- [23] Munk P. Equilibrium and Nonequilibrium Polymer Micelles. In: Webber SE, Munk P, Tuzar Z, editors. *Nato Adv Sci Inst Se*. Dordrecht: Springer Netherlands; 1996. p. 19-32.
- [24] Zhu JT, Hayward RC. Spontaneous generation of amphiphilic block copolymer micelles with multiple morphologies through interfacial instabilities. *J Am Chem Soc*. 2008;130:7496-502.
- [25] Zhu J, Hayward RC. Hierarchically structured microparticles formed by interfacial instabilities of emulsion droplets containing amphiphilic block copolymers. *Angew Chem Int Edit*. 2008;47:2113-6.
- [26] Zhu JT, Hayward RC. Interfacial tension of evaporating emulsion droplets containing amphiphilic block copolymers: Effects of solvent and polymer composition. *J Colloid Interf Sci*. 2012;365:275-9.
- [27] Zhu J, Ferrer N, Hayward RC. Tuning the assembly of amphiphilic block copolymers through instabilities of solvent/water interfaces in the presence of aqueous surfactants. *Soft Matter*. 2009;5:2471-8.
- [28] Jain S, Bates FS. On the origins of morphological complexity in block copolymer surfactants. *Science*. 2003;300:460-4.
- [29] Tao D, Feng C, Cui Y, Yang X, Manners I, Winnik MA, et al. Monodisperse Fiber-like Micelles of Controlled Length and Composition with an Oligo(*p*-phenylenevinylene) Core via "Living" Crystallization-Driven Self-Assembly. *J Am Chem Soc*. 2017;139:7136-9.
- [30] Gilroy JB, Gadt T, Whittell GR, Chabanne L, Mitchels JM, Richardson RM, et al. Monodisperse cylindrical micelles by crystallization-driven living self-assembly. *Nat Chem*. 2010;2:566-70.

- [31] Qiu HB, Gao Y, Boott CE, Gould OEC, Harniman RL, Miles MJ, et al. Uniform patchy and hollow rectangular platelet micelles from crystallizable polymer blends. *Science*. 2016;352:697-701.
- [32] He XM, He YX, Hsiao MS, Harniman RL, Pearce S, Winnik MA, et al. Complex and Hierarchical 2D Assemblies via Crystallization-Driven Self-Assembly of Poly(L-lactide) Homopolymers with Charged Termini. *J Am Chem Soc*. 2017;139:9221-8.
- [33] He XM, Hsiao MS, Boott CE, Harniman RL, Nazemi A, Li XY, et al. Two-dimensional assemblies from crystallizable homopolymers with charged termini. *Nat Mater*. 2017;16:481-+.
- [34] Qiu HB, Hudson ZM, Winnik MA, Manners I. Multidimensional hierarchical self-assembly of amphiphilic cylindrical block comicelles. *Science*. 2015;347:1329-32.
- [35] Li XY, Gao Y, Boott CE, Winnik MA, Manners I. Non-covalent synthesis of supermicelles with complex architectures using spatially confined hydrogen-bonding interactions. *Nat Commun*. 2015;6:8127.
- [36] Qiu HB, Cambridge G, Winnik MA, Manners I. Multi-Armed Micelles and Block Co-micelles via Crystallization-Driven Self-Assembly with Homopolymer Nanocrystals as Initiators. *J Am Chem Soc*. 2013;135:12180-3.
- [37] Blanazs A, Verber R, Mykhaylyk OO, Ryan AJ, Heath JZ, Douglas CWI, et al. Sterilizable Gels from Thermoresponsive Block Copolymer Worms. *J Am Chem Soc*. 2012;134:9741-8.
- [38] Fielding LA, Lane JA, Derry MJ, Mykhaylyk OO, Armes SP. Thermo-responsive Diblock Copolymer Worm Gels in Non-polar Solvents. *J Am Chem Soc*. 2014;136:5790-8.
- [39] Shum HC, Kim JW, Weitz DA. Microfluidic fabrication of monodisperse biocompatible and biodegradable polymersomes with controlled permeability. *J Am Chem Soc*. 2008;130:9543-9.
- [40] Discher BM, Won YY, Ege DS, Lee JCM, Bates FS, Discher DE, et al. Polymersomes: Tough vesicles made from diblock copolymers. *Science*. 1999;284:1143-6.
- [41] Lakes R. Materials with Structural Hierarchy. *Nature*. 1993;361:511-5.
- [42] Spatz JP, Roescher A, Moller M. Gold nanoparticles in micellar poly(styrene)-b-poly(ethylene oxide) films-size and interparticle distance control in monoparticulate films. *Adv Mater*. 1996;8:337-40.
- [43] Spatz JP, Mossmer S, Hartmann C, Moller M, Herzog T, Krieger M, et al. Ordered deposition of inorganic clusters from micellar block copolymer films. *Langmuir*. 2000;16:407-15.
- [44] Spatz JP, Chan VZH, Mossmer S, Kamm FM, Plettl A, Ziemann P, et al. A combined top-down/bottom-up approach to the microscopic localization of metallic nanodots. *Adv Mater*. 2002;14:1827-32.
- [45] Glass R, Moller M, Spatz JP. Block copolymer micelle nanolithography. *Nanotechnology*. 2003;14:1153-60.
- [46] Dimitrov AS, Nagayama K. Continuous convective assembling of fine particles into two-dimensional arrays on solid surfaces. *Langmuir*. 1996;12:1303-11.
- [47] Denkov ND, Yoshimura H, Nagayama K, Kouyama T. Nanoparticle arrays in freely suspended vitrified films. *Phys Rev Lett*. 1996;76:2354-7.
- [48] Yun SH, Il Yoo S, Jung JC, Zin WC, Sohn BH. Highly ordered arrays of nanoparticles in large areas from diblock copolymer micelles in hexagonal self-assembly. *Chem Mater*. 2006;18:5646-8.

- [49] Glass R, Arnold M, Blummel J, Kuller A, Moller M, Spatz JP. Micro-nanostructured interfaces fabricated by the use of inorganic block copolymer micellar monolayers as negative resist for electron-beam lithography. *Advanced Functional Materials*. 2003;13:569-75.
- [50] Arnold M, Cavalcanti-Adam EA, Glass R, Blummel J, Eck W, Kantelehner M, et al. Activation of integrin function by nanopatterned adhesive interfaces. *Chemphyschem*. 2004;5:383-8.
- [51] Glass R, Arnold M, Cavalcanti-Adam EA, Blummel J, Haferkemper C, Dodd C, et al. Block copolymer micelle nanolithography on non-conductive substrates. *New J Phys*. 2004;6.
- [52] Selhuber C, Blummel J, Czerwinski F, Spatz JP. Tuning surface energies with nanopatterned substrates. *Nano Lett*. 2006;6:267-70.
- [53] Graeter SV, Huang JH, Perschmann N, Lopez-Garcia M, Kessler H, Ding JD, et al. Mimicking cellular environments by nanostructured soft interfaces. *Nano Lett*. 2007;7:1413-8.
- [54] Arnold M, Hirschfeld-Warneken VC, Lohmuller T, Heil P, Blummel J, Cavalcanti-Adam EA, et al. Induction of cell polarization and migration by a gradient of nanoscale variations in adhesive ligand spacing. *Nano Lett*. 2008;8:2063-9.
- [55] Lohmuller T, Helgert M, Sundermann M, Brunner R, Spatz JP. Biomimetic interfaces for high-performance optics in the deep-UV light range. *Nano Lett*. 2008;8:1429-33.
- [56] Kruss S, Wolfram T, Martin R, Neubauer S, Kessler H, Spatz JP. Stimulation of Cell Adhesion at Nanostructured Teflon Interfaces. *Adv Mater*. 2010;22:5499-506.
- [57] Lohmuller T, Aydin D, Schwieder M, Morhard C, Louban I, Pacholski C, et al. Nanopatterning by block copolymer micelle nanolithography and bioinspired applications. *Biointerphases*. 2011;6:Mr1-Mr12.
- [58] Guasch J, Diemer J, Riahinezhad H, Neubauer S, Kessler H, Spatz JP. Synthesis of Binary Nanopatterns on Hydrogels for Initiating Cellular Responses. *Chem Mater*. 2016;28:1806-15.
- [59] Lohmueller T, Bock E, Spatz JP. Synthesis of quasi-hexagonal ordered arrays of metallic nanoparticles with tuneable particle size. *Adv Mater*. 2008;20:2297-+.
- [60] Han W, Byun M, Li B, Pang XC, Lin ZQ. A Simple Route to Hierarchically Assembled Micelles and Inorganic Nanoparticles. *Angew Chem Int Edit*. 2012;51:12588-92.
- [61] Cunningham VJ, Ratcliffe LPD, Blanazs A, Warren NJ, Smith AJ, Mykhaylyk OO, et al. Tuning the critical gelation temperature of thermo-responsive diblock copolymer worm gels. *Polym Chem-Uk*. 2014;5:6307-17.
- [62] Park S, Kim B, Yavuzcetin O, Tuominen MT, Russell TP. Ordering of PS-b-P4VP on patterned silicon surfaces. *ACS Nano*. 2008;2:1363-70.
- [63] Kadem LF, Lamprecht C, Purto J, Selhuber-Unkel C. Controlled Self-Assembly of Hexagonal Nanoparticle Patterns on Nanotopographies. *Langmuir*. 2015;31:9261-5.
- [64] Bennett RD, Hart AJ, Miller AC, Hammond PT, Irvine DJ, Cohen RE. Creating patterned carbon nanotube catalysts through the microcontact printing of block copolymer micellar thin films. *Langmuir*. 2006;22:8273-6.
- [65] Cao L, Massey JA, Winnik MA, Manners I, Riethmuller S, Banhart F, et al. Reactive ion etching of cylindrical polyferrocenylsilane block copolymer micelles: Fabrication of ceramic nanolines on semiconducting substrates. *Advanced Functional Materials*. 2003;13:271-6.

- [66] Gould OEC, Qiu HB, Lunn DJ, Rowden J, Harniman RL, Hudson ZM, et al. Transformation and patterning of supermicelles using dynamic holographic assembly. *Nat Commun*. 2015;6:10009.
- [67] Glazer PJ, Bergen L, Jennings L, Houtepen AJ, Mendes E, Boukany PE. Generating Aligned Micellar Nanowire Arrays by Dewetting of Micropatterned Surfaces. *Small*. 2014;10:1729-34.
- [68] Zhang K, Glazer PJ, Jennings L, Vedaraman S, Oldenhof S, Wang Y, et al. A facile approach for the fabrication of 2D supermicelle networks. *Chem Commun (Camb)*. 2016;52:12360-3.
- [69] Glazer PJ, Leuven J, An H, Lemay SG, Mendes E. Multi-Stimuli Responsive Hydrogel Cilia. *Advanced Functional Materials*. 2013;23:2964-70.
- [70] Raghavan SR, Douglas JF. The conundrum of gel formation by molecular nanofibers, wormlike micelles, and filamentous proteins: gelation without cross-links? *Soft Matter*. 2012;8:8539-46.
- [71] El-Sherbiny IM, Yacoub MH. Hydrogel scaffolds for tissue engineering: Progress and challenges. *Global cardiology science & practice*. 2013;2013:316-42.
- [72] Silva GA, Czeisler C, Niece KL, Beniash E, Harrington DA, Kessler JA, et al. Selective differentiation of neural progenitor cells by high-epitope density nanofibers. *Science*. 2004;303:1352-5.
- [73] He CL, Kim SW, Lee DS. In situ gelling stimuli-sensitive block copolymer hydrogels for drug delivery. *J Control Release*. 2008;127:189-207.
- [74] Won YY, Davis HT, Bates FS. Giant wormlike rubber micelles. *Science*. 1999;283:960-3.
- [75] Velasco D, Chau M, Therien-Aubin H, Kumachev A, Tumarkin E, Jia ZF, et al. Nanofibrillar thermoreversible micellar microgels. *Soft Matter*. 2013;9:2380-3.
- [76] Du X, Zhou J, Shi J, Xu B. Supramolecular Hydrogelators and Hydrogels: From Soft Matter to Molecular Biomaterials. *Chem Rev*. 2015;115:13165-307.
- [77] Lee KY, Mooney DJ. Hydrogels for tissue engineering. *Chem Rev*. 2001;101:1869-79.
- [78] Sun JY, Zhao X, Illeperuma WR, Chaudhuri O, Oh KH, Mooney DJ, et al. Highly stretchable and tough hydrogels. *Nature*. 2012;489:133-6.



# **Hydrogels from block copolymer nanofibrillar micelles: thermal fusion crosslinking of micellar cores and/or chemical crosslinking of coronas**

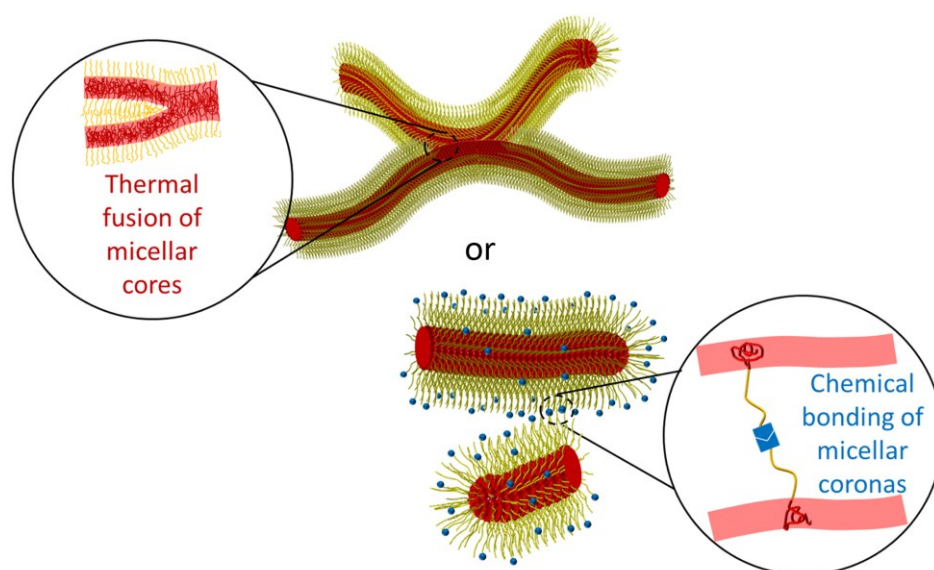
# 2

The content of this chapter is based on:

K. Zhang, A. Suratkar, S. Vedaraman, V. Lakshminarayanan, L. Jennings, P.J. Glazer, J.H. van Esch and E. Mendes,  
*Under revision.*

## Abstract

While the formation of (tri-)block copolymer hydrogels has been extensively investigated, such studies mostly focused on equilibrium self-assembling whereas the use of pre-formed structures as building blocks such as out of equilibrium, quenched, nanofibrillar micelles is still a challenge. Here, we demonstrate that quenched, ultralong polystyrene-*b*-poly(ethylene oxide) (PS-*b*-PEO) micelles can be used as robust precursors of hydrogels. Two crosslinking strategies, i) thermal fusion of micellar cores and ii) chemical crosslinking of pre-formed micellar coronas were studied. The gelation process and the structure of the micellar networks were investigated by in-situ rheological measurements, confocal microscopy and transmission electron microscopy. Direct observation of core fusion of pre-formed quenched micelles is provided validating this method as a robust gelation route. Using time sweep rheological experiments, it was found for both crosslinking methods that these 3D “mikado” gels are formed in three different stages, containing (1) initiation, (2) transition (growth) and (3) stabilization regimes.



## 2.1. Introduction

Hydrogels, as an important class of soft materials, are usually composed of entrapped dispersion medium (aqueous phase) and three-dimensional networks of dispersed matter, which are formed by either chemical crosslinks or physical associations of hydrophilic polymers or supramolecular assemblies. In the first case, the prototypical hydrogels are derived from small molecular precursors (including monomers and crosslinkers) that are covalently bonded together to form a three dimension network[1], such as the classical polyacrylamide hydrogel[2]. In contrast, physically crosslinked hydrogels are formed by various physical associative interactions, including hydrogen bond[3], ionic complexation[4], hydrophobic interaction and topological entanglements[5] etc., between the building blocks. Among this kind of hydrogels, micellar hydrogels, in which the build blocks are micelles, have attracted increasing attention recently[6-17].

In general, two main categories of micellar hydrogels can be classified based on the materials used. One is formed by conventional small molecular surfactants, while the other one is constructed by block copolymers which can self-assemble into a variety of morphologies[18], including spherical micelles, vesicles, worm-like (or fibril) micelles and other complex nanostructures[19-25]. Compared to conventional surfactants, micellar systems formed by block copolymers exhibit higher stability and easier functionalization properties, offering more design flexibility and broad range of applications. Depending on the structure of block copolymer micelles, a variety of micellar hydrogels can be formed. For example, a fast multi-responsive micellar gel was formed by well-defined packing spherical micelles into an ordered structure[17]. Nanofibrillar micellar hydrogels were first reported by Bates and co-workers, which were constructed by core crosslinked wormlike micelles[7, 8]. Using a new strategy, called polymerization induced self-assembly, Armes et al. successfully prepared soft worm gels[15, 16, 26]. Although many studies have been carried out for micellar hydrogels, it is still a challenge to prepare micellar hydrogels with non-equilibrium, nano-fibrillar micelles, which can mimic or at least exhibit similar morphology and (non-linear) mechanical properties as the filamentous extracellular matrix.

In the present work, we report a new kind of nano-fibrillar micellar hydrogels formed by either thermal crosslinking of glassy cores or chemical inter-corona crosslinking of very long, rod-like quenched micelles. Briefly, either a gel was formed by formation of physical junctions between adjacent micelles via increasing temperature above the glass transition temperature of the polystyrene (PS) micelle core, or by chemical cross-linkages between methacrylate functionalized poly(ethylene oxide) (PEO) chains forming the micellar corona. In this case, photo-crosslinking was used to control the reaction (Figure 2.1). The gelation process as a function of micelle concentration and time was studied by rheology and the



corresponding micro-structures were examined by confocal microscopy and transmission electron microscopy. The critical gelation concentration (CGC) for physically (core) and chemically (corona) crosslinked gels were found to be around 5.84 mg/ml and 1.00 mg/ml, respectively. Below CGC, instead of forming micellar gels, agglomerates of micelles were formed.

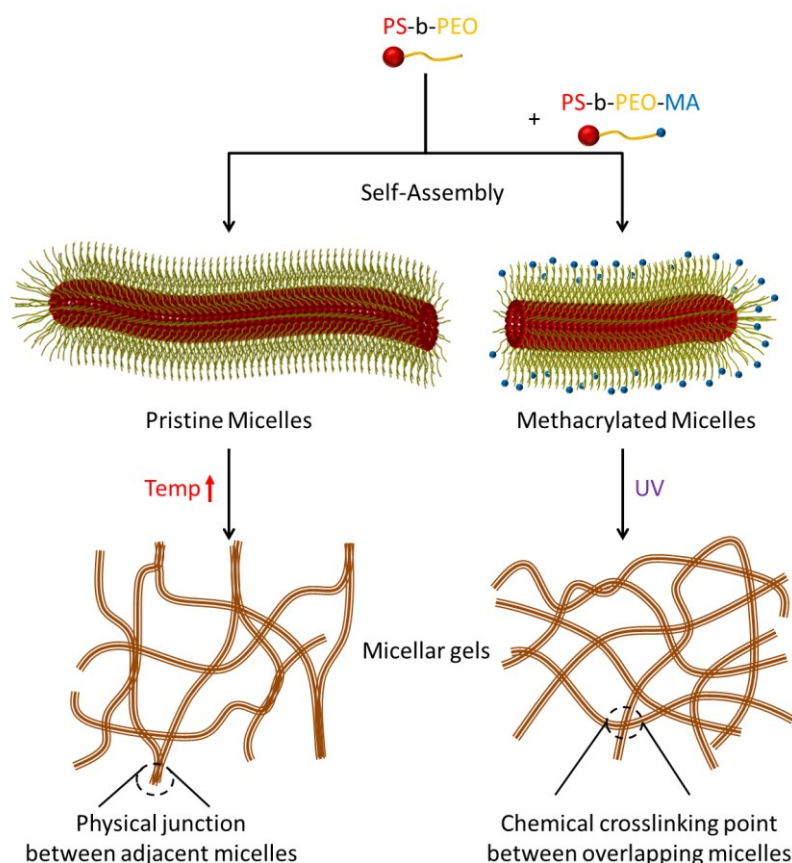


**Figure 2.1.** Schematics of physically and chemically crosslinked micellar gels formed by non-equilibrium glassy micelles of block copolymers.

## 2.2. Results and Discussion

### 2.2.1. Formation of wormlike micelles

Figures 2.2a and 2.2b display the morphologies of pristine PS-b-PEO micelles and 10% PS-b-PEO-MA functionalized micelles, respectively. Both of them displayed the fibrous structures, whose lengths are in the micro-scale range with diameters in nano-scale range (Figure 2.2c and 2.2d). Although 10 wt% methacrylated PS-b-PEO was doped into micelles, no significant difference between pristine PS-b-PEO micelles and 10% PS-b-PEO-MA micelles can be observed in fibril structure or in their diameters (around 40 nm). Nevertheless, compared to PS-b-PEO-MA decorated micelles, it seems that original PS-b-PEO micelles exhibit much longer contour length (as shown in Figure 2.2e). These results indicate that adding 10% PS-b-

PEO-MA for the formation of micelles may influence the out of equilibrium assembly behaviour of PS-b-PEO.

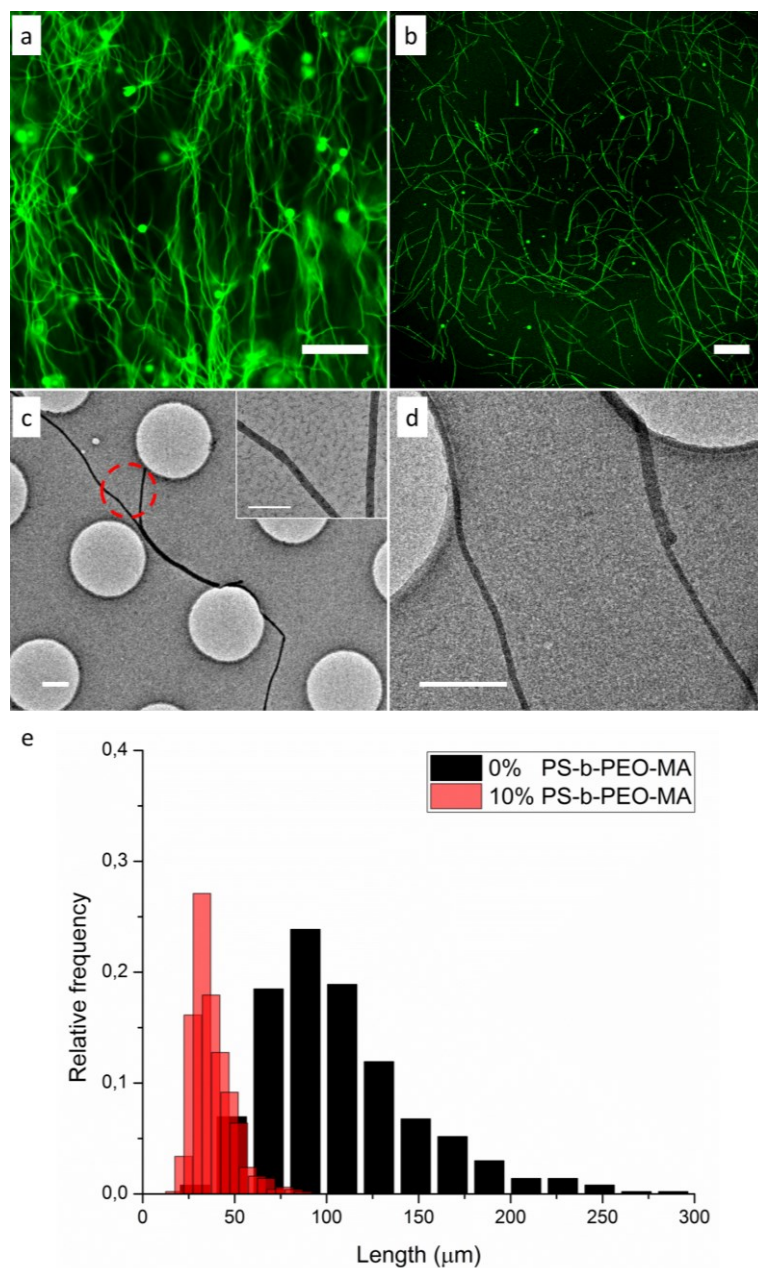


**Figure 2.2.** Confocal microscopy images of nano-fibrous micelles formed by self-assembly of PS-b-PEO (a) without PS-b-PEO-MA and (b) with 10 wt% PS-b-PEO-MA. TEM images of micelles formed by PS-b-PEO (c) without and (d) with 10 wt% PS-b-PEO-MA. The inset image shows the magnification of red dash circle area. (e) Statistical contour length histograms of micelles formed by PS-b-PEO without and with PS-b-PEO-MA. Scale bars: 20  $\mu\text{m}$  in (a) and (b), 500 nm in (c) and (d), 200 nm in inset image of (c).

To reveal the effect of PS-b-PEO-MA on assembling behaviour, a series of PS-b-PEO-MA micelles was investigated. As shown in Figure 2.3, fibrillar micelle structures can be formed in all range of PS-b-PEO-MA percentages (From 0% to 100%). However, agglomerates were

also formed with increasing the amount of PS-*b*-PEO-MA. Especially in the case of using pure PS-*b*-PEO-MA to prepare micelles, single wormlike micelles can be barely observed and the micelles tend to aggregate together forming clusters (Figure 2.3d). According to basic principles of block copolymer self-assembly, it is well known that the morphologies of assemblies depend on the intrinsic ratio between hydrophobic and hydrophilic part, which can be roughly represented by a geometrical factor, packing parameter[27].

$$P=V_c/a_0l_c \quad (1)$$

where  $V_c$  is the volume of the hydrophobic chain,  $a_0$  is the area of the hydrophilic head and  $l_c$  is the length of the hydrophobic chain. Owing to the hydrophobic nature of methacrylate group in PS-*b*-PEO-MA, the packing parameter of the original PS-*b*-PEO was probably changed. Compared to PS-*b*-PEO, the ratio between hydrophobic and hydrophilic parts of PS-*b*-PEO-MA was increased, resulting in the transition of aggregate morphologies. As shown in Figure 2.3, some agglomerates were formed when the fraction of PS-*b*-PEO-MA was increased to 20%. The possible reason is that hydrophobic heads (MA) diminishes the expansion of the corona chains, leading to a less effective shield of hydrophobic PS subunits. Then, PS blocks have more tendencies to aggregate via hydrophobic interactions and switch the morphologies. It is similar to self-assembly as controlled by regulating the corona volume[28].

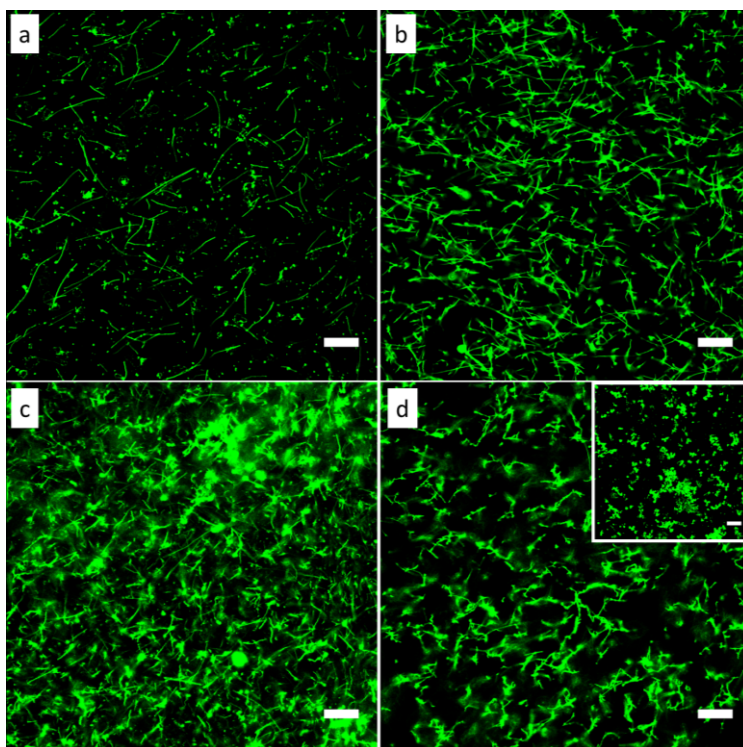


**Figure 2.3.** Confocal microscopy images of fibril micelles formed by self-assembly of PS-*b*-PEO with (a) 20 wt%, (b) 40 wt%, (c) 60 wt%, (d) 100 wt% of PS-*b*-PEO-MA. The inset shows the agglomerates formed in case of 100 wt% of PS-*b*-PEO-MA. All scale bars: 20  $\mu$ m.

Moreover, Figure 2.2e illustrates the effect of MA groups on the contour length of micelles. It can be clearly seen that after introducing PS-*b*-PEO-MA, the average length of wormlike micelles reduced from around 100  $\mu\text{m}$  to 30  $\mu\text{m}$ . This indicates that hydrophobic MA groups give rise to the formation of shorter fibril micelles as a result of corona volume effect. In order to generate the micellar hydrogels based on the glassy nanofibrillar micelles, we need to choose the system which not only maintains the fibril structure but also contains some crosslinkable groups in the corona part. Based on the above results, the system of 10% PS-*b*-PEO-MA micelles was chosen as the basis for the study of chemically crosslinked micellar hydrogels.

### 2.2.2. Physically crosslinked micellar hydrogels

For pure PS-*b*-PEO micelles, we note that these fibril micelles exhibit an aspect ratio of around 2000~3000, which can be called “ultra-long” micelles as compared to the literature. In such case, it is to be expected that the topological interactions, entanglements or liquid crystalline like interactions between them could easily be built in mildly concentrated solutions, forming a highly viscous gel-like solution[29]. To learn more about such effects, micellar solutions with different concentrations were prepared. As shown in Figure S3, with increasing concentration of micelles, micellar solutions became more turbid while the viscosity increased (indicated by the meniscus edge of micellar solutions). A gel state was even observed as the concentration of micelles is up to 140 mg/ml, indicating that gelation of these ultra-long micelles can spontaneously occur in certain concentration.

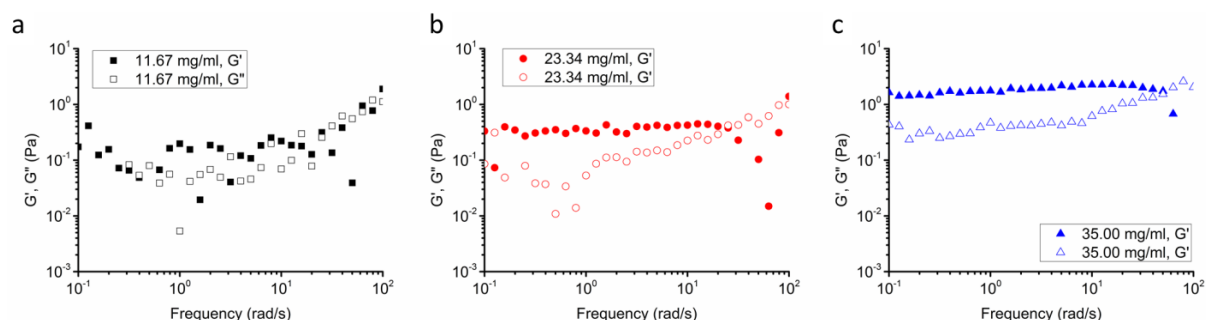


**Figure 2.4.** Frequency sweeps for PS-*b*-PEO fibril micellar solutions with different concentrations at 25 °C: (a) 11.67 mg/ml, (b) 23.34 mg/ml and (c) 35.00 mg/ml.

Rheological properties of these micellar solutions were further investigated. As shown in Figure S4 and Figure 2.4, micellar solutions with relative low concentrations (<11.67 mg/ml) exhibit very weak viscoelastic properties and the effect of geometry inertia and compliance is unneglectable, resulting in appreciable noise. High concentration samples show that viscoelastic properties of micellar solutions change from predominantly viscous (Figure 2.4a) to highly elastic (Figure 2.4b). A weak gel state, in which  $G'$  and  $G''$  became almost frequency independent, was observed at 23.34 mg/ml and 35.00 mg/ml of micellar solutions. The

reason behind this could be that increasing micelle concentration facilitate the formation of “entanglements” between these ultra-long micelles, yielding a gel network. Surprisingly, an interesting structure, micellar knot (Figure S5), was observed in air dried condition. This fact supports our assumption of micelle “entanglements” and explains that more inter-worm entanglements can be formed at the high concentration (140 mg/ml), resulting in the apparent fibrillary gel-like structure[30, 31].

Nevertheless, from the low values of  $G'$  (around 2.0 Pa) at 35.00 mg/ml concentration, we know that this kind of weak gel formed by micelle entanglements is not stable. To improve their mechanical properties and form more stable micellar gels, we, herein, proposed to increase the temperature of micellar solutions, leading to the formation of more stable crosslinks between micelles. As shown in Figure S6, gel formation of a micellar solution (35.00 mg/ml) can be observed at 70°C. For further investigation, a real-time rheological technique was employed to monitor the gelation process. Figure 2.5 shows that  $G'$  started increasing around 70 °C, which agrees with the range of glass transition temperature of polystyrene block in PS-b-PEO (Figure S2). Moreover, due to the temperature dependent dehydration behaviour of PEO corona, increasing temperature is favourable to form links between neighbouring micelles. Shikata et al.[32] have reported that with increasing temperature, the hydration number per ethylene oxide monomer unit decrease gradually and change from 4 to 2 at 70°C. In such way, PS-b-PEO ultra-long fibril micelles became less soluble in aqueous solution at high temperature, resulting in the partial collapse of the PEO corona and more interactions between micelles. Eventually, more bundling and crosslinks were formed to build up a micellar network.

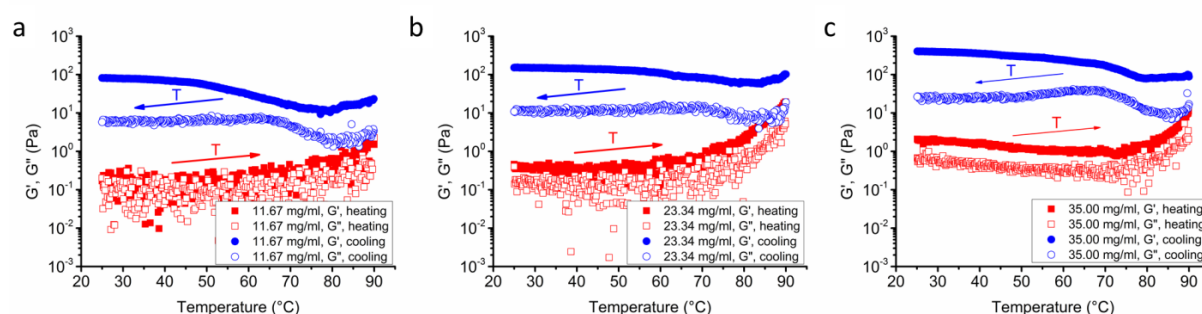


**Figure 2.5.** Storage moduli  $G'$  and loss moduli  $G''$  of PS-b-PEO fibril micellar solutions with different concentrations as a function of temperature during heating-cooling cycle. (a) 11.67 mg/ml, (b) 23.34 mg/ml, (c) 35.00 mg/ml. The red and blue arrows indicate the heating and cooling process, respectively.

Compared with noisy signal in low concentration (Figure S7), an increasing tendency of  $G'$  and  $G''$  was clearly observed with increasing temperature (Figure 2.5) indicating that more cross-linkages were formed at high concentrations ( $\geq 11.67$  mg/ml). During the cooling



process, three stages were observed in all cases. At high concentrations ( $\geq 11.67$  mg/ml),  $G'$  and  $G''$  first decreased slightly till around  $80^\circ\text{C}$  and then increased to a plateau. However, in case of low concentrations ( $\leq 1.61$  mg/ml),  $G'$  and  $G''$  first increased slowly before about  $80^\circ\text{C}$  and then climbed fast to reach an apex, followed by a decline. This difference can be explained by the formation of micellar network at high concentrations while it is difficult to construct a network at low concentrations. We noticed that in the case of  $5.84$  mg/ml, the tendency of  $G'$  combines the former two situations, namely,  $G'$  increased slowly at the beginning and then climbed to a plateau (Figure S7c). This implies that  $5.84$  mg/ml could be the critical gelation concentration (CGC), above which the micellar gels can be formed after heating-cooling cycle.

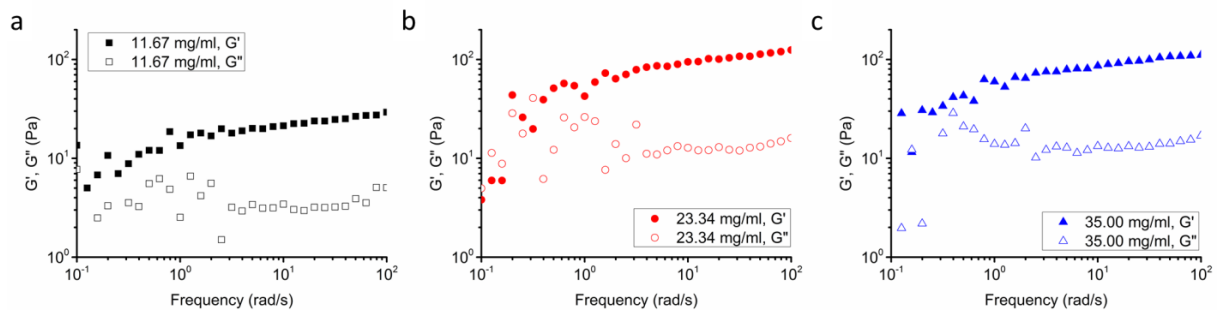


**Figure 2.6.** Frequency sweeps for PS-b-PEO fibril micellar solutions with different concentrations at  $90^\circ\text{C}$ : (a)  $11.67$  mg/ml, (b)  $23.34$  mg/ml and  $35.00$  mg/ml.

We also investigated further the rheology properties of micellar solutions at  $90^\circ\text{C}$ . For high concentrations ( $\geq 11.67$  mg/ml),  $G'$  and  $G''$  exhibited a frequency dependence as compared to that obtained at  $25^\circ\text{C}$ , before heating. The elastic properties dominate over the viscous properties (Figure 2.6). In contrast, the viscoelastic behaviour was found at low concentrations (Figure S8), which is similar to that obtained before heating. According to the crossover of  $G'$  and  $G''$ , the characteristic relaxation time can be estimated through the following equation [10]

$$\tau = 1/(2\pi f) \quad (2)$$

where  $f$  is the frequency at the crossover point. The estimated  $\tau$  of micellar solutions with high concentrations ( $\geq 11.67$  mg/ml) at  $90^\circ\text{C}$  is of order of second. These weak physical gels can be referred to as “soft gels” [33, 34], which are characterized as a solution of cylindrical micelles of sufficient length and very long relaxation times ( $\sim$  seconds) responsible for an elastic response to an oscillatory stress.

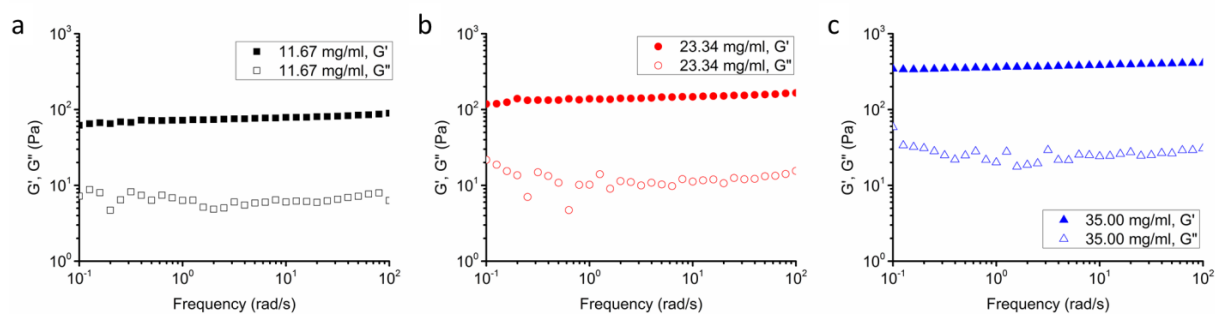


**Figure 2.7.** Frequency sweeps for PS-b-PEO fibril micellar solutions with different concentrations after heating-cooling cycle: (a) 11.67 mg/ml, (b) 23.34 mg/ml and 35.00 mg/ml.

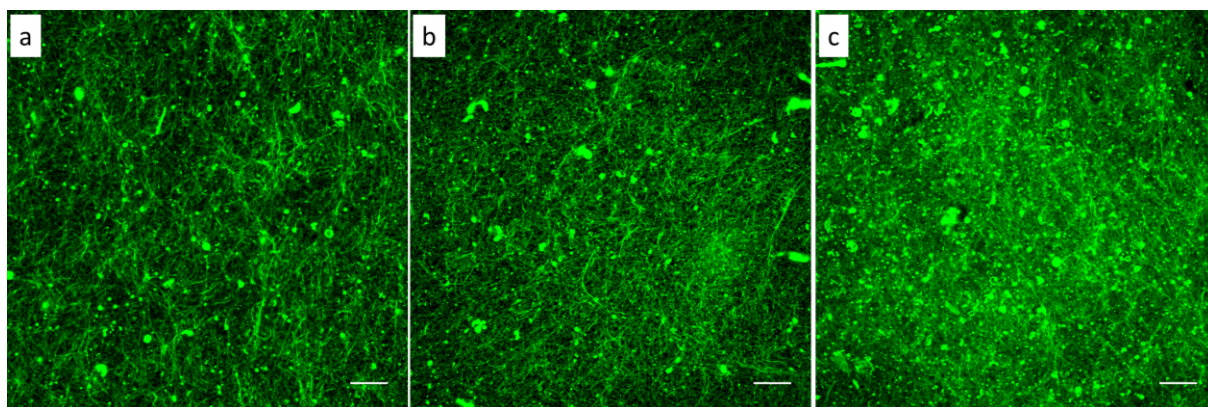


**Figure 2.8.** Confocal microscopy images of micellar hydrogels with various concentrations: (a) 11.67 mg/ml, (b) 23.34 mg/ml and 35.00 mg/ml. Scale bars: 20  $\mu\text{m}$ .

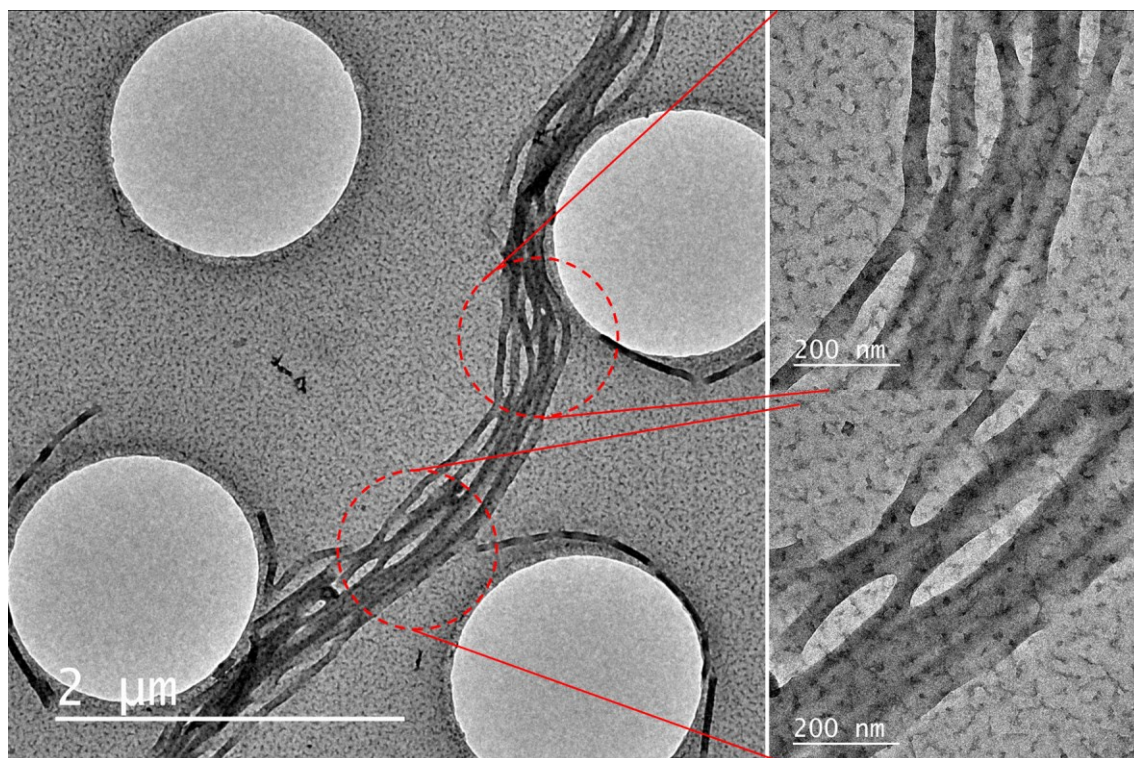


**Figure 2.9.** TEM images of micellar solution (35.00 mg/ml) after heating at 70°C for 30 min.

After cooling to room temperature (25°C),  $G'$  and  $G''$  became more frequency independent (Figure 2.7) as a result of the formation of micellar networks. Meanwhile, a weak network state was observed at low concentrations ( $\leq 1.61$  mg/ml) (Figure S9). As shown in Figure 2.8 and Figure S10, the dense micellar networks were constructed at high concentrations while no obvious micelle clusters or networks were observed at low concentrations. This can be attributed to the higher concentration of micelles, forming crosslinks easier between micelles. To further understand these “crosslinks”, we used TEM to investigate the structure of these systems. As shown in Figure 2.9, micellar clusters were observed showing that the PS core of micelles were fused together at some positions to form these “crosslinks”, which is consistent with our previous findings[35]. Regarding the glassy nature of PS at room temperature, these crosslinks are more stable at 25°C than at 90°C. In other words, the micellar networks are stronger at room temperature as compared to that at higher temperatures (90°C), which is consistent with the rheological data. It also explained why the stable micellar gels can be formed after heating-cooling cycle while “soft gels” were observed at high temperature (90°C). The morphologies of cross-links observed in Figure 2.8 differ drastically from what one expects from simple polymer gels and they resemble here to partially fused parallel cables.

### 2.2.3. Chemically crosslinked micellar hydrogels

According to the above results, we note that physically crosslinked micellar hydrogels are formed by the fusion (or “physical crosslinking”) of glassy PS cores between micelles. In comparison, we, herein, proposed to make the micellar gels with corona crosslinks followed by investigating the gelation process and corresponding properties. First, we functionalized block copolymer PS-*b*-PEO by coupling a methacrylate group to the end of the PEO block, yielding PS-*b*-PEO-MA. After incorporating PS-*b*-PEO-MA into micelles during assembling of block copolymers, the micelles with methacrylate terminal groups in the end of corona part were formed. Then, these functionalized micelles can be crosslinked via neighbouring groups.

To study the gelation behaviour of these micelles (10% PS-*b*-PEO-MA), we first simply investigated the effect of micelle concentrations on the formation of gels. As shown in Figure S11, micellar gels were formed above the concentration of 1.0 mg/ml. With increasing micelle concentrations, the gels became more and more turbid. Although a decrease of micelle average length was observed after adding PS-*b*-PEO-MA (Figure 2.2e), CGC of functionalized micelles is much lower than that of pristine micelles. This may be caused by an easier chemical crosslinking between micelle coronas. To further study the dependence of gel formation of methacrylated micelles on the concentrations, the microstructures of gels or sols formed after crosslinking were investigated. As shown in Figure 2.10, 3D micellar networks were built up above concentration of 1.00 mg/ml while agglomerates were formed



at low concentrations (0.90 mg/ml). Increasing micelle concentration also increase the possibility for connecting adjacent micelles or clusters. Compared to samples of 0.90 mg/ml (Figure 2.10a and 2.10b), it can be clearly seen that many clusters were connected with micelles at concentration of 23.34 mg/ml (Figure 2.10f), indicating that at higher micelle concentrations, denser micellar networks were formed.

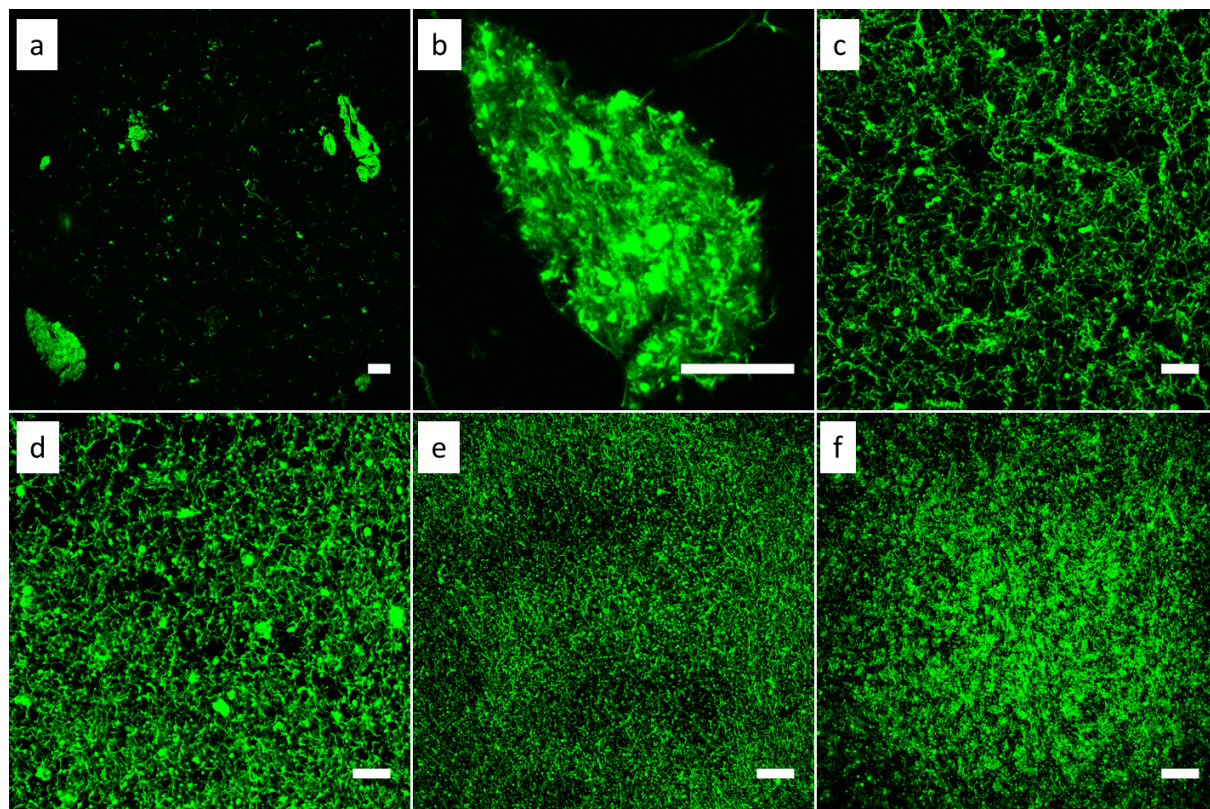


**Figure 2.10.** Confocal microscopy images of micellar networks at various concentrations of block copolymers: (a) 0.90 mg/ml; (c) 1.00 mg/ml; (d) 5.84 mg/ml; (e) 11.60 mg/ml; (f) 23.30 mg/ml. (b) magnified image of agglomerate at bottom left of (a). Scale bars: 20  $\mu\text{m}$ .

To shed light on the gelation process of this new type of glassy micellar gels, the shear storage moduli  $G'$  and loss moduli  $G''$  were recorded during the cross-linking process. Figure 2.11 shows the time dependence of  $G'$  and  $G''$  for different copolymer concentrations. Take the sample of 35.00 mg/ml concentration as an example, it can be observed that after a certain induction period, the storage modulus rises from around 10 Pa toward a long-time asymptote around 7000 Pa. The loss modulus  $G''$  exhibits a similar behaviour and also has three different regions, which can be defined as: (1) an initiation period where  $G'$  and  $G''$  are very small and similar, (2) a sol-gel transition period where  $G'$  and  $G''$  increase rapidly, (3) a plateau period where  $G'$  and  $G''$  slightly increase to reach a plateau value.

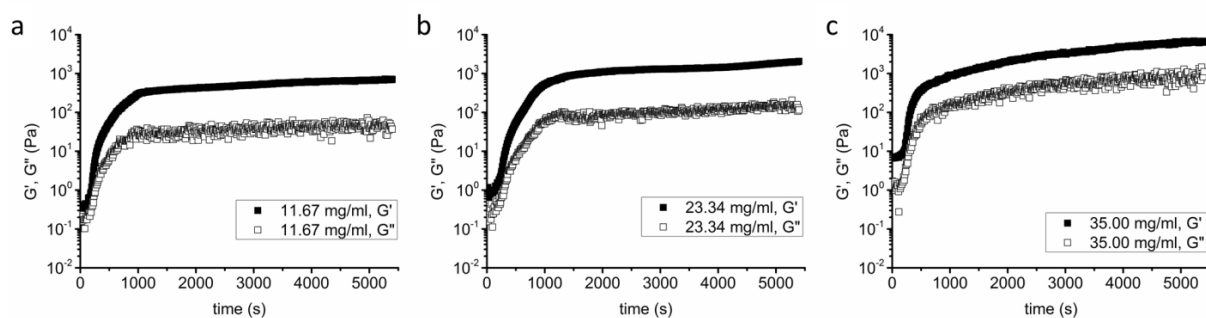


**Figure 2.11.** Time dependence of storage moduli  $G'$  and loss moduli  $G''$  during photo cross-linking reaction of 10% PS-b-PEO-MA micelles for different copolymer concentrations: (a) 11.67 mg/ml, (b) 23.34 mg/ml and 35.00 mg/ml.

Here, it can be observed that  $G'$  and  $G''$  increased with increasing concentration of micelles, which agrees with the results of physically crosslinked micellar gels. It is interesting to note that the initiation time, which is defined as the time used for the first induction plateau in  $G'$  curve, also increased (from  $\sim 115$ s to  $\sim 209$ s) with increasing concentration of micelles (from 11.67 mg/ml to 35.00 mg/ml). As the concentrations of micelles increased, it became easier for micelles to “encounter” and then bond with each other, especially at low concentrations. However, as the concentration increased further, more micellar entanglements are formed resulting in the physical micellar networks. In such situation, the contribution of micellar networks formed by chemically crosslinking is eclipsed at the beginning stage of crosslinking process. It requires more time to build chemically crosslinked networks, which have more crosslinks and larger modulus than that of the entangled ones, to eventually dominate the network properties at high concentrations. For example, a pronounced initial plateau in  $G'$  and  $G''$  was clearly observed with  $G'$  larger than  $G''$  in magnitude (Figure 2.11c). This suggests that physical networks of fibril micelles were formed before the reaction, which is consistent with our former results and is also similar to other systems such as cellulose microfibrils reinforced hydrogels[36]. Meanwhile, the higher concentration of micelles leads to lower diffusion rate of micelles, resulting in more time required for micelles to “encounter” with each other and to further crosslink.

As a result of further chemical crosslinking, more stable networks were constructed leading to the fast increment of  $G'$  until a second plateau is reached. If we associate the slope of the  $G'$  curve with time in the sol-gel transition period as a growth rate of the gel network, it can be seen that the growth rate increases for higher concentrations. This can be explained by that higher concentration of functional crosslinking groups in micellar solutions give rise to increase the rate of crosslinking reaction.

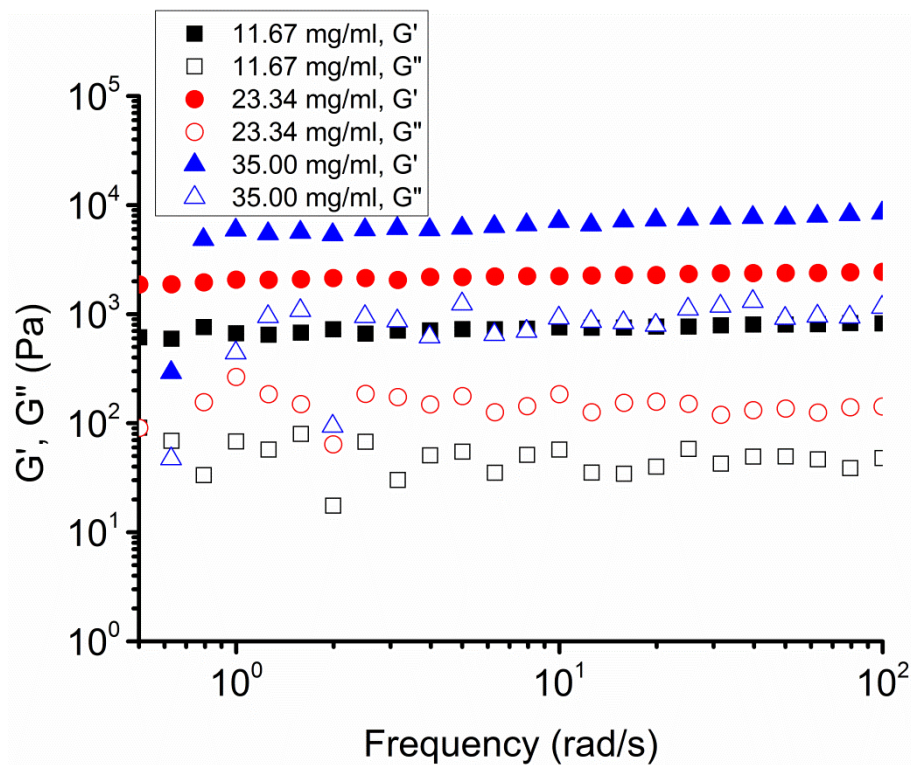


**Figure 2.12.** Plots of  $G'$  (filled symbols) and  $G''$  (open symbols) as a function of frequency measured for micellar solutions with various concentrations after crosslinking.

In order to quantify the status of cured solutions, frequency sweep was performed after crosslinking. Figures 2.12 show the  $G'$  and  $G''$  as a function of frequency at various concentrations. After crosslinking, no significant crossover of  $G'$  and  $G''$  was obtained for all concentrations, even in lower concentrations (Figure S13). Storage modulus  $G'$  is always larger than loss modulus  $G''$  over the measured frequency range, indicating the formation of a gel network. The structures of cured micellar solutions were rationalized by using a scaling approach as it is known that the storage modulus follows a power law near the gel point. However, when we associate a power law dependence,  $G' \sim \omega^n$ , to various concentrations of micelles, weak exponents were found. The extracted exponent,  $n$ , is around 0.07 (Figure 2.13). It is however, not very far from the weak power-law behaviour ( $G' \sim \omega^{0.17}$ ) behave as soft glassy materials [37, 38]. According to the theory of glassy wormlike chain model (GMLC)[39], instead of appearing flat, the “plateau” region shows an increase tendency in a weak power law. This could explain the weak frequency dependence observed for the micellar gel formed after crosslinking. Note, however, that a low value of exponent ( $n < 0.2$ ) was also reported before for thermoplastic elastomers gelled with physical crosslinking[40].

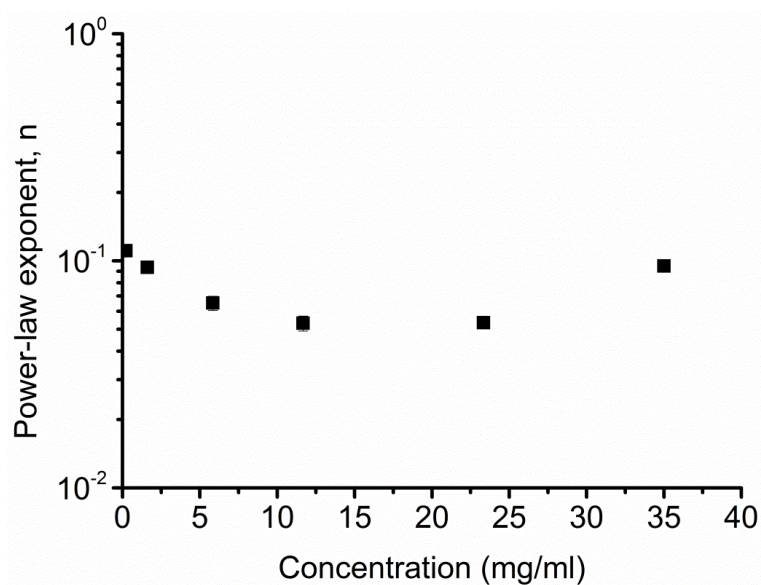


**Figure 2.13.** The power-law exponent  $n$  as a function of micelle concentration.

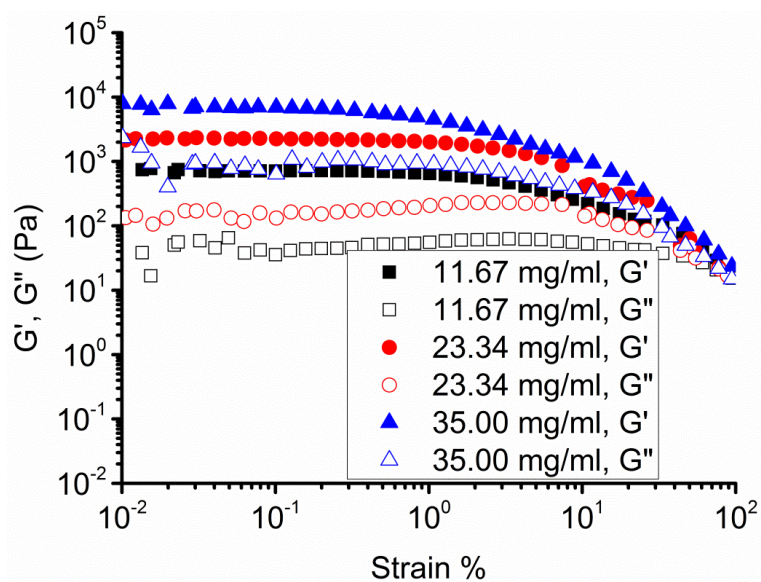


**Figure 2.14.** Plots of  $G'$  (filled symbols) and  $G''$  (open symbols) as a function of strain measured for micellar solutions with various concentrations after crosslinking.

As shown in Figure 14,  $G'$  and  $G''$  were measured as a function of increasing strain amplitude.  $G'$  remains constant over the range of low strains. When the concentration of micelles is above CGC, the critical strain of the linear region seems to decrease with increasing concentration of micelles probably because higher micelle concentrations lead to higher crosslinking degrees of micellar networks, resulting in denser and less flexible micellar gels. However, for lower concentrations (below CGC), the value is much smaller as no large network of micelles was formed (Figure S14), which is consistent with the observed microstructures (Figure 2.10).

## 2.3. Conclusion

In the present work, we used for the first time a glassy, ultra-long, nanofibrillar micelles of block copolymers to form micellar hydrogels by two different strategies: physical and chemical crosslinking. Physical crosslinking was obtained by a heating and cooling cycle of previously formed ultra-long micellar solutions with glassy polystyrene cores which were shown to partially fuse. Chemical crosslinking was obtained via modification of the corona outer monomer allowing for the formation of covalent bonds under UV irradiation. The gelation processes as function of micelle concentrations were investigated by using an in-situ rheological method. At low concentrations, instead of forming micellar gels, micelle agglomerates were formed. The CGC for physically and chemically crosslinked gels were found to be around 5.84 mg/ml and 1.00 mg/ml, respectively. Both gelation processes show three regions, including (1) initiation, (2) sol-gel transition, and (3) a plateau region, and the storage modulus  $G'$  increased with increasing micelle concentrations. When a frequency dependent scaling law was used to describe  $G'$  for these glassy micellar systems with chemical crosslinks, a weak power-law behaviour was observed (exponent is around 0.07), which is similar to that of living cells.

## 2.4. Experimental section

### 2.4.1. Materials

Diblock copolymer, polystyrene-*b*-polyethylene oxide (PS-*b*-PEO), having an –OH terminal group in PEO block was purchased from Polymer Source, Inc. (Canada). Polydispersity index of PS-*b*-PEO is 1.09 and the molecular weights of PS and PEO blocks are 16.0 kg/mol and 7.5 kg/mol, respectively. The dye used for visualization of micelles in confocal microscopy was 1,1'-Diocadecyl-3,3,3',3'-Tetramethylindocarbocyanine Perchlorate (DiI), which was purchased from Sigma-Aldrich and has excitation maxima at 549 nm. Triethylamine (Et<sub>3</sub>N), methacryloyl chloride (MAC), ethanol, anhydrous chloroform, anhydrous hexane and anhydrous tetrahydrofuran (THF) were also purchased from Sigma-Aldrich. All chemicals were used as received without further purification.

### 2.4.2. Modification of PS-*b*-PEO

A typical protocol for the modification of PS-*b*-PEO is as follows: PS-*b*-PEO (0.5 g, 0.02 mmol) was fully dissolved in 50 mL of THF and Et<sub>3</sub>N (1.25 mL, 13 mmol) was then added under vigorous stirring at room temperature. After purging the mixture with N<sub>2</sub> for 10 min, MAC (1.25 mL, 13 mmol) was dripping into the reaction solution under cooling of ice bath. Subsequently, the reaction was continued under stirring for 24h at 25°C to substitute terminal alcohol of PS-*b*-PEO by methacryloyl (MA) group. After reaction, the resulting



solution was centrifuged at 10000 rpm for 15 min and decanted to remove the formed trimethylamine hydrochloride salts. To ensure most salts were mostly removed before precipitation, the centrifugation step was repeated several times. Then, block copolymers were precipitated in hexane and washed with ethanol thoroughly, followed by drying in vacuum oven at 50°C for 2 days. Methacryloyl terminal functionalized PS-b-PEO block copolymers were denoted with “MA”, PS-b-PEO-MA.  $^1\text{H}$  NMR spectroscopy indicated the successful modification.

### **2.4.3. Preparation of nano-fibrous micelles and micellar gels**

Block copolymer micelles were prepared using an evaporation-induced self-assembly method, which you can find elsewhere[35, 41]. Briefly, block copolymers were completely dissolved in chloroform to make the stock solutions with concentration of 10 mg/ml. To prepare the micelles with MA groups, PS-b-PEO-MA was mixed with PS-b-PEO at certain weight percentages and the corresponding samples were labelled as PS-b-PEO-MA micelles. For example, the micelle sample prepared with 10% PS-b-PEO-MA and 90% PS-b-PEO was named as 10% PS-b-PEO-MA micelles. To visualise the micelles with confocal laser scanning microscopy after their formation, 0.02 wt% of the fluorescent dye, Dil, was added. Subsequently, 100  $\mu\text{L}$  of these stock solutions with Dil were injected into a 20 mL vial containing 2.3 mL of MilliQ water and stirred until chloroform was completely evaporated. Then, the resulting solutions containing micelles were collected. The micellar solutions with higher concentrations were prepared by concentrating the micelles with centrifugal filters (Centriprep centrifugal filter unit with Ultracel-30 membrane, Merck Millipore BV, The Netherlands). For physically crosslinked micellar hydrogels, pristine PS-b-PEO micellar solutions were treated with a heating-cooling cycle. To make chemically crosslinked micellar hydrogels, the water soluble photo initiator, lithium phenyl-2,4,6-trimethylbenzoylphosphine (LAP), was added to the functionalized micellar solutions leading to a concentration of LAP of 1 mg/ml. Then, micellar solutions with various concentrations were crosslinked under UV light for 10 min to form micellar gels.

### **2.4.4. Characterization**

$^1\text{H}$  NMR ( $\text{CDCl}_3$ ) spectra were recorded using a 400 MHz Agilent 400-MR spectrometer (128 scans averaged per spectrum). The micelles and micellar gels were visualized using a laser scanning confocal microscope (LSM 710, Carl Zeiss Microscopy GmbH, Germany) with a Fluor 40 $\times$ /1.30 oil M27 objective lens. To measure the length of cylinder micelles, software Image J was employed for analysis of confocal images of micelles deposited on glass slides. More than 500 micelles were measured for each sample. The resulting cylindrical micellar morphologies were also investigated by atomic force microscopy (AFM) in tapping mode and

transmission electron microscopy (TEM), which was performed by using a JEOL JEM-1400 electron microscope at 120 kV.

Rheological measurements were carried out using an AR-G2 rheometer (TA instruments) equipped with a Peltier plate for temperature control. In order to prevent the effect of water evaporation on gelation process, a solvent trap was used. Both physically and chemically crosslinking process were monitored with a parallel-plate geometry. A steel plate with 40 mm diameter was employed in the former case, while an quartz plate with 50 mm diameter and a home-make UV light source fixed on the bottom of motor shell was used for chemically crosslinked case (Figure S1). For all rheological experiments, 0.4 mL of micellar solutions (with LAP in chemically crosslinked cases) was placed on the Peltier plate and then the upper plate was set at a desired gap to make sure it was fully filled with micellar solution. Then, for the physical case, a temperature ramp was conducted at frequency of 1 Hz and 0.05% strain. The temperature increased from 25°C to 90°C and then decreased to 25°C at a speed of 1 °C/min. Frequency sweep (0.05% strain) was performed before heating (25°C), in heating (90°C) and after cooling (25°C), followed by strain sweep (frequency 1 Hz). For the chemical case, time sweep was conducted at frequency of 1Hz and strain of 0.05% for 90 min under UV irradiation, followed by frequency sweep (0.05% strain) and strain sweep (frequency 1 Hz). The 0.05% strain was selected to ensure that measurements were performed in the linear deformation region.

Differential scanning calorimetry (DSC) analysis of block copolymer PS-b-PEO was conducted on a PerkinElmer Thermal Analysis instrument. PS-b-PEO (~11mg) was carefully loaded into pre-weighted aluminum pans with a cap. A heating rate of 10°C/min was used to obtain DSC thermograms with an empty pan as reference. (Figure S2) For the thermal studies, the samples were heated in a water bath, following by equilibration of 30min at target temperature. Then, tubes were tilted to investigate the sol-gel transition behaviour.

## 2.5. References

- [1] Flory PJ. Introductory lecture. Faraday Discussions of the Chemical Society. 1974;57:7-18.
- [2] Tanaka T. Gels. Sci Am. 1981;244:124-38.
- [3] Noro A, Matsushita Y, Lodge TP. Gelation Mechanism of Thermoreversible Supramacromolecular Ion Gels via Hydrogen Bonding. Macromolecules. 2009;42:5802-10.
- [4] Augst AD, Kong HJ, Mooney DJ. Alginate hydrogels as biomaterials. Macromol Biosci. 2006;6:623-33.
- [5] Raghavan SR, Douglas JF. The conundrum of gel formation by molecular nanofibers, wormlike micelles, and filamentous proteins: gelation without cross-links? Soft Matter. 2012;8:8539-46.
- [6] Pekař M. Hydrogels with Micellar Hydrophobic (Nano)Domains. Frontiers in Materials. 2015;1.
- [7] Won YY, Davis HT, Bates FS. Giant wormlike rubber micelles. Science. 1999;283:960-3.

- [8] Won YY, Paso K, Davis HT, Bates FS. Comparison of original and cross-linked wormlike micelles of poly(ethylene oxide-*b*-butadiene) in water: Rheological properties and effects of poly(ethylene oxide) addition. *J Phys Chem B*. 2001;105:8302-11.
- [9] Bhatia SR, Mourchid A. Gelation of micellar block polyelectrolytes: Evidence of glassy behavior in an attractive system. *Langmuir*. 2002;18:6469-72.
- [10] O'Lenick TG, Jin NX, Woodcock JW, Zhao B. Rheological Properties of Aqueous Micellar Gels of a Thermo- and pH-Sensitive ABA Triblock Copolymer. *J Phys Chem B*. 2011;115:2870-81.
- [11] Velasco D, Chau M, Therien-Aubin H, Kumachev A, Tumarkin E, Jia ZF, et al. Nanofibrillar thermoreversible micellar microgels. *Soft Matter*. 2013;9:2380-3.
- [12] Moeinzadeh S, Jabbari E. Gelation characteristics, physico-mechanical properties and degradation kinetics of micellar hydrogels. *Eur Polym J*. 2015;72:566-76.
- [13] Can V, Kochovski Z, Reiter V, Severin N, Siebenburger M, Kent B, et al. Nanostructural Evolution and Self-Healing Mechanism of Micellar Hydrogels. *Macromolecules*. 2016;49:2281-7.
- [14] Zhang ZL, He ZF, Liang RL, Ma Y, Huang WJ, Jiang R, et al. Fabrication of a Micellar Supramolecular Hydrogel for Ocular Drug Delivery. *Biomacromolecules*. 2016;17:798-807.
- [15] Blanazs A, Verber R, Mykhaylyk OO, Ryan AJ, Heath JZ, Douglas CWI, et al. Sterilizable Gels from Thermoresponsive Block Copolymer Worms. *J Am Chem Soc*. 2012;134:9741-8.
- [16] Fielding LA, Lane JA, Derry MJ, Mykhaylyk OO, Armes SP. Thermo-responsive Diblock Copolymer Worm Gels in Non-polar Solvents. *J Am Chem Soc*. 2014;136:5790-8.
- [17] Willet N, Gohy JF, Lei LC, Heinrich M, Auvray L, Varshney S, et al. Fast multiresponsive micellar gels from a smart ABC triblock copolymer. *Angew Chem Int Edit*. 2007;46:7988-92.
- [18] Mai YY, Eisenberg A. Self-assembly of block copolymers. *Chemical Society Reviews*. 2012;41:5969-85.
- [19] Gadt T, leong NS, Cambridge G, Winnik MA, Manners I. Complex and hierarchical micelle architectures from diblock copolymers using living, crystallization-driven polymerizations. *Nat Mater*. 2009;8:144-50.
- [20] Qiu H, Du VA, Winnik MA, Manners I. Branched cylindrical micelles via crystallization-driven self-assembly. *J Am Chem Soc*. 2013;135:17739-42.
- [21] Qiu HB, Cambridge G, Winnik MA, Manners I. Multi-Armed Micelles and Block Co-micelles via Crystallization-Driven Self-Assembly with Homopolymer Nanocrystals as Initiators. *J Am Chem Soc*. 2013;135:12180-3.
- [22] Gould OEC, Qiu HB, Lunn DJ, Rowden J, Harniman RL, Hudson ZM, et al. Transformation and patterning of supermicelles using dynamic holographic assembly. *Nat Commun*. 2015;6:10009.
- [23] Li XY, Gao Y, Boott CE, Winnik MA, Manners I. Non-covalent synthesis of supermicelles with complex architectures using spatially confined hydrogen-bonding interactions. *Nat Commun*. 2015;6:8127.
- [24] Qiu HB, Hudson ZM, Winnik MA, Manners I. Multidimensional hierarchical self-assembly of amphiphilic cylindrical block comicelles. *Science*. 2015;347:1329-32.
- [25] He XM, Hsiao MS, Boott CE, Harniman RL, Nazemi A, Li XY, et al. Two-dimensional assemblies from crystallizable homopolymers with charged termini. *Nat Mater*. 2017;16:481-8.



- [26] Warren NJ, Rosselgong J, Madsen J, Armes SP. Disulfide-Functionalized Diblock Copolymer Worm Gels. *Biomacromolecules*. 2015;16:2514-21.
- [27] Blanz A, Armes SP, Ryan AJ. Self-Assembled Block Copolymer Aggregates: From Micelles to Vesicles and their Biological Applications. *Macromol Rapid Comm*. 2009;30:267-77.
- [28] Groschel AH, Schacher FH, Schmalz H, Borisov OV, Zhulina EB, Walther A, et al. Precise hierarchical self-assembly of multicompartiment micelles. *Nat Commun*. 2012;3.
- [29] Pei XM, Zhao JX, Ye YZ, You Y, Wei XL. Wormlike micelles and gels reinforced by hydrogen bonding in aqueous cationic gemini surfactant systems. *Soft Matter*. 2011;7:2953-60.
- [30] Clausen TM, Vinson PK, Minter JR, Davis HT, Talmon Y, Miller WG. Viscoelastic Micellar Solutions - Microscopy and Rheology. *J Phys Chem-Us*. 1992;96:474-84.
- [31] Cates ME. Flow behaviour of entangled surfactant micelles. *J Phys-Condens Mat*. 1996;8:9167-76.
- [32] Shikata T, Okuzono M, Sugimoto N. Temperature-Dependent Hydration/Dehydration Behavior of Poly(ethylene oxide)s in Aqueous Solution. *Macromolecules*. 2013;46:1956-61.
- [33] Li H, Yu G-E, Price C, Booth C, Hecht E, Hoffmann H. Concentrated Aqueous Micellar Solutions of Diblock Copoly(oxyethylene/oxybutylene) E41B8: A Study of Phase Behavior. *Macromolecules*. 1997;30:1347-54.
- [34] Hvidt S, Jorgensen EB, Brown W, Schillen K. Micellization and Gelation of Aqueous-Solutions of a Triblock Copolymer Studied by Rheological Techniques and Scanning Calorimetry. *J Phys Chem-Us*. 1994;98:12320-8.
- [35] Zhang K, Glazer PJ, Jennings L, Vedaraman S, Oldenhof S, Wang Y, et al. A facile approach for the fabrication of 2D supermicelle networks. *Chem Commun*. 2016;52:12360-3.
- [36] Harini M, Deshpande AP. Rheology of poly(sodium acrylate) hydrogels during cross-linking with and without cellulose microfibrils. *J Rheol*. 2009;53:31-47.
- [37] Deng LH, Treppe X, Butler JP, Millet E, Morgan KG, Weitz DA, et al. Fast and slow dynamics of the cytoskeleton. *Nat Mater*. 2006;5:636-40.
- [38] Fabry B, Maksym GN, Butler JP, Glogauer M, Navajas D, Fredberg JJ. Scaling the microrheology of living cells. *Phys Rev Lett*. 2001;87.
- [39] Broedersz CP, MacKintosh FC. Modeling semiflexible polymer networks. *Rev Mod Phys*. 2014;86:995-1036.
- [40] Richtering HW, Gagnon KD, Lenz RW, Fuller RC, Winter HH. Physical Gelation of a Bacterial Thermoplastic Elastomer. *Macromolecules*. 1992;25:2429-33.
- [41] Jennings L, Ivashchenko O, Marsman IJ, Laan AC, Denkova AG, Waton G, et al. In vivo biodistribution of stable spherical and filamentous micelles probed by high-sensitivity SPECT. *Biomater Sci*. 2016;4:1202-11.

## 2.6. Appendix

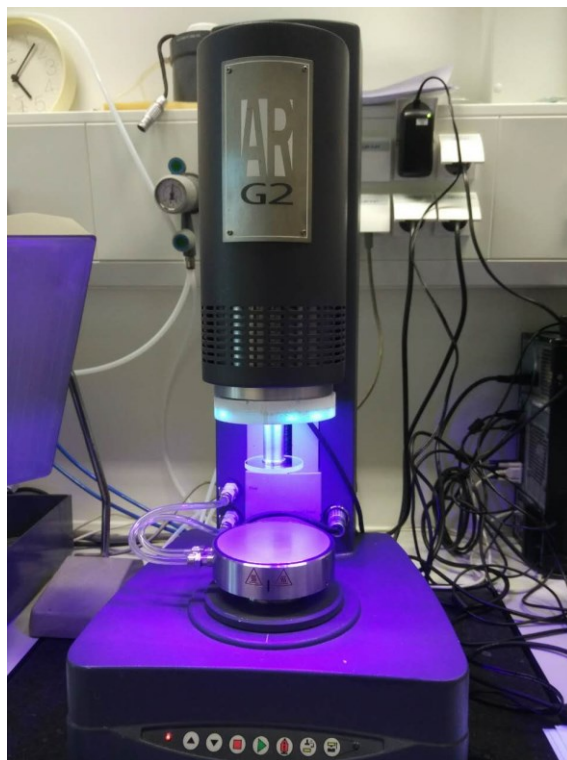


**Figure S1.** Home-made UV light source installed in rheometer.

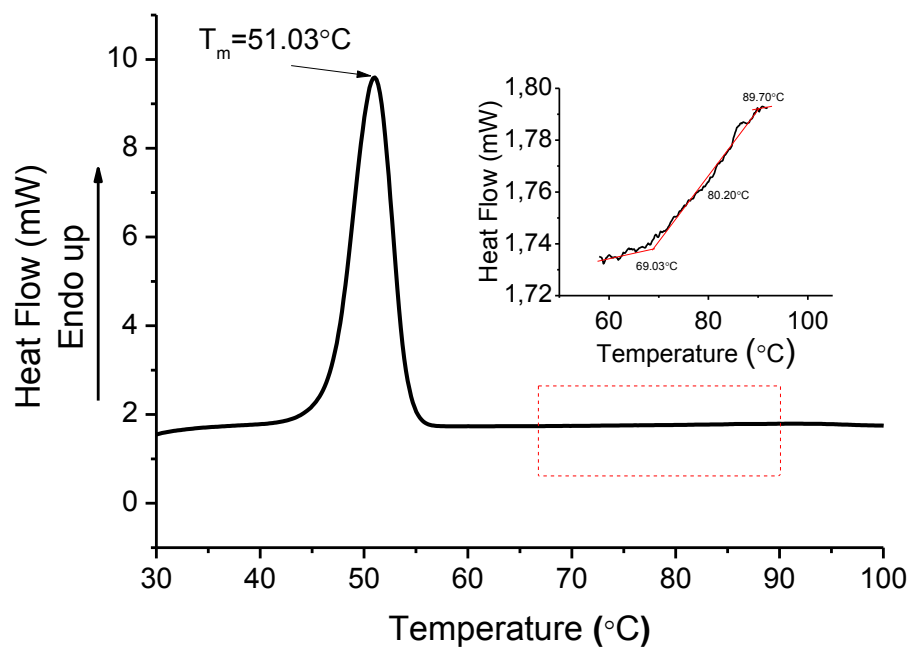


**Figure S2.** Differential scanning calorimetry thermograms of PS16k-b-PEO7.5k diblock copolymers. The heating rate was 10.00 $^\circ\text{C}/\text{min}$ . The inset is the amplification of the marked area in the main curve.

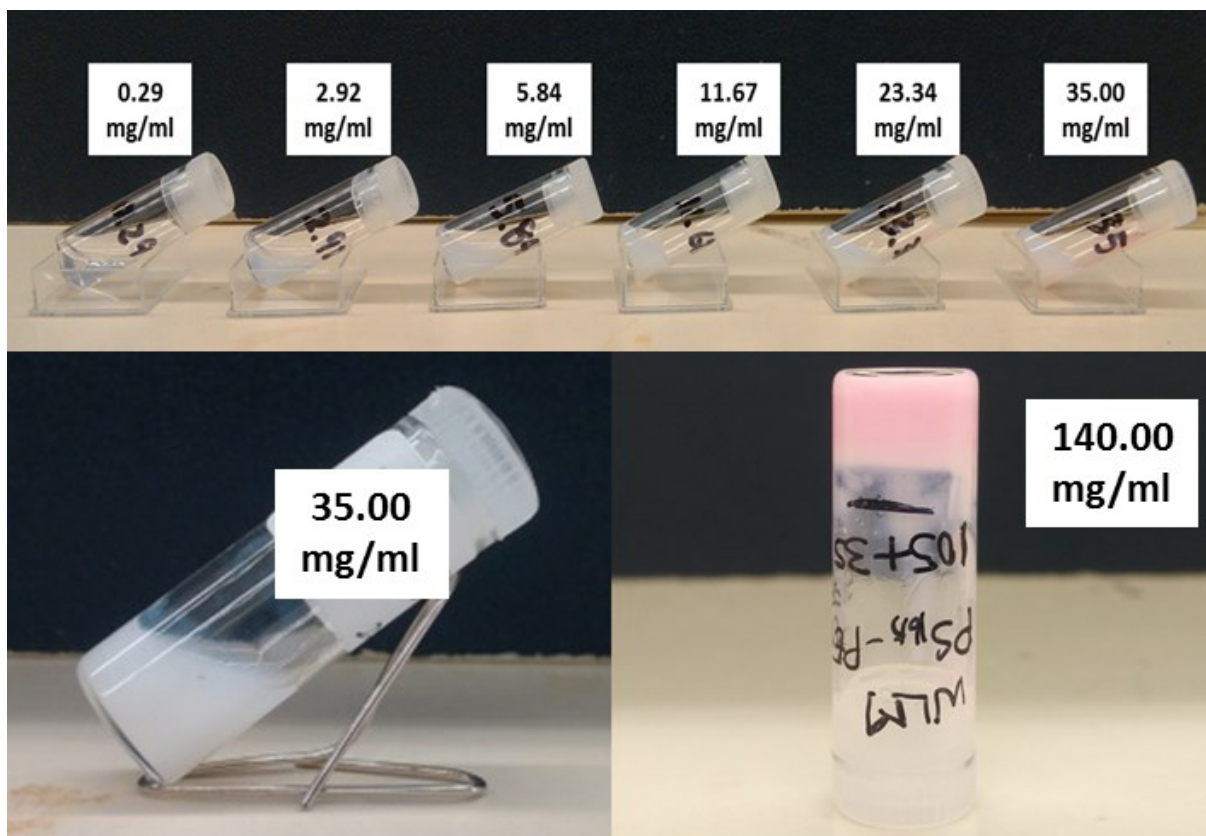


**Figure S3.** Photographs of PS-b-PEO micellar solutions with different concentrations. With increasing the concentration of micelles, the solutions became more viscous and the 140.00 mg/ml sample passed the tube inversion test showing a characteristic gel behaviour. Note the pink colour in 140.00 mg/ml sample was caused by the increased concentration of dye encapsulated in micelles.

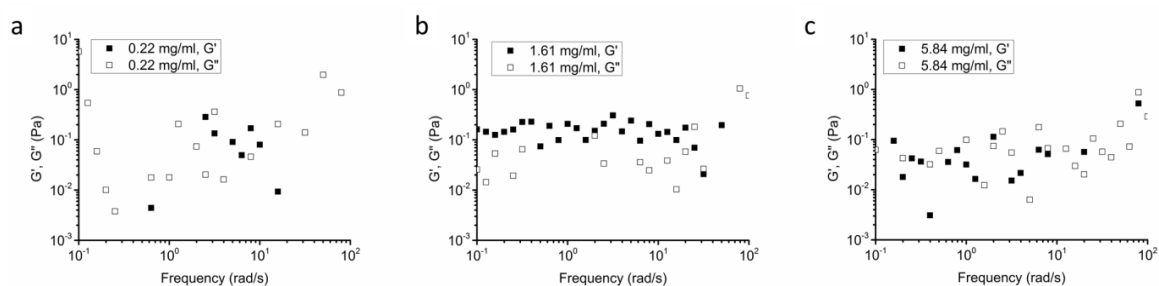


**Figure S4.** Frequency sweeps for PS-b-PEO fibril micellar solutions with different concentrations at 25 °C.

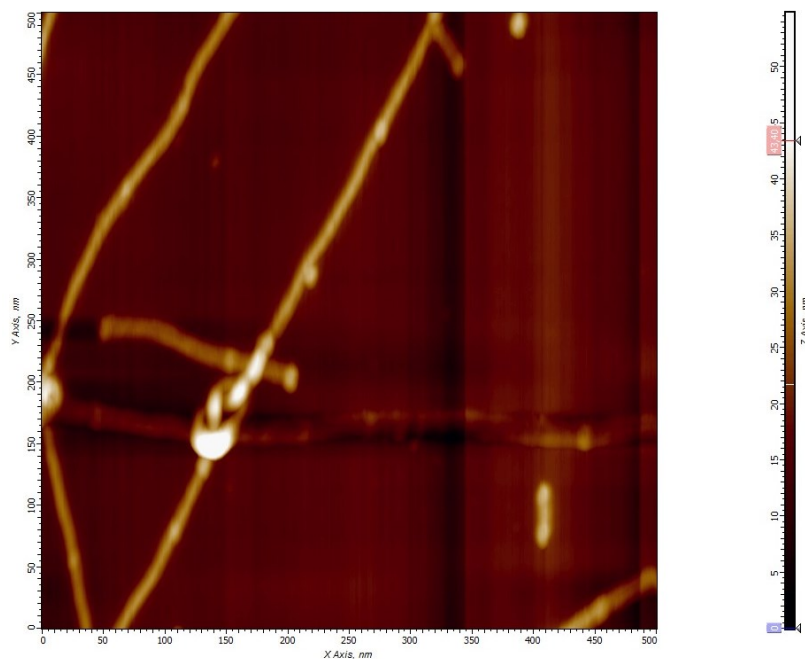


**Figure S5.** AFM image of PS-b-PEO micelle knot.

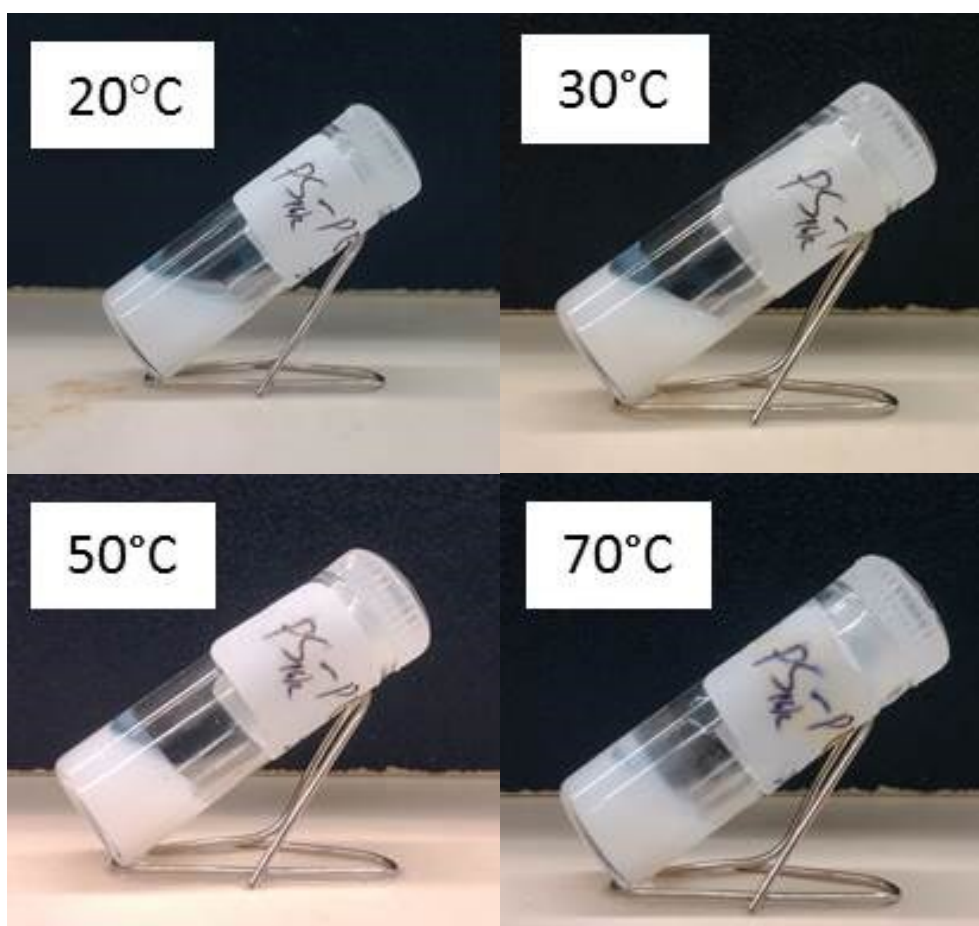


**Figure S6.** Vial-titling test of 35.00 mg/ml micelles solution at different temperatures.

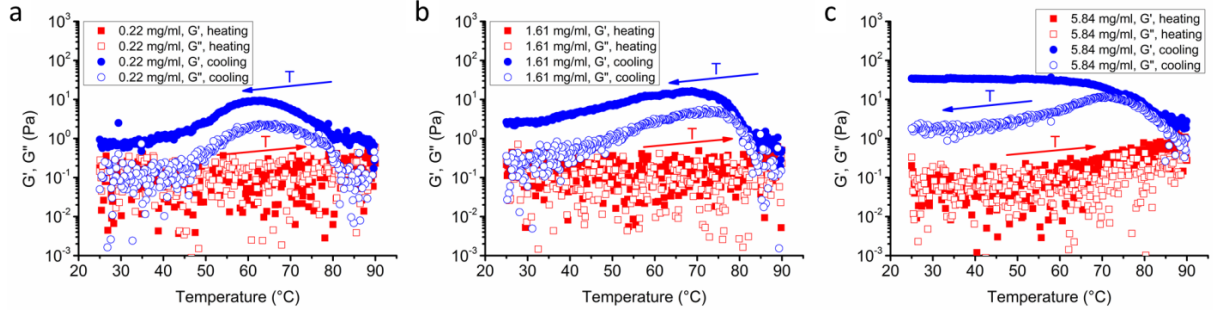


**Figure S7.** Storage moduli  $G'$  and loss moduli  $G''$  of PS-b-PEO fibril micellar solutions with different concentrations as a function of temperature during heating-cooling cycle. (a) 0.22 mg/ml, (b) 1.61 mg/ml, (c) 5.84 mg/ml. The red and blue arrows indicate the heating and cooling process, respectively.

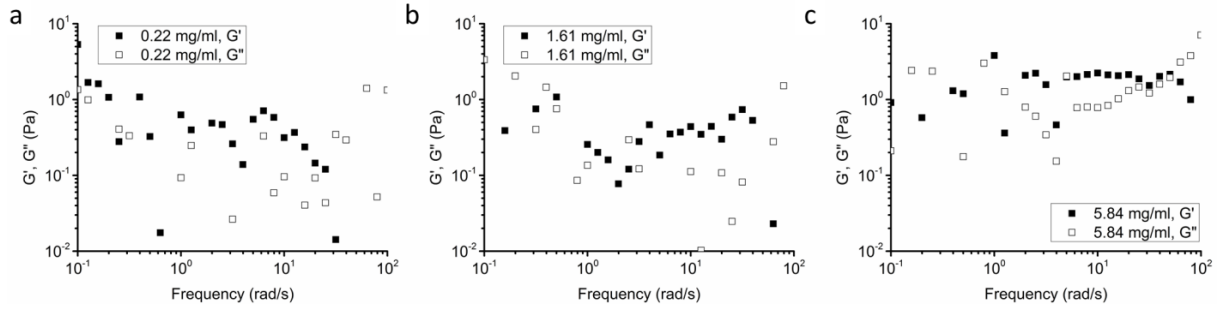


**Figure S8.** Frequency sweeps for PS-b-PEO fibril micellar solutions with different concentrations at 90 °C: (a) 0.22 mg/ml, (b) 1.61 mg/ml, (c) 5.84 mg/ml.

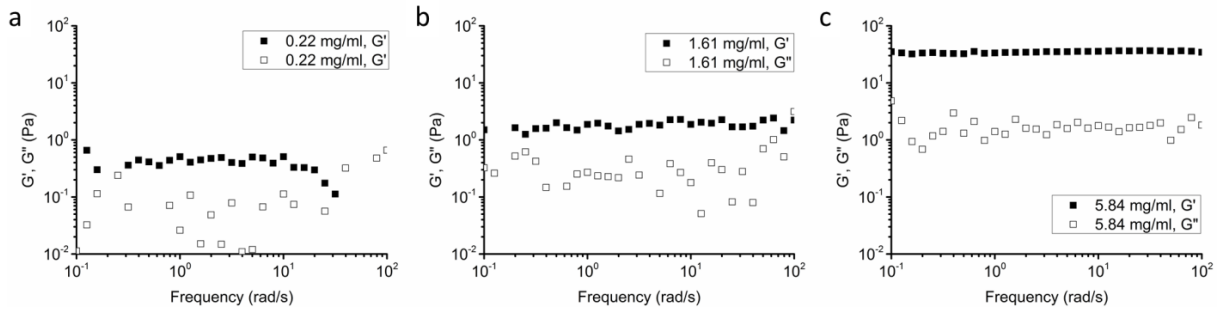


**Figure S9.** Frequency sweeps for PS-b-PEO fibril micellar solutions with different concentrations after heating-cooling cycle: (a) 0.22 mg/ml, (b) 1.61 mg/ml, (c) 5.84 mg/ml.



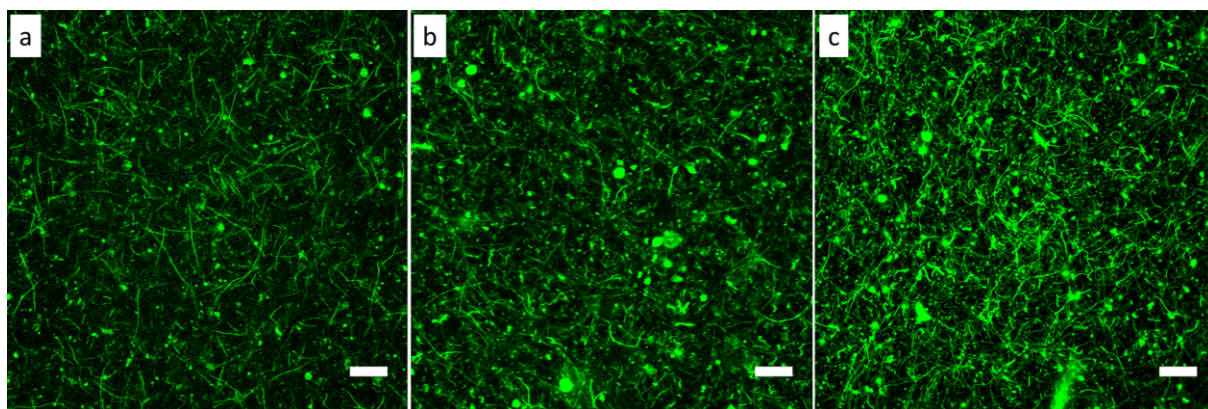


**Figure S10.** Confocal microscopy images of micellar hydrogels with various concentrations: (a) 0.22 mg/ml, (b) 1.61 mg/ml, (c) 5.84 mg/ml.

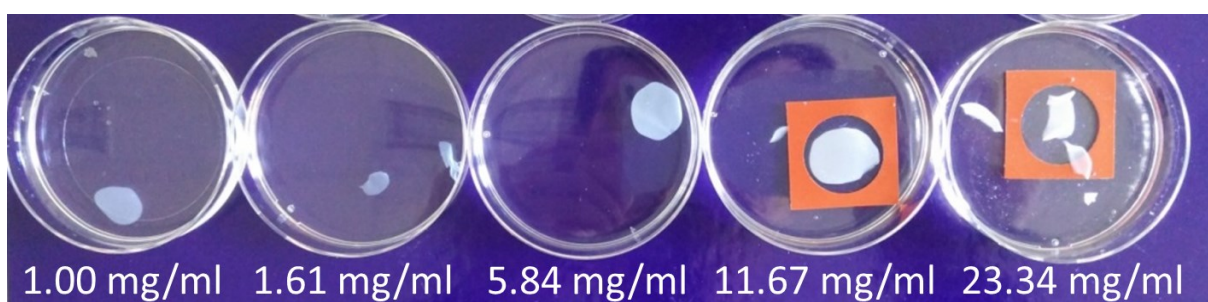


**Figure S11.** Optical image of micellar hydrogels formed at different concentrations of micelles. Note: as these micellar gels are very fragile, they can be easily broke into small pieces during transfer. The small pieces in image was caused by this. The cases of micellar solution crosslinked at the lower concentrations were not shown here as only solution of agglomerates was observed instead of gels.

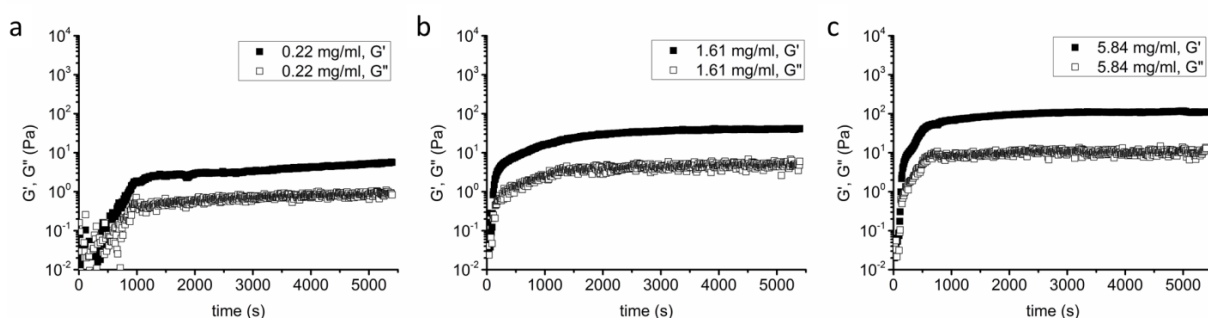


**Figure S12.** Time dependence of storage moduli  $G'$  and loss moduli  $G''$  during photo cross-linking reaction of 10% PS-*b*-PEO-MA micelles for different copolymer concentrations: (a) 0.22 mg/ml, (b) 1.61 mg/ml and (c) 5.84 mg/ml.

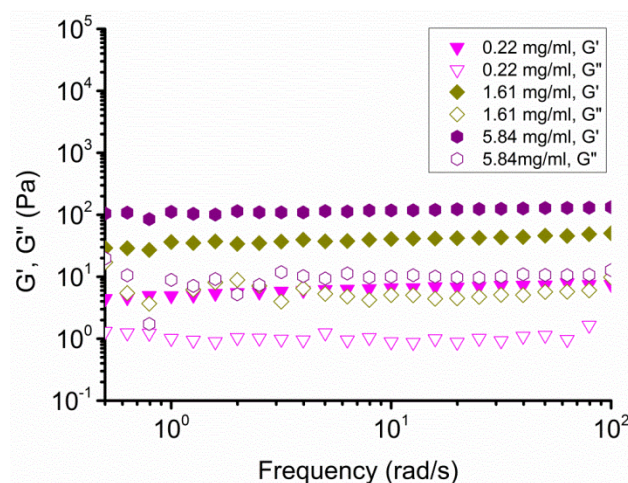


**Figure S13.** Plots of  $G'$  (filled symbols) and  $G''$  (open symbols) as a function of frequency measured for micellar solutions with various concentrations after crosslinking.

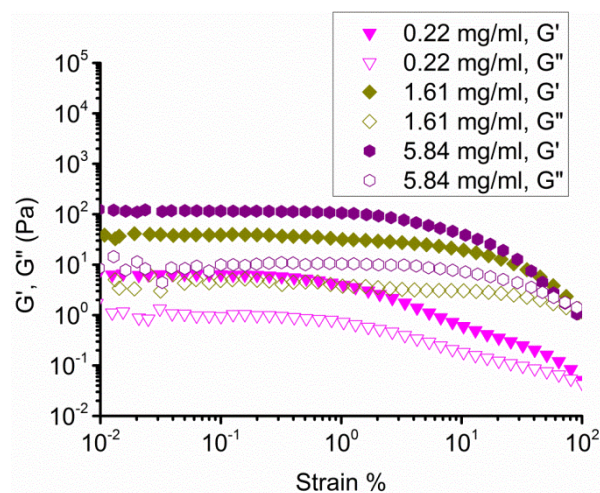


**Figure S14.** Plots of  $G'$  (filled symbols) and  $G''$  (open symbols) as a function of strain measured for micellar solutions with various concentrations after crosslinking.

# A facile approach for the fabrication of 2D supermicelle networks

# 3

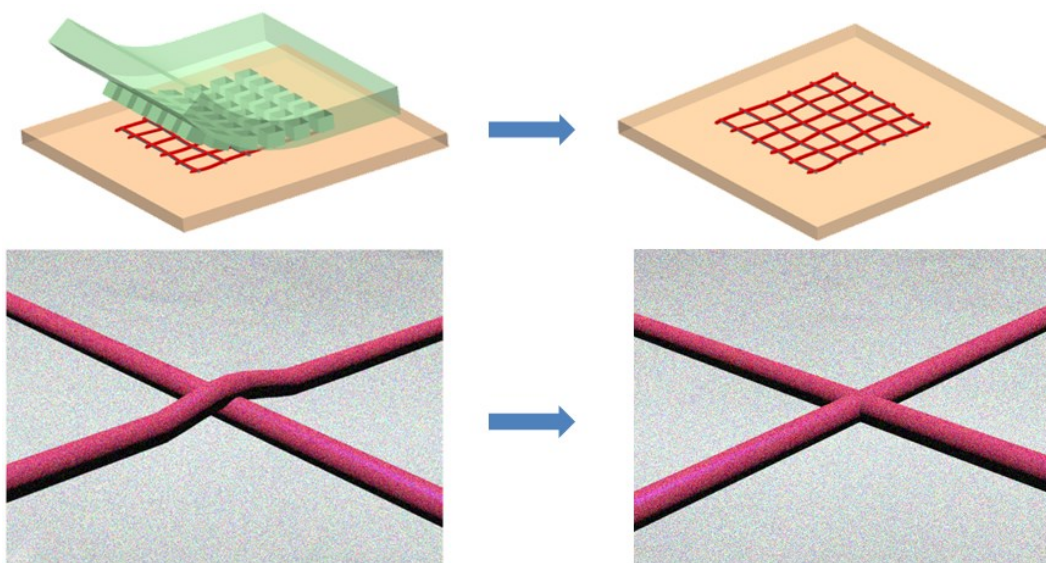
This chapter has been published in :

K. Zhang, P.J. Glazer, L. Jennings, S. Vedaraman, S. Oldenhof, Y. Wang, F. Schosseler, J.H. van Esch and E. Mendes, *Chem. Commun.*, **2016**, 52, 12360-12363.



## Abstract

A novel and facile approach to fabricate well-organized macroscopic 2D networks of cylindrical micelles is reported, based on transfer printing and thermal welding of aligned supramolecular micelles of block copolymers. This versatile approach provides a new strategy for fabricating functional 2D superstructures with a higher level of order.



### 3.1. Introduction

The controlled fabrication of ordered macroscopic structures from supramolecular assemblies has drawn much attention due to their wide-ranging applications, such as in tissue engineering[1] and electronics[2]. While amphiphilic block copolymers (BCPs) can self-assemble into various nano-structures, including spheres, cylinders, vesicles and other morphologies, by simply controlling block length ratio, solvent, concentration and temperature,[3, 4] more complex and higher-level structures were recently reported, broadening the range of hierarchical materials based on BCPs micelles and their advanced applications. For instance, Spatz and Möller et al.[5-8] combined the self-assembly of BCPs with conventional lithography methods, namely block copolymer micelle nanolithography (BCMN), to control and guide organization of spherical micelles on flat surfaces. Cohen et al.[9] created patterned carbon nanotubes by microcontact printing of block copolymer micellar thin films. Manners et al. recently reported some interesting structures, such as “I”-shaped, “windmill” or “cross” supermicelles,[10, 11] formed by the programmed assembly of cylindrical micelles with crystalline cores. However, a simple method for the fabrication of complex and artificial supermicelle structures, such as a fishnet, is still a challenge. Herein, we present a novel and facile method for the preparation of such two dimensional (2D) supermicelle networks, that is based on a combination of guided de-wetting, transfer-printing and thermal welding of ultralong, out of equilibrium BCPs micelles. The flexibility of stamp fabrication, wetting and micelles printing involved in this approach shows its simplicity and potential for fabrication of new functional superstructures with controlled size and shape.

### 3.2. Results and Discussion

The fabrication process of a 2D supermicelle networks is schematically illustrated in Figure 3.1. First, poly(dimethylsiloxane) (PDMS) stamps were prepared by casting and curing the polymer on a reverse Si-wafer template, which was fabricated by deep reactive ion etching technique.[17] The stamp consisted of an array of square micropillars with sizes of  $3.5 \times 3.5 \times 3.0 \mu\text{m}$  (length $\times$ width $\times$ height) separated by  $2.0 \mu\text{m}$  (Figure S1). These dimensions were found to promote dewetting and alignment process of the micelles (See Table S1). Ultralong ( $\sim 200 \mu\text{m}$ ) quenched cylindrical micelles with PEO corona and glassy polystyrene core were obtained as previously reported.[17] Subsequently, a micelle solution ( $20 \mu\text{L}$ ) of polystyrene-*b*-poly(ethylene oxide) (PS-*b*-PEO) was deposited on the edge area of the stamp pattern. An optical lens tissue was employed to drag the micelle solution to guide the de-wetting process on PDMS stamp (Figure 3.1b). As the micellar solution moves over the pillar tops, air trapped in between the pillars provides a continuous interface at the pillar top while pillars act as wetting defects to hold the drop receding contact line locally, leading to the

suspension and ordering of micelles along pillar tops.[16, 17] As a result, an “inked” stamp with well-aligned micelle arrays on micropillars tops was formed (as shown in Figure 3.1c). Next, the “inked” stamp was placed on the receiving substrate, such as glass cover slide, and mild pressure was applied to attain conformal contact. After slowly peeling the PDMS stamp off, the aligned micelles were released from the pillars of the stamp and transfer-printed onto the receiving substrate (Figure 3.1d). By repeating the former steps a-c, more fresh “inked” stamps can be prepared and used to print subsequent micelle layers on top of the former micelle arrays with a certain degree, such as 90°. As a result, a grid that consists of layered orthogonal micelle arrays was formed (Figure 3.1e). Upon heat treatment, a 2D network of supermicelles was built through a simple thermal welding process at the junctions (Figure 3.1f).

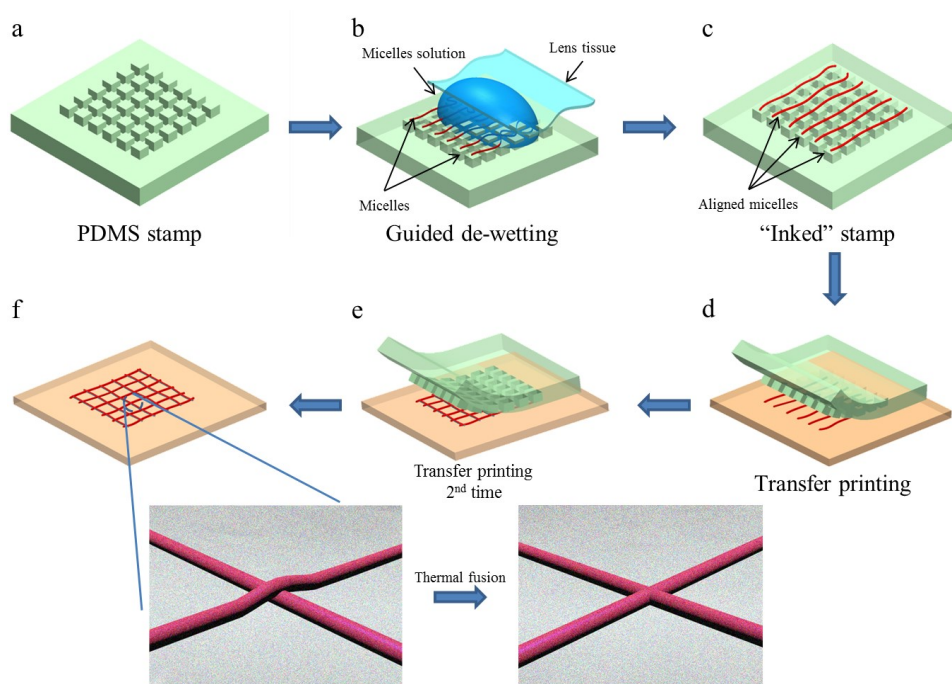


**Figure 3.1.** Schematic illustration of the fabrication process of 2D supermicelle network: (a) Preparation of PDMS stamp; (b) Aligned cylinder micelles on PDMS stamp by guided de-wetting technology; (c) “Inked” stamp; (d) Transfer printing of aligned micelles onto the target substrate; (e) 2nd Transfer printing with another “inked” stamp perpendicular to 1st array; (f) Thermal welding of the printed two layers of micelles.

In this approach, the alignment and printing of micelles is crucial in the formation of 2D network. We previously reported the process of alignment while in this work we detail the process of printing.[17] For successful stepwise build-up of a 2D network, transfer printing after alignment is critical. To achieve a successful transfer, the work of adhesion at micelle-substrate interface  $W_{m-sub}$  should be larger than that at the micelle-stamp interface  $W_{m-st}$ , i.e.,  $W_{m-sub} > W_{m-st}$ . [18] Here, PDMS was used to prepare the stamp for transfer printing, which has a good chemical stability, high resolution moulding capability and conformable

nature. Its low surface energy ( $21.6 \text{ dynes/cm}^2$ ) enables the reliable release during printing[19] while the viscoelastic behaviour of PDMS offers a kinetic manipulation of adhesion at the ink-stamp interface (velocity-dependent adhesion).[20] When the stamp was peeled off at slow rate (approximately  $1 \text{ mm/s}$  or slower), the micelles adhered preferentially onto the glass. In contrast, fast peeling velocity (approximately  $10 \text{ cm/s}$  or faster) results in the micelles left on PDMS stamp after printing. Laser scanning confocal microscopy images of the micelle arrays aligned on PDMS stamp before transfer and on glass surface after transfer are shown in Figure 3.2a and 3.2b, respectively. As indicated by the dash squares in Figure 3.2a, it can be seen that the micelles were well aligned on micropillars of PDMS stamp.

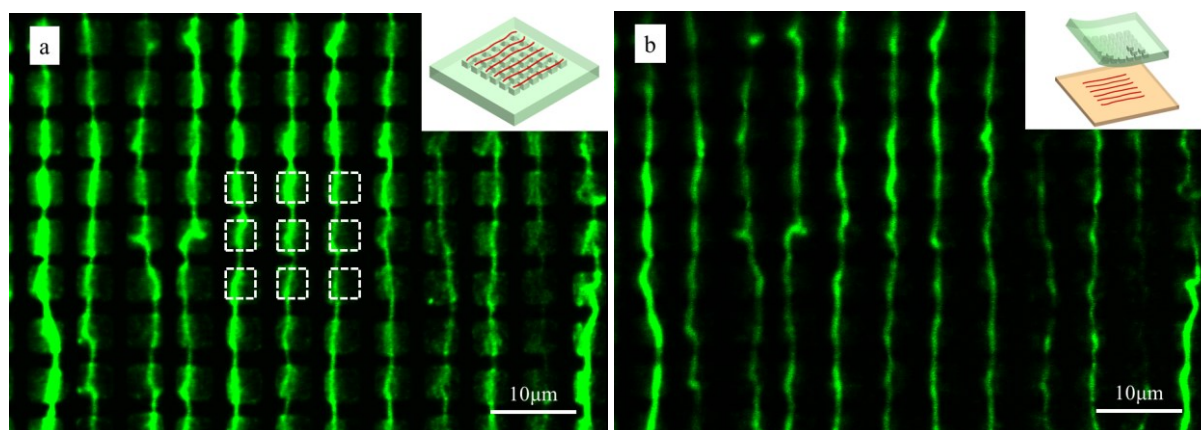


**Figure 3.2.** Confocal microscopy images of aligned micelles before (a) and after (b) micelles transfer onto a glass slide. Note: The micelles were fluorescently labelled with Dil. The white dashed boxes in (a) stand for the outline of the PDMS micropillars.

Subsequently, the aligned micelles can be efficiently printed onto a glass slide when the stamp was peeled off from the receiving substrate, at low velocity (around  $1 \text{ mm/s}$  or slower). As shown in Figure 3.2b, nearly all the micelles were transferred to the glass surface with the identical alignment. The transfer process can be understood by comparing the estimated work of adhesion at the micelle-PDMS interface with that of the micelle-glass interface. Owing to the core-corona structure of micelles, we used PEO instead of the micelle to calculate the adhesion. The work of adhesion between micelle (PEO) and PDMS is  $W_{\text{PDMS-PEO}} = 50.1 \text{ mN/m}$ , which is smaller than that between glass and micelle (PEO)  $W_{\text{Glass-PEO}} = 91.1 \text{ mN/m}$  (see Supporting Information). This is in agreement with our findings. The same printing procedure is also suitable for other substrates as long as the work of adhesion between micelle and substrate is larger than  $W_{\text{PDMS-PEO}}$ , such as silicon wafer ( $W_{\text{Silicon-PEO}} = 83.8 \text{ mN/m}$ ), as shown in Figure S4. However, transfer printing failed on the substrates with extremely low surface energy, such as polytetrafluoroethylene (PTFE). The interfacial work of adhesion between PTFE and micelle ( $W_{\text{PTFE-PEO}}$ ) is  $51.8 \text{ mN/m}$ , which is comparable to  $W_{\text{PDMS-PEO}}$  and results in the failure of transfer process (results not shown).



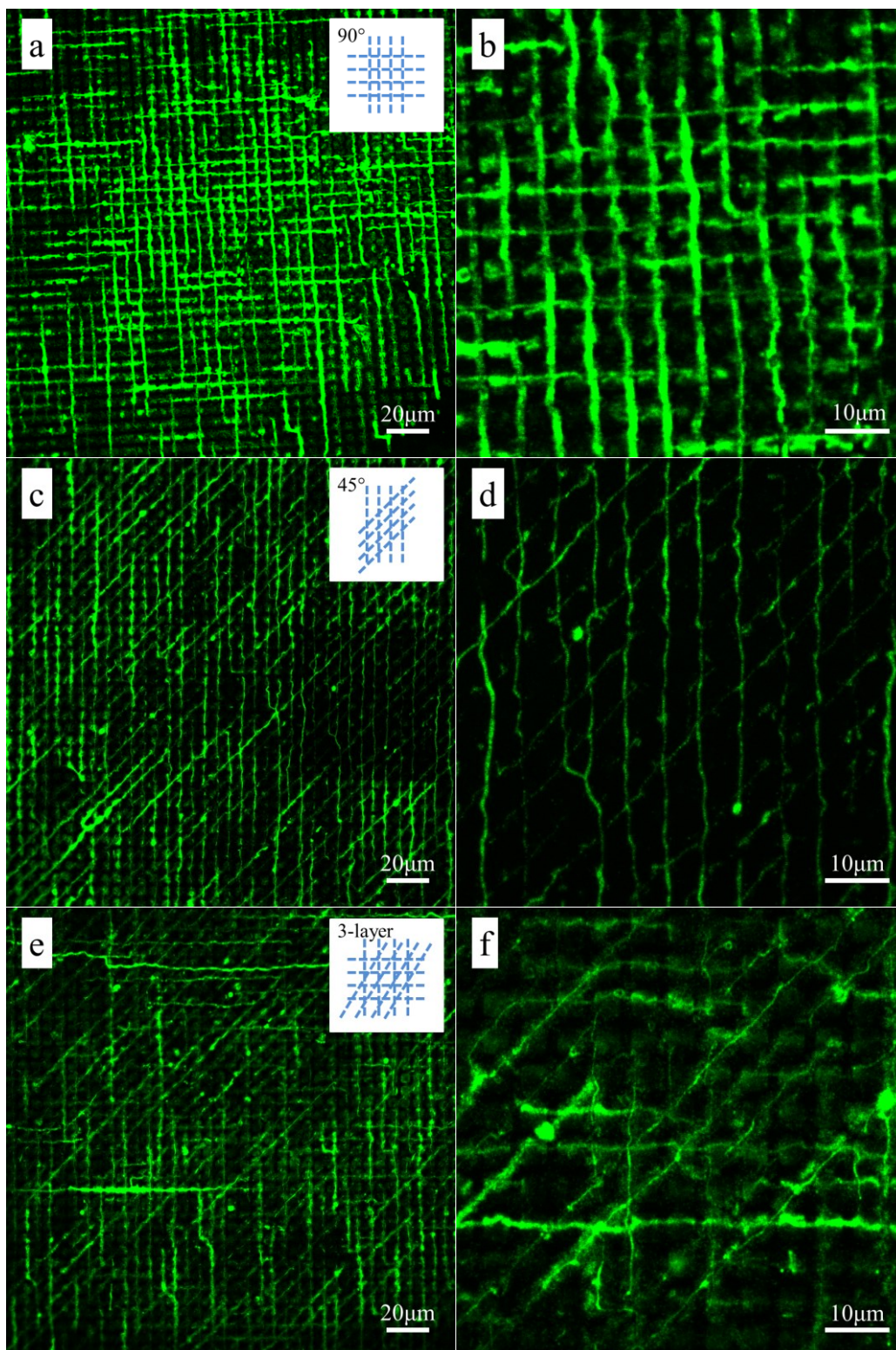


**Figure 3.3.** Multiple transfer printings of aligned micelles with different alignment angles. Images (a) and (b) correspond to an orthogonal double-layer; (c) and (d) to a double-layer forming 45°; (e) and (f) a triple-layer with 45° and 90° in relation to the first printed micelle array.

In order to construct 2D micelle network, the same transfer printing process was applied several times on the same receiving substrate. As shown in Figure 3.3a and 3.3b, a grid

structure was obtained by printing the second layer perpendicularly to the first one. By simply changing the angle of the second printing, other alignments such as 45° can also be obtained (Figure 3.3c and 3.3d). A triple-layer structure was even formed by sequentially printing three layers of aligned micelles (Figure 3.3e and 3.3f), which shows the possibility to build more complex and multi-layered structures by combining various micelles with different materials and sizes. Here, we need to note that  $W_{\text{PEO-PEO}}=85.8 \text{ mN/m}$  is in the same order of magnitude as  $W_{\text{Glass-PEO}}$  and therefore multiple layers of micelles do not significantly influence transfer printing efficiency.

After the deposition of these 2D micelle grids, we applied temperature treatment to induce welding of the block copolymer micelles in order to form a non-covalent superstructure of micelles. This method offers a simple way to physically connect the micelles together without the need for a chemical reaction, as shown in Figure 3.1f. By increasing the temperature, the morphologies of micelles, especially in the junctions, exhibit changes as imaged by atomic force microscopy (AFM) (Figure 3.4a). It can be seen that at room temperature (25°C), micelles superimpose and the height of the junctions is around 94 nm (Figure S5a and S5b), in agreement with twice as the height of a single micelle (around 48 nm) (Figure S5c and S5d). As the temperature increased, the orthogonally aligned micelles soften and fuse together at junctions. The height of junction points decreased from 94 nm to 57 nm at 85°C, which is just above the observed glass transition temperature (80°C) of polystyrene core (Figure S6).[21]

Figure 3.4b shows the heights of micelle junction and single aligned micelle on glass at different temperatures. When the temperature reached around 50°C, the height of micelle junction starts to reduce. From this plot, we can see that the height decrease of the junction is around 19 nm, which is about three times higher than what is observed for the decrease of a single micelle (around 6 nm). This corresponds to the melting process of PEO corona, which has a melting point of approximately 50°C (Figure S6). With further increase of the temperature, the height of junctions also decreased further. This was attributed to the softening of the thicker polystyrene (PS) core. As the temperature increased above 90°C, the height of junction reached an equilibrium state without any significant change, which is in agreement with the glass transition of PS (Figure S6). Upon cooling down to room temperature, the height of the micelles and junctions didn't recover to the original value, showing indeed that irreversible thermal induced micelle fusion occurred generating a fishnet like higher-ordered superstructure. We noticed that the decrease of junction height (~37 nm) is larger than the twice the height decrease of a single micelle (~13 nm). It suggests that besides the thermal melting of each single micelle, the micelles also fused together at the junctions. Hence, during the whole thermal fusion process, there are two main stages involved: (1) melting process of PEO corona and (2) soften and fusion step of glassy PS core

when the temperature was above the glass transition temperature of PS. After thermal fusion, micelles were bound together and two-dimensional superstructures were formed (Figure S7).

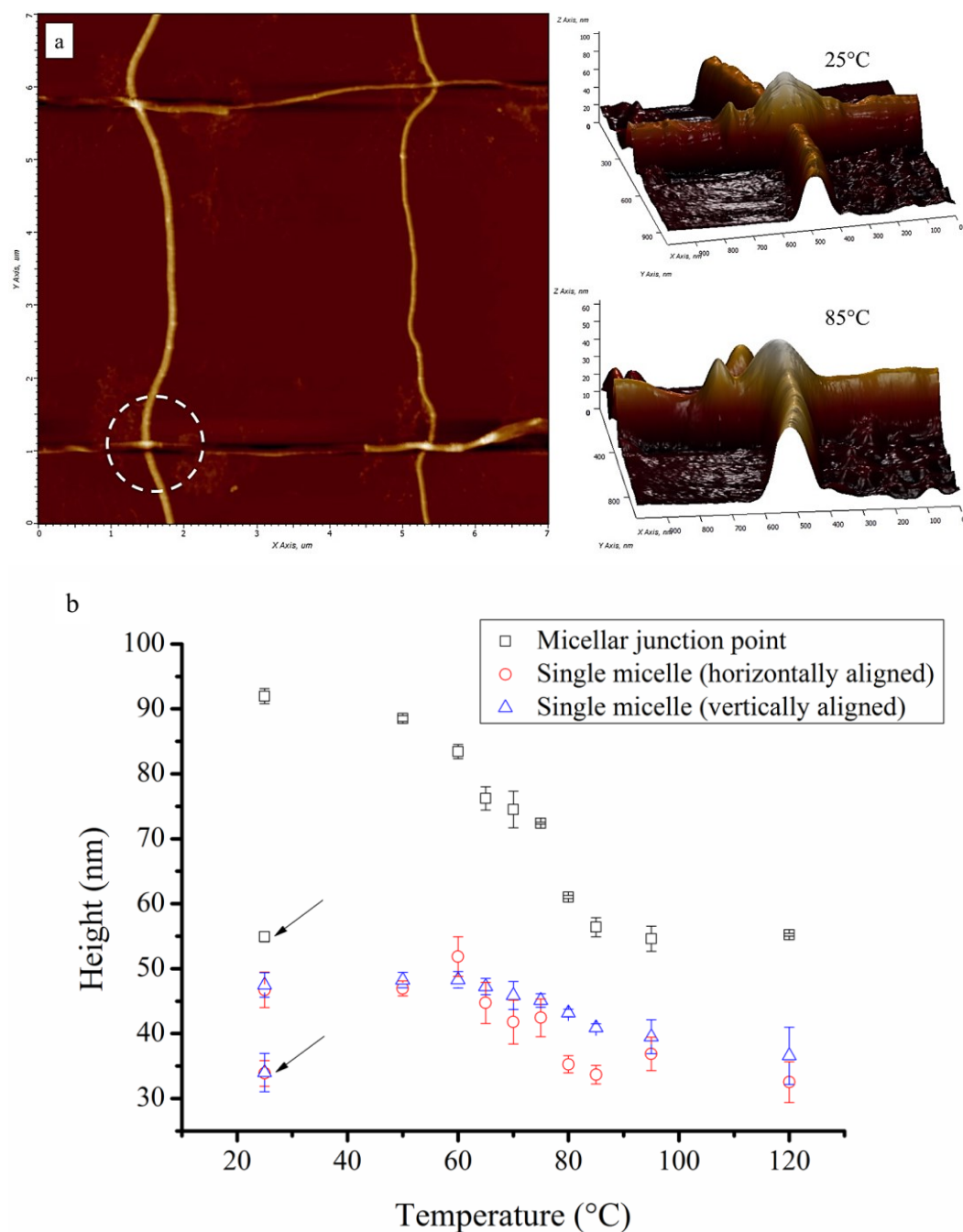


**Figure 3.4.** Thermal welding process of micelle network: (a) AFM images of 2D micelle network on glass substrate. AFM 3D scans of a micelle junction (dashed line) measured at 25°C before heating and at 85°C are shown on top right, respectively. (b) Height of the micellar junction and single micelles as a function of increasing temperature. The heights of single micelles plotted correspond to micelles aligned in vertical and horizontal directions in (a). The arrows in (b) indicate the heights measured after cooling to room temperature.

### 3.3. Conclusion

In summary, we have introduced a novel and facile approach for the fabrication of 2D supermicelle networks. This new methodology utilizes the de-wetting alignment of ultralong ( $\sim 200\mu\text{m}$ ) cylindrical micelles followed by employment of multiple transfer-printing cycles, and enables the fabrication of finely patterned 2D micelle network on a solid substrate. It can be applied to the fabrication of macroscopic patterning of self-assembled monolayer with nanometer resolution using these micelle networks as templates. Moreover, micelle superstructures are generated after thermal welding which involves the melting of PEO corona and softening of glassy PS core. Due to the flexibility of stamp fabrication, wetting step, and printing direction, the mesh size and shape of these 2D networks could be easily controlled. This approach opens a new way to prepare new functional superstructures by using the functionalized micelles. Their potential applications in filtration, sensing and nano-electronics can be envisaged.

### 3.4. Experimental section

#### 3.4.1. Preparation of Ultralong micelles

Amphiphilic block copolymer, polystyrene-*b*-polyethylene oxide (PS-*b*-PEO), with total molecular weight  $23.5\text{ kg mol}^{-1}$  ( $16.0\text{--}7.5\text{ kg mol}^{-1}$ , polydispersity index (PDI)=1.09) was purchased from Polymer Source, Inc. and used without any further purification. 1,1'-dioctadecyl-3,3,3',3'-tetramethylindocarbocyanine perchlorate (DiI) was purchased from Sigma-Aldrich and used as the fluorescent dye for copolymer micelles. The detailed preparation of cylindrical micelles by evaporation-induced self-assembly method have been reported elsewhere.[12] By using this method, we can obtain the ultralong cylindrical micelles as shown in Figure S2. The micelle solutions with a concentration of  $0.1\text{ mg/ml}$  were used throughout this study unless specifically noted.

#### 3.4.2. Fabrication of PDMS stamp

First, a silicon template was made by the deep reactive ion etching technique. For preparing poly(dimethyl siloxane) (PDMS) stamp, prepolymers and curing agent (Sylgard 184, Dow Corning Co. Ltd.) were mixed with a weight ratio of 10:1. The mixture was degassed under vacuum for 2h to eliminate the air bubbles inside and then poured onto the silicon wafer. Before baking at  $68^\circ\text{C}$  for 24h, the mixture with silicon wafer was degassed again for 0.5h to get rid of bubbles formed during pouring process. Then, the prepared PDMS stamp, which has a pattern of square pillars with sizes of  $3.5\times 3.5\times 3.0\mu\text{m}$  (length $\times$ width $\times$ height, i.e.  $l\times w\times h$ ) and  $2.0\mu\text{m}$  of gaps (See Figure S1) was peeled off from silicon wafer and immersed in a bath of ethanol for 16h to remove unreacted compound and dried in the air.



Size and spacing of micropillars may affect the formation of air cushions and liquid bridges between the pillars during the passage of the drop on pillar tops (dewetting) and consequent deposition of aligned micelles. The protocol was tuned by using various pillar sizes and shapes as depicted in Table S1. Basically, for a fixed concentration of 0.1 mg/ml micelle solution, simply inspection of micelle alignment, branching and coverage of the stamps of various sizes and shapes, indicated which ones were suited for this study.

Original choices for pillars sizes and shapes were, however, made with basis on previous studies that consider two competitive forces on the formation of liquid bridges between two adjacent pillars. [13] One is the capillary force,  $F_c$ , and the other one is the structural cohesive force,  $F_s$ , of non-Newtonian fluids. Following the previous study,[13] when the sizes of pillars and gaps are appropriate such that these two forces match each other, a good alignment of the micelles can be achieved during dewetting. Furthermore, squared pillars are shown to enhance or direct micelles stretching (Figure 2) as compared to circular ones (stamp 2).[14]

### **3.4.3. Alignment of ultralong micelles**

20 $\mu$ l of micelles solution was deposited on the edge area of the stamp pattern. And then, by using a lens tissue to drag the micelles solution, the wetting process can be controlled resulting in the well-aligned micelles array on top of micro-pillars. After alignment, the stamp is called “inked stamp” in this study. The mechanism of this alignment is similar to Lee’s study [15, 16], in which DNA nanowire array was patterned on micropillar-structured surface. Here, we need to notice that the concentration of micelles plays an important role in the formation of micelle array during alignment process. As shown in Figure S3, with reducing the concentration of cylindrical micelle solution, a decrease in the density of micelles aligned on PDMS stamp was observed.

### **3.4.4. Transfer printing of aligned micelles onto receiver substrate**

Following dewetting, visual inspection of the stamp was performed to ensure that no extra water droplet was present on the stamp and the micelles were then immediately transferred to glass without any further drying. The inked stamp was brought into contact with the receiving substrate, such as glass slide, and gently pressed to make sure that stamp was placed in conformal contact with the substrate. And then, the stamp was slowly peeled off to leave the micelle arrays on the receiver substrate. After printing the single layer of micelle arrays, the second layer of micelle arrays will be printed perpendicularly to the first one using the same protocol.

### 3.4.5. Characterization

The patterns of PDMS stamps were investigated by scanning electron microscopy (JEOL, 6010, Japan) at an accelerating voltage of 5.0kV.

Confocal fluorescence imaging was performed using a Laser scanning confocal microscopy (LSM 710, Carl Zeiss Microscopy GmbH, Germany) with a Fluar 40×/1.30 oil M27 objective lens. The dye, Dil, was excited using a HeNe laser operating at 543nm. In order to measure the lengths of these ultralong micelles, a dilute micelle solution (0.01mg/ml) was drop-casted onto a glass slide. After analysis of 500 micelles with software ImageJ, the distribution of micelle lengths can be obtained.

For the observation and analysis of the micelles' thermal fusion, atomic force microscopy (AFM) experiments were performed on an NT-MDT (NTEGRA) microscope with NT-MDT HA\_NA tips (resonance frequency around 240kHz). The accessory, heating stage, was used to control the sample temperature during measurements. After printing, samples were left to dry in the air for at least 24h up to few weeks before heating process. Similar results were found in all cases. All the images were recorded in tapping mode in the air at different temperatures. Before measurements, the samples were equilibrated for 0.5h at each temperature. To obtain the micelle structure by AFM, 50μl micelle solution was placed on a small piece of silicon wafer, which was treated by plasma for 140s, followed by spin coating at 2000rpm. Then, tapping mode was used to measure the micelles in the air.

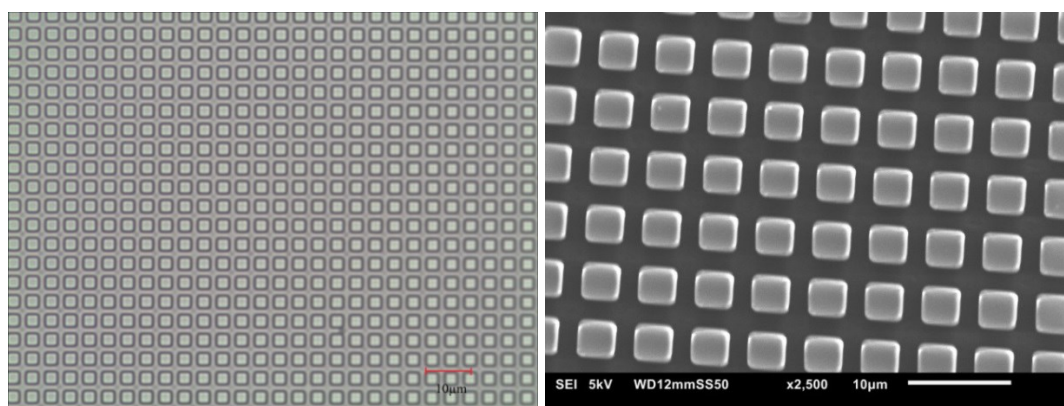
Differential scanning calorimetry (DSC) analysis of PS-b-PEO was conducted on a PerkinElmer Thermal Analysis instrument. PS-b-PEO copolymer (~11mg) was carefully loaded into a preweighted aluminum pan with cap. A heating rate of 10°C/min was used to obtain DSC thermograms with an empty pan as reference.

### 3.5. References

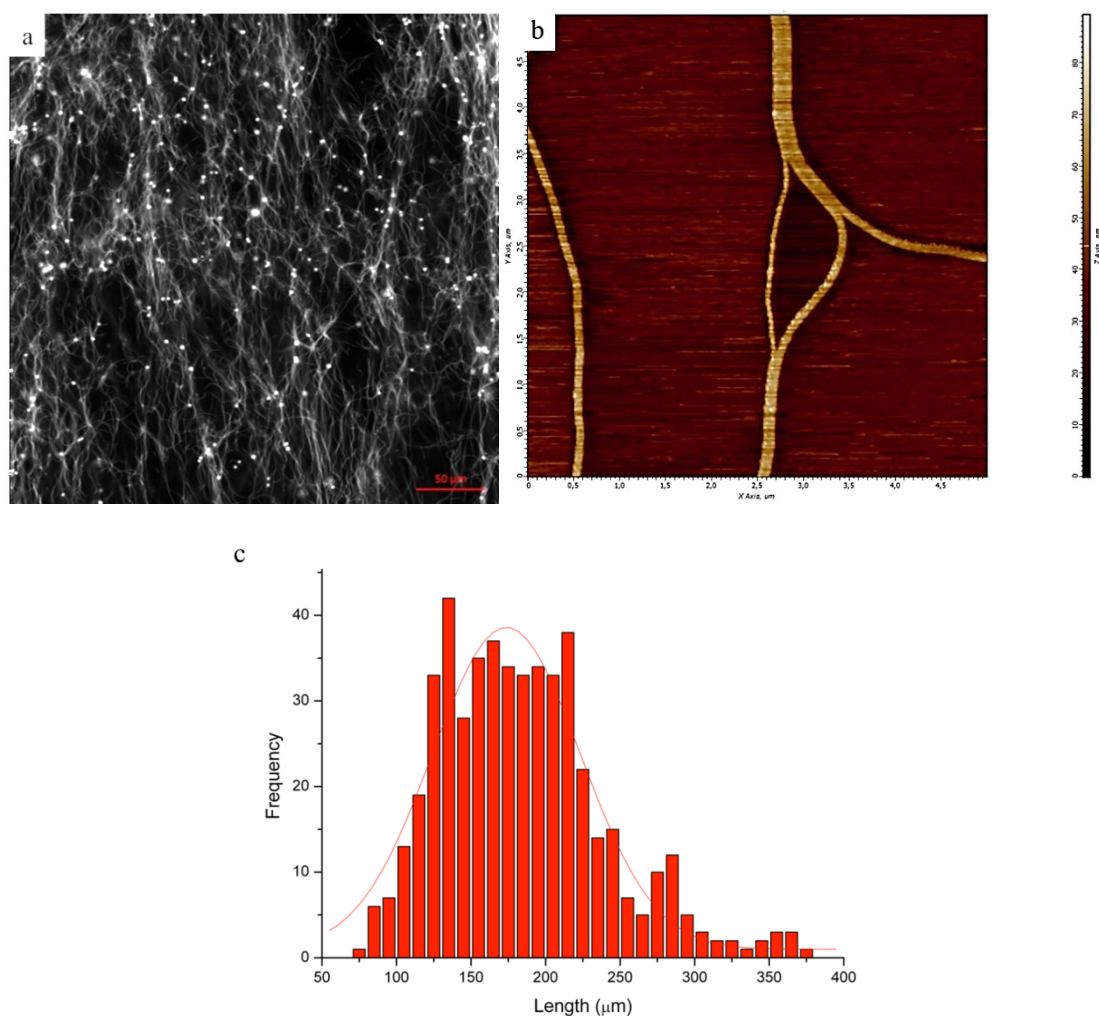
- [1] Cheng MJ, Wang Y, Yu LL, Su HJ, Han WD, Lin ZF, et al. Macroscopic Supramolecular Assembly to Fabricate 3D Ordered Structures: Towards Potential Tissue Scaffolds with Targeted Modification. *Advanced Functional Materials*. 2015;25:6851-7.
- [2] Gracias DH, Tien J, Breen TL, Hsu C, Whitesides GM. Forming electrical networks in three dimensions by self-assembly. *Science*. 2000;289:1170-2.
- [3] Mai YY, Eisenberg A. Self-assembly of block copolymers. *Chemical Society Reviews*. 2012;41:5969-85.
- [4] Wyman I, Njikang G, Liu GJ. When emulsification meets self-assembly: The role of emulsification in directing block copolymer assembly. *Prog Polym Sci*. 2011;36:1152-83.
- [5] Spatz JP, Herzog T, Mossmer S, Ziemann P, Moller M. Micellar inorganic-polymer hybrid systems - A tool for nanolithography. *Adv Mater*. 1999;11:149-53.

- [6] Lohmuller T, Aydin D, Schwieder M, Morhard C, Louban I, Pacholski C, et al. Nanopatterning by block copolymer micelle nanolithography and bioinspired applications. *Biointerphases*. 2011;6:Mr1-Mr12.
- [7] Glass R, Moller M, Spatz JP. Block copolymer micelle nanolithography. *Nanotechnology*. 2003;14:1153-60.
- [8] Glass R, Arnold M, Cavalcanti-Adam EA, Blummel J, Haferkemper C, Dodd C, et al. Block copolymer micelle nanolithography on non-conductive substrates. *New J Phys*. 2004;6.
- [9] Bennett RD, Hart AJ, Miller AC, Hammond PT, Irvine DJ, Cohen RE. Creating patterned carbon nanotube catalysts through the microcontact printing of block copolymer micellar thin films. *Langmuir*. 2006;22:8273-6.
- [10] Li XY, Gao Y, Boott CE, Winnik MA, Manners I. Non-covalent synthesis of supermicelles with complex architectures using spatially confined hydrogen-bonding interactions. *Nat Commun*. 2015;6:8127.
- [11] Li X, Gao Y, Boott CE, Hayward DW, Harniman R, Whittell GR, et al. "Cross" Supermicelles via the Hierarchical Assembly of Amphiphilic Cylindrical Triblock Comicelles. *J Am Chem Soc*. 2016;138:4087-95.
- [12] Jennings L. Kinetically Frozen Copolymer Nanocarriers: From non-equilibrium self-assembly into in vitro and in vivo evaluation [PhD thesis]. Strasbourg: University of Strasbourg; 2015.
- [13] Su B, Wang ST, Ma J, Wu YC, Chen X, Song YL, et al. Elaborate Positioning of Nanowire Arrays Contributed by Highly Adhesive Superhydrophobic Pillar-Structured Substrates. *Adv Mater*. 2012;24:559-64.
- [14] Guan JJ, Boukany PE, Hemminger O, Chiou NR, Zha WB, Cavanaugh M, et al. Large Laterally Ordered Nanochannel Arrays from DNA Combing and Imprinting. *Adv Mater*. 2010;22:3997-4001.
- [15] Liao WC, Hu X, Wang WX, Lee LJ. Simulation of single DNA molecule stretching and immobilization in a de-wetting two-phase flow over micropillar-patterned surface. *Biomicrofluidics*. 2013;7.
- [16] Guan JJ, Yu B, Lee LJ. Forming highly ordered arrays of functionalized polymer nanowires by dewetting on micropillars. *Advanced Materials*. 2007;19:1212-7.
- [17] Glazer PJ, Bergen L, Jennings L, Houtepen AJ, Mendes E, Boukany PE. Generating Aligned Micellar Nanowire Arrays by Dewetting of Micropatterned Surfaces. *Small*. 2014;10:1729-34.
- [18] Rogers JA, Lee HH. Patterning Based on Work of Adhesion. *Unconventional Nanopatterning Techniques and Applications: John Wiley & Sons, Inc.*; 2008. p. 67-94.
- [19] Gates BD, Xu Q, Stewart M, Ryan D, Willson CG, Whitesides GM. New approaches to nanofabrication: molding, printing, and other techniques. *Chem Rev*. 2005;105:1171-96.
- [20] Meitl MA, Zhu ZT, Kumar V, Lee KJ, Feng X, Huang YY, et al. Transfer printing by kinetic control of adhesion to an elastomeric stamp. *Nat Mater*. 2006;5:33-8.
- [21] Willet N, Gohy JF, Lei LC, Heinrich M, Auvray L, Varshney S, et al. Fast multiresponsive micellar gels from a smart ABC triblock copolymer. *Angew Chem Int Edit*. 2007;46:7988-92.

### 3.6. Appendix



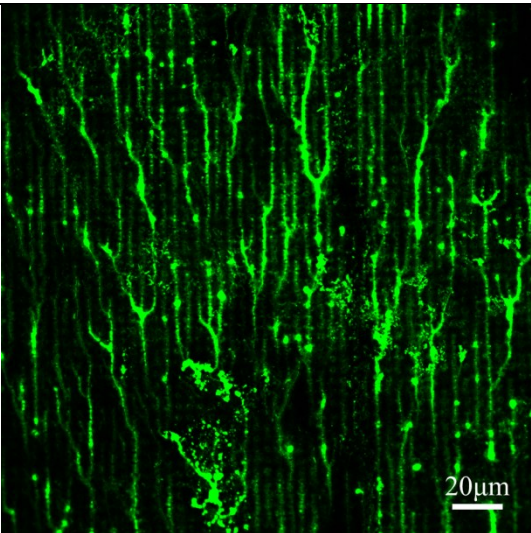
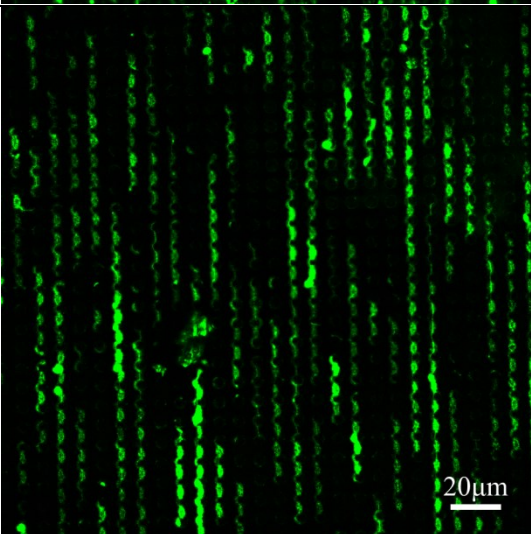
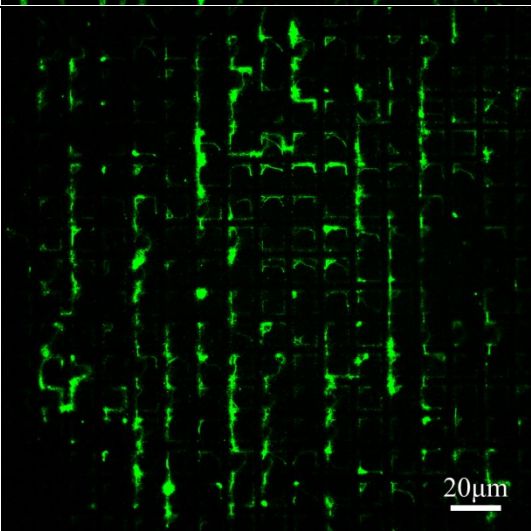
**Figure S1.** Optical microscopy image and SEM image of PDMS stamp ( $3.5 \times 3.5 \times 3.0 \mu\text{m}$ ,  $l \times w \times h$ ).



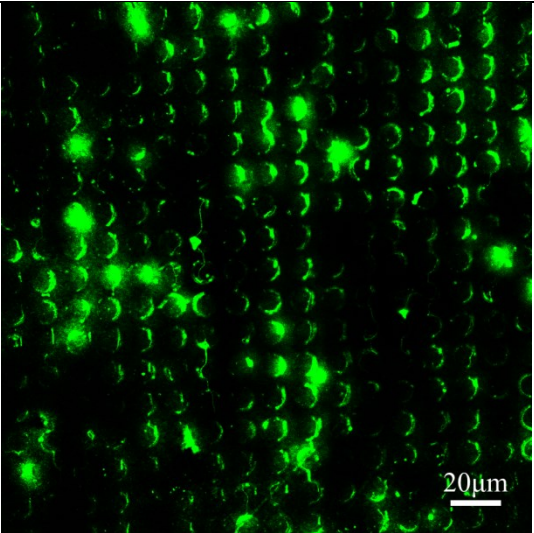
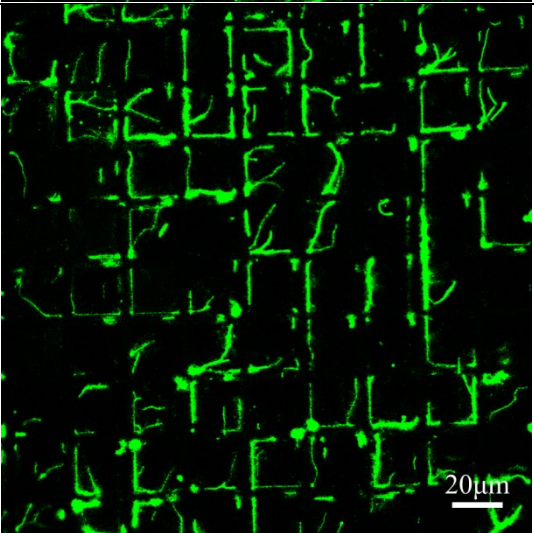
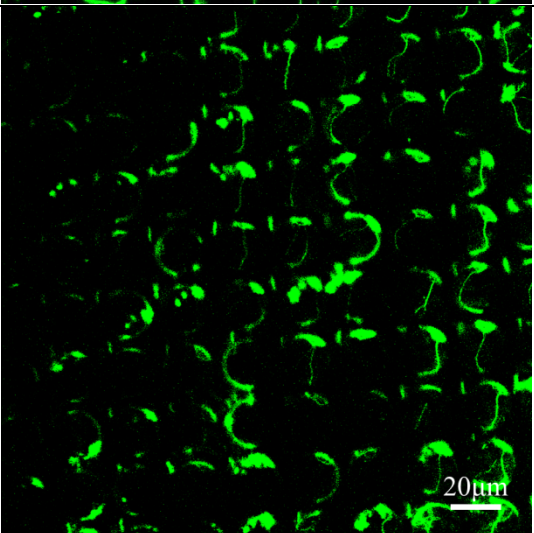
**Figure S2.** Morphology and length distribution of micelles from a solution of concentration of  $0.1 \text{ mg/mL}$  as used throughout this study (unless specifically noted). (a) Confocal microscopy image of cylindrical micelles in solution; (b) AFM image of cylindrical micelles spin-coated on silicon wafer; (c) Statistical histograms of micelle contour length. Note that some bundling /branching is observed in some cases.

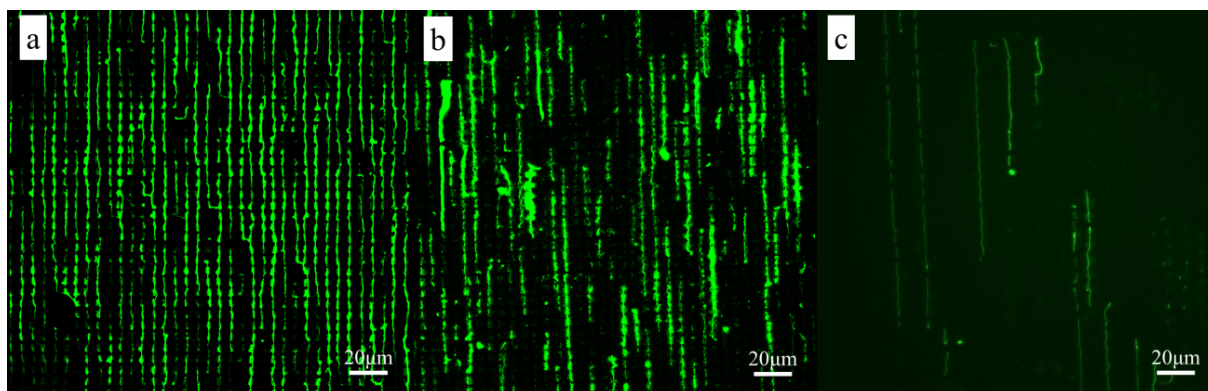
**Table S1.** list of PDMS stamps with other different shapes and sizes used for micelle alignment

Note: All the experiments were performed with 0.1mg/ml micelle solution

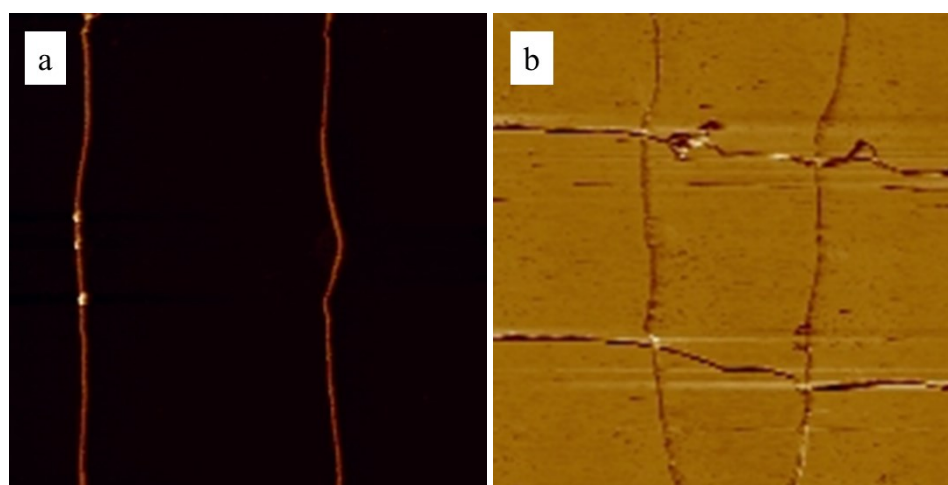
Stamp No.	Shape and sizes (l×w×h or d×h, gap, μm)	Confocal image of aligned micelles
1	Square, 1.5×1.5×3.0, 1.0	
2	Circle, 5.0×3.0, 3.0	
3	Square, 10.0×10.0×3.0, 3.0	



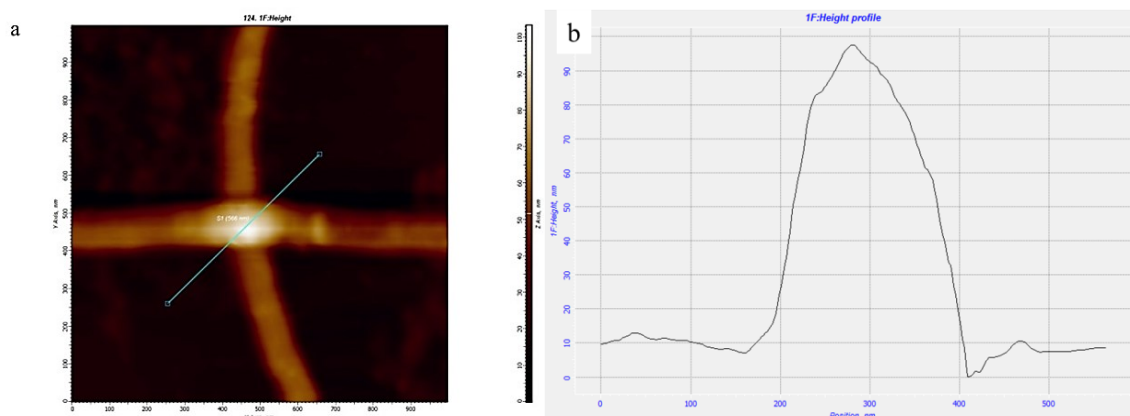
4	Circle, 10.0×3.0, 3.0	 A fluorescence microscopy image showing a grid of circular patterns. Each circle contains several bright, localized spots of light. A scale bar in the bottom right corner indicates 20μm.
5	Square, 20.0×20.0×3.0, 4.0	 A fluorescence microscopy image showing a grid of square patterns. The squares are formed by bright, interconnected lines. A scale bar in the bottom right corner indicates 20μm.
6	Circle, 20.0×3.0, 4.0	 A fluorescence microscopy image showing a grid of circular patterns. Each circle contains several bright, localized spots of light. A scale bar in the bottom right corner indicates 20μm.



**Figure S3.** The effect of micellar concentration on spacing of micelles. Confocal images of micelles aligned on PDMS stamp (l×w×h: 3.5×3.5×3.0μm, gap: 2.0μm). Concentrations used: (a) 0.1mg/ml; (b) 0.05mg/ml; (c) 0.01mg/ml.



**Figure S4.** AFM images of transfer printed (a) micelles and (b) micelle network on silicon wafer.



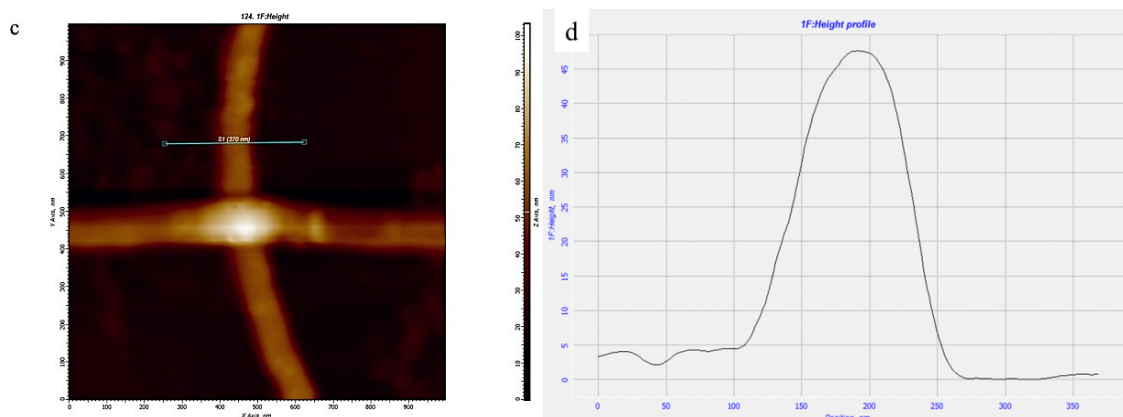


**Figure S5.** AFM images and corresponding height curves of (a, b) micelles junction measured at 25°C; (c, d) single micelle measure at 25°C.

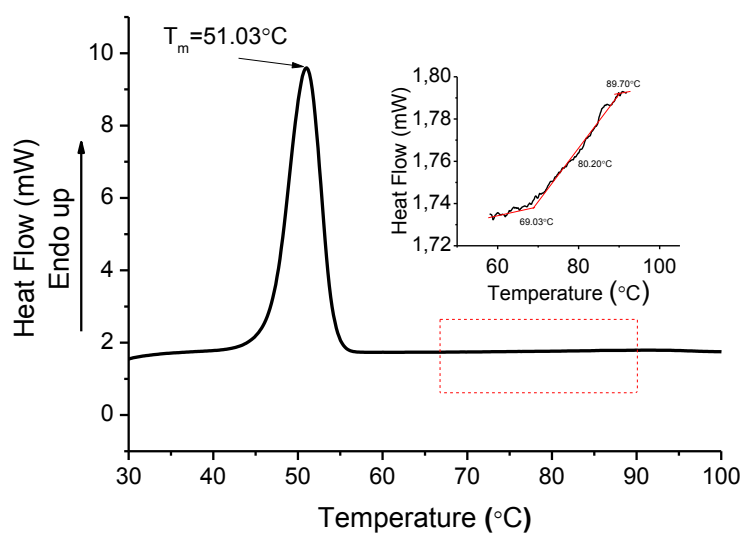


**Figure S6.** Differential scanning calorimetry thermograms of PS-b-PEO. The heating rate was 10.00°C/min. The inset is the amplification of the marked area in the main curve.



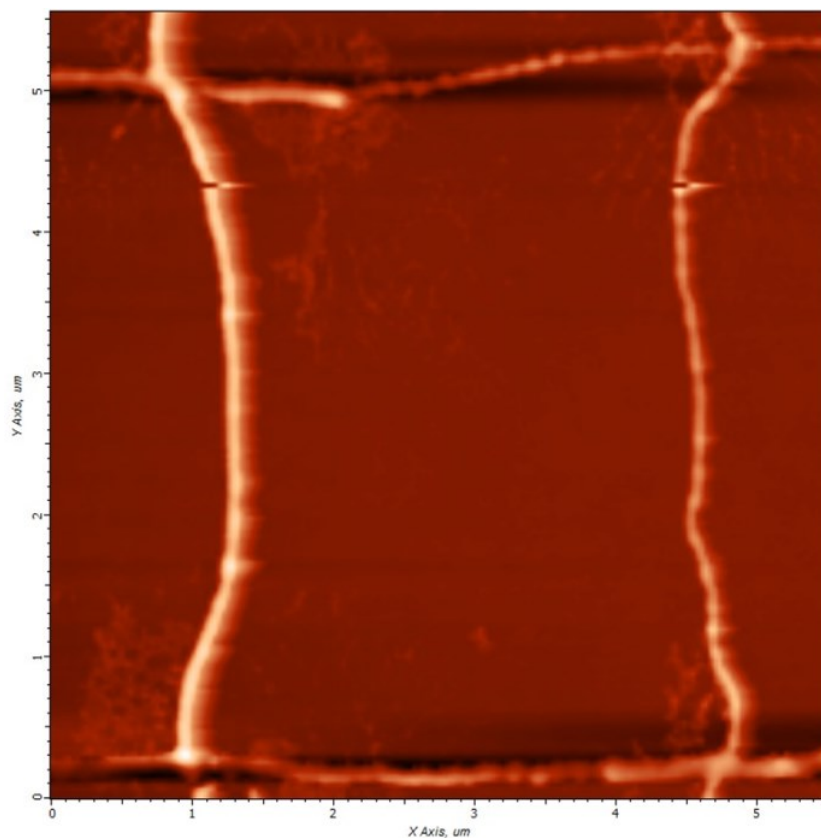


**Figure S7.** AFM image of 2D micelle network after thermal welding and cooling.

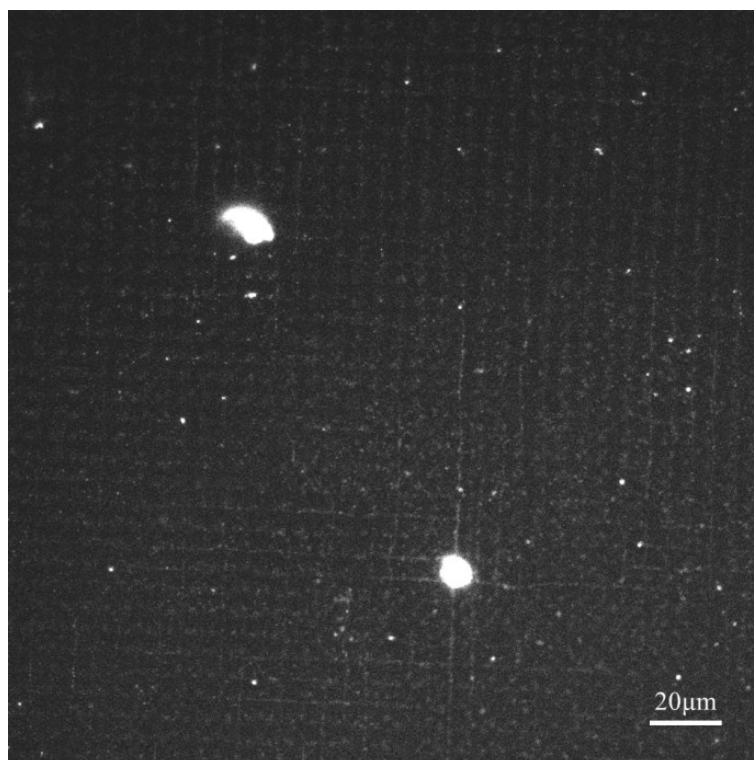


**Figure S8.** Confocal microscopy image of 2D micelle network after thermal welding and cooling illustrating that after heating process, the fluorescing dye partially leaked out from the micelles leading to a decrease of light intensity of the network.

## Interfacial work of adhesion

To estimate the possibility of transferring process, we briefly discussed the interfacial work of adhesion between micelles and stamp (also micelles and substrate) by using the following harmonic-mean equation[1].

$$W_{ij} = \frac{4\gamma_i^d \gamma_j^d}{\gamma_i^d + \gamma_j^d} + \frac{4\gamma_i^p \gamma_j^p}{\gamma_i^p + \gamma_j^p}$$

Where  $W_{ij}$  is the work of adhesion between two surfaces,  $i$  and  $j$ ,  $\gamma$  is the surface tension and the subscripts  $d$  and  $p$  represent the dispersion (nonpolar) and polar components, respectively. The surface free energy data of PDMS, PEO, silicon wafer (with an oxide layer), polytetrafluoroethylene (PTFE) and glass are obtained from literature and listed in Table S1.

Table S1: Surface free energy (mN/m) of PDMS, PEO, silicon wafer(with an oxide layer), polytetrafluoroethylene (PTFE) and glass

	$\gamma$	$\gamma^d$	$\gamma^p$
PDMS[2]	19.8	19.0	0.8
PEO[2]	42.9	30.9	12.0
PTFE[2]	20.0	18.4	1.6
Silicon[1]	46.7	22.1	24.6
Glass[3]	70.5	23.0	47.5

Then, we can calculate the work of adhesion between different materials surface.

$$W_{\text{PDMS-PEO}} = 50.1 \text{ mN/m}$$

$$W_{\text{PTFE-PEO}} = 51.8 \text{ mN/m}$$

$$W_{\text{Silicon-PEO}} = 83.8 \text{ mN/m}$$

$$W_{\text{Glass-PEO}} = 91.1 \text{ mN/m}$$

$$W_{\text{PEO-PEO}} = 85.8 \text{ mN/m}$$

It can be seen that the work of adhesion between PDMS and PEO is smaller than that at the silicon-PEO or glass-PEO interface, i.e.,  $W_{\text{PDMS-PEO}} < W_{\text{Silicon-PEO}}, W_{\text{PDMS-PEO}} < W_{\text{Glass-PEO}}$ . This suggests that PS-PEO micelles can be transferred from PDMS stamp to glass substrate and silicon wafer. Since the adhesion between PTFE and micelles is similar to that at PDMS-PEO interface, the transfer process from PMDS to PTFE is difficult to succeed.

## **References**

- [1] Rogers JA, Lee HH. Patterning Based on Work of Adhesion. Unconventional Nanopatterning Techniques and Applications: John Wiley & Sons, Inc.; 2008. p. 67-94.
- [2] Solid surface energy data (SFE) for common polymers. 2007.
- [3] Rowe RC. Surface Free-Energy and Polarity Effects in the Granulation of a Model System. Int J Pharmaceut. 1989;53:75-8.

# **Patterned nano-fibrous micelles of block copolymers for controlled cell alignment**

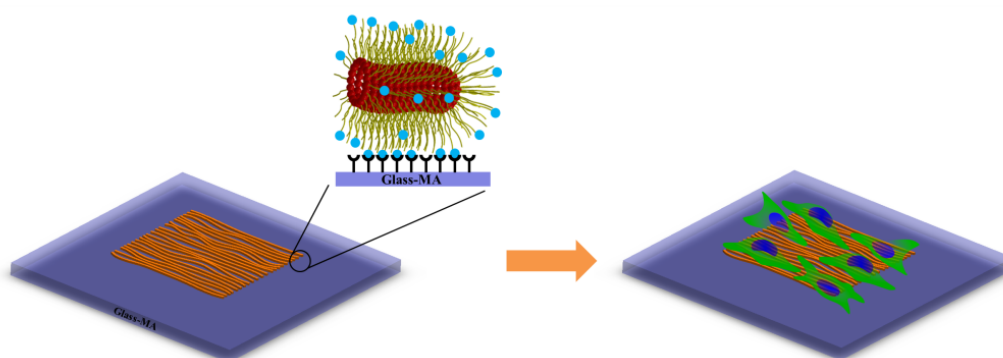
# 4

The content of this chapter is based on:

K. Zhang, A. Arranja, H. Chen, S. Mytnyk, Y. Wang, S. Oldenhof, J.H. van Esch and E. Mendes, *Under review*.

## Abstract

The last decade has witnessed a great progress in understanding and manipulating self-assembly of block copolymers in solution. A wide variety of micellar structures can be created and many promising applications in bioscience have been reported. In particular, nano-fibrous micelles provide a great platform to mimic the filamentous structure of native extracellular matrix (ECM). However, the evaluation of this kind of filomicellar systems with potential use in tissue engineering is virtually unexplored. The question behind it, such as if the block copolymer nano-fibrous micelles can regulate cellular response, still lingers for many years because of the difficulties in preparation and 3D manipulation of these tiny objects. Here, by using a combination approach of self-assembly of block copolymers and soft lithography, we establish a novel and unique nano-fibrous 2D platform of organized micelles and demonstrate that patterned micelles enable control over the cellular alignment behaviour. The area density and orientation of fibrous micelles determine the alignment degree and directionality of cells, respectively. Furthermore, when cells were cultured on multi-directionally aligned micelles, competitive response was observed. Due to the virtually infinite possibilities of functionalization of micelle corona, our work opens a new route to further mimic the native fibrous networks with artificial micelles containing various functionalities.



## 4.1. Introduction

Tissue engineering has attracted growing attention to create living constructs that closely resemble native tissues in order to rescue patients from organ failure or tissue malfunction[1]. As a crucial element in tissue engineering, the extracellular matrix (ECM) in which cells reside provides a variety of essential biophysical and biochemical milieu for cell growth, proliferation, migration and function[2-4]. Therefore, developing a tailored artificial scaffold to mimic the native ECM that consists of complex and organized nano-/micro-fibrous structures is highly desirable.

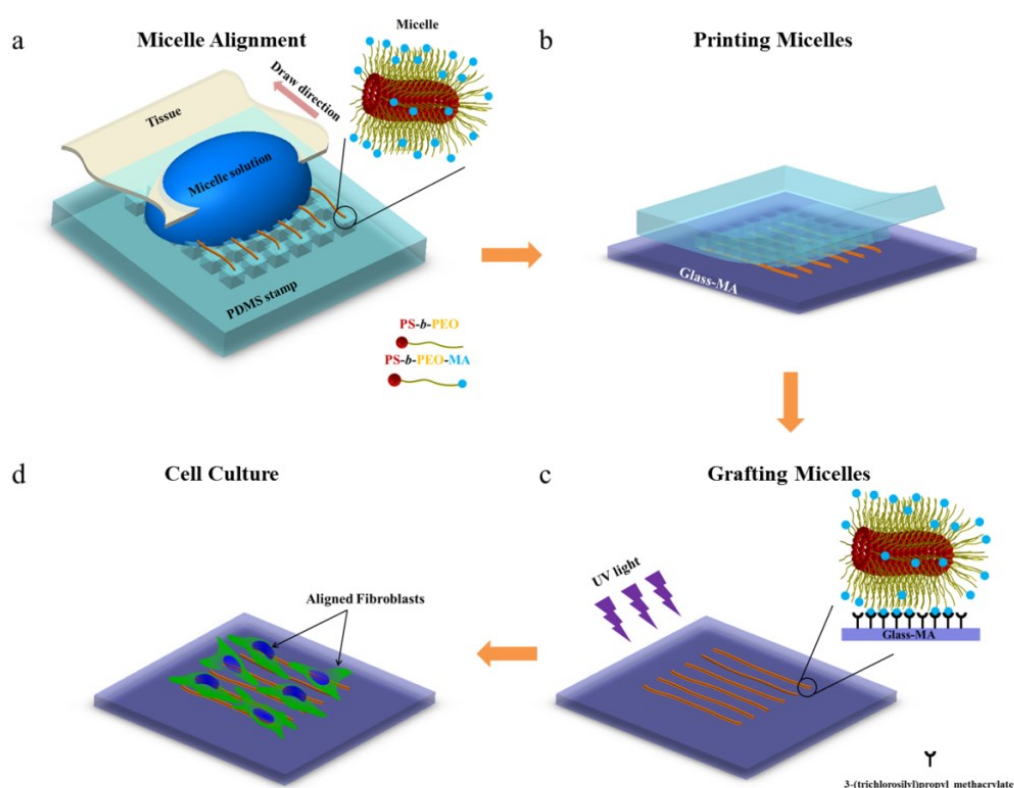
To address this challenge, a wide variety of materials and technologies has been developed[5, 6]. For example, electrospinning is usually used to create fibrous meshes and even 3D scaffolds with controlled orientation and mechanical properties[7, 8], while phase separation methods are applied for fabricating porous scaffolds with minimal setup requirements and easy control of scaffold porosity[9-11]. More recently, inspired by an ubiquitous process in nature, self-assembly strategy has become increasingly important not only in biological but also in synthetic systems[12]. It provides a facile route to construct complex and hierarchical structures, such as triple-helix morphology of collagen[13]. Based on this principle, many synthetic materials with self-assembly properties have been developed[14]. Amphiphilic block copolymers that consist of two or more chemically distinct polymers is one important sort of these materials. Due to the micro-phase separation between different blocks, block copolymers can self-assemble into various micellar structures in solution, offering many potential applications in bioscience fields[15, 16]. Especially, nano-fibrous micelles provide a great platform to mimic the filamentous structure of native ECM.

However, to our best knowledge, no study has been reported to use this kind of block copolymer assemblies to mimic the ECM due to the challenges in relation to preparation of long enough (hundreds of microns) semi-flexible filomicelles as well as limitations to their physical manipulation. In this work, we give a step in this direction by producing a flat surface as a unique nano-fibrous platform with quenched, ordered, ultra-long block copolymer micelles. Using this platform, we investigate the effects of patterned block copolymer micelles on the alignment behaviour of cells. We find that by adjusting the area density and orientation of micelles, one can control the extent of cellular alignment and orientation degree, respectively. Moreover, competitive guidance was also observed when cells were cultured on substrates with micelles aligned in two or more directions simultaneously. This study demonstrates the ability of block copolymer fibrous micelles to topologically regulate cellular alignment and it also opens the door to the possible use of ultra-long block copolymer filomicelles in tissue engineering.

## 4.2. Results and Discussion

### 4.2.1. Fabrication of micellar platform

To investigate whether the block copolymer fibrous micelles are capable of regulating cellular response, a key challenge is the directional manipulation of nano-fibril micelles of block copolymers. Here, we combined the quenched, out-of-equilibrium assembly of block copolymers and soft lithography approaches to fabricate a patterned micellar structures for this study. A schematic illustration of the manufacturing process of micellar platform for cell alignment is depicted in Scheme 1. First, cross-linkable PS-*b*-PEO micelles were prepared by evaporation-induced self-assembly method and aligned on micro-pillars of PDMS stamps using our former reported dewetting approach[18, 19] (Scheme 1a). Next, due to the specific viscoelastic behaviour of PDMS, the aligned micelles can be successfully transfer-printed to the acrylated glass coverslides (Scheme 1b). Repeating the first two steps offered an easy way to control the area densities of aligned micelles on the glass surface. To immobilize the patterned micelles, the glass slide with aligned micelles was irradiated under UV light for 20 minutes to bond the micelles on the glass surface (Scheme 1c), followed by water rinsing to remove the residual photo initiator. The final new nanofibrous platform was formed and used for further cell culture experiments (Scheme 1d).



**Scheme 1.** Schematic representation of the micro-contact printing ( $\mu$ CP) technique used to fabricate a fibrous micelle array on a glass substrate with controlled area fraction of micelles: (a) alignment of

functionalized PS-b-PEO micelles on a PDMS stamp; (b) transfer printing of micelles onto the methacrylate groups modified glass slide; (c) UV irradiation of aligned micelles to bond them onto the glass surface, and (d) cellular alignment induced by the aligned micelles.

As shown in Figure 4.1, the density of micelles printed on glass surface increased with increasing number of micelles printing times. The individual aligned micelles were distinguishable in the case of low printing times (Figure 4.1a, 4.1b), while it became much harder to image the samples with ten and twenty printing times (Figure 4.1c, 4.1d). In order to analyze the alignment of micelles after multiple printings, Fast Fourier Transform (FFT) of the confocal images were taken. As shown in the inserted FFT images of Figure 4.1a-4.1d, all of them have the ellipsoidal shape, which indicates a clear directionality of printed micelles. This suggests that the amount of printing times has no detectable influence on the alignment of micelles.

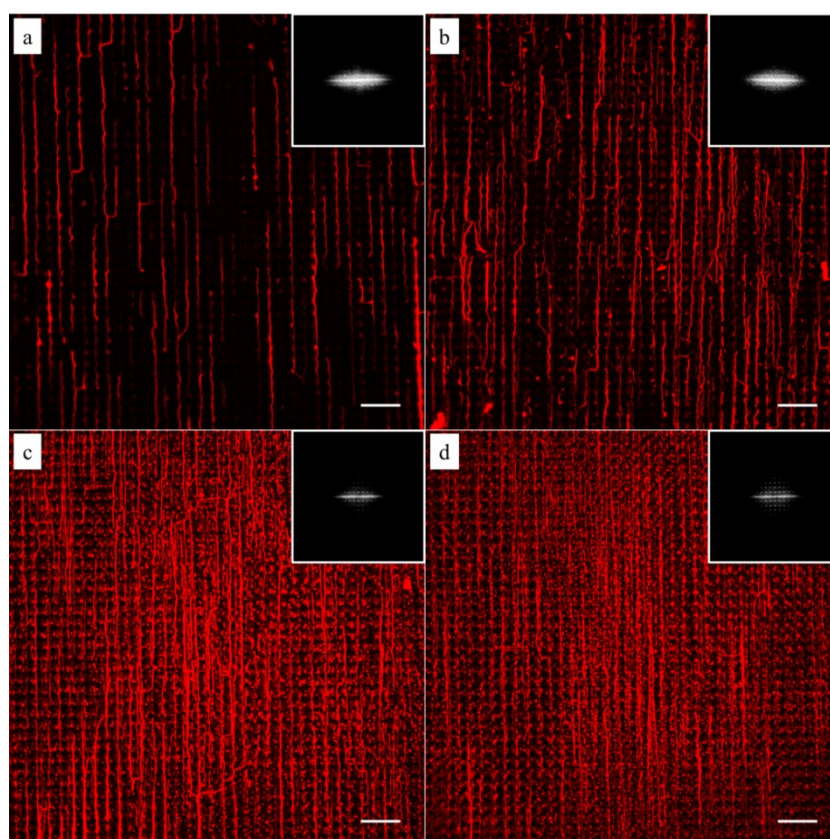


**Figure 4.1.** Confocal microscopy images of the immobilized micelles after multiple printing: (a) 1, (b) 5, (c) 10 and (d) 20 times. The inserts are the corresponding FFT output images. Scale bars are 20  $\mu\text{m}$ .

To gain a deeper insight in the dependence of micelle density on printing times, AFM measurements were performed on the glass surfaces grafted with micelles. As can be seen in Figure 4.2, by increasing the number of printing steps, we could graft more micelles on the glass surface, i.e. achieve higher surface coverage of micelles. The height of a single micelle is around 50 nm (Figure S2), which agrees well with our previous study[27] and is above the



threshold size (35 nm) for contact guidance of fibroblast alignment[28]. Figure 4.2e illustrates the relationship between printing times and covering area percentage of micelles. The area percentage of micelle coverage raised from around 4.4% to 31.4% as the printing times increased from 1 time to 20 times. A linear relationship was observed, showing that the micelle density on substrate is fully controllable.

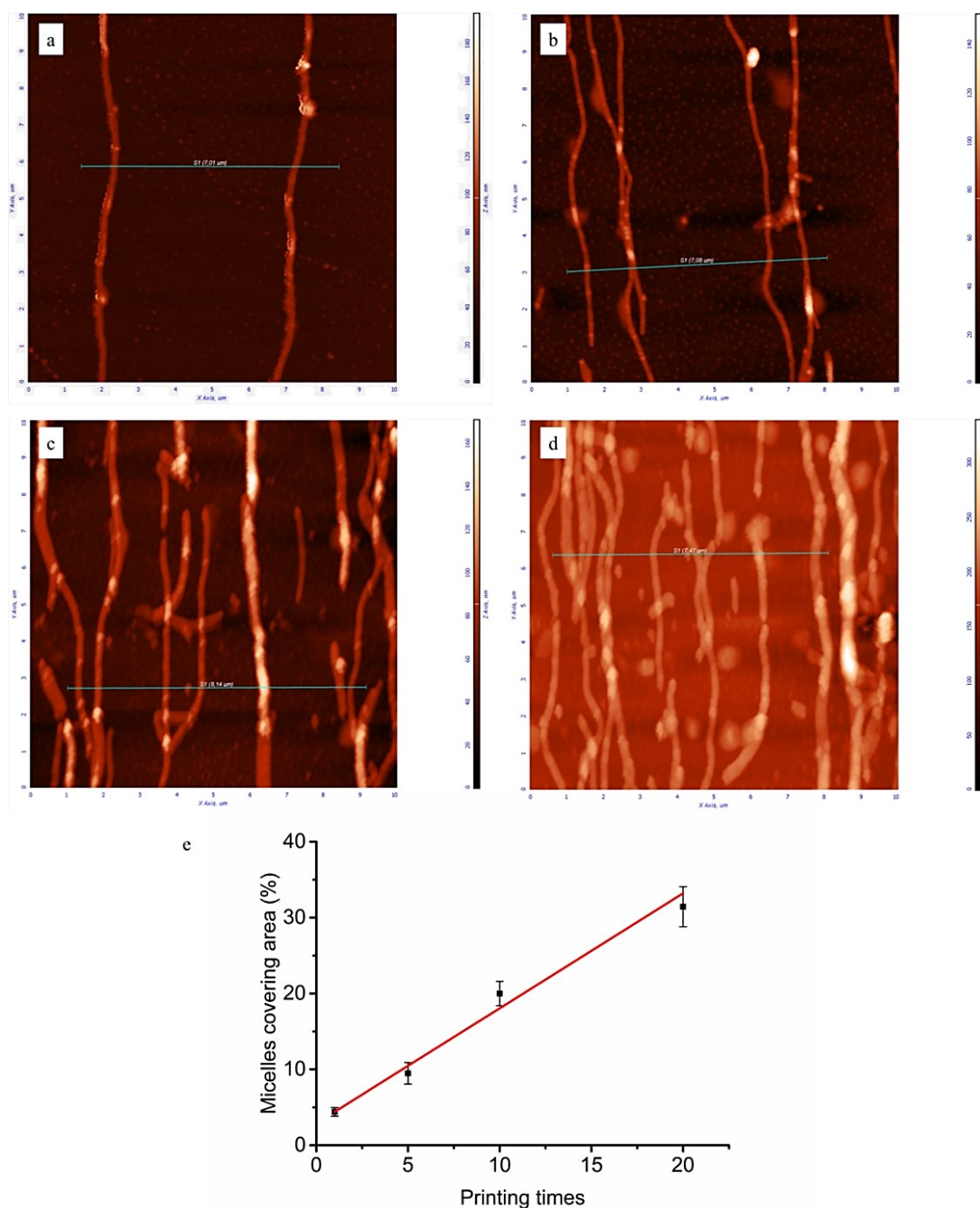


**Figure 4.2.** Representative AFM images (10×10 μm) of micelles printed and cross-linked on the glass surface: (a) 1, (b) 5, (c) 10, (d) 20 printing times. Line scan profiles corresponding to green lines in AFM images were shown in Figure S2 of SI. (e) Area percentages covered by aligned micelles as a function of printing times.

### 4.2.2. Unidirectional micelles

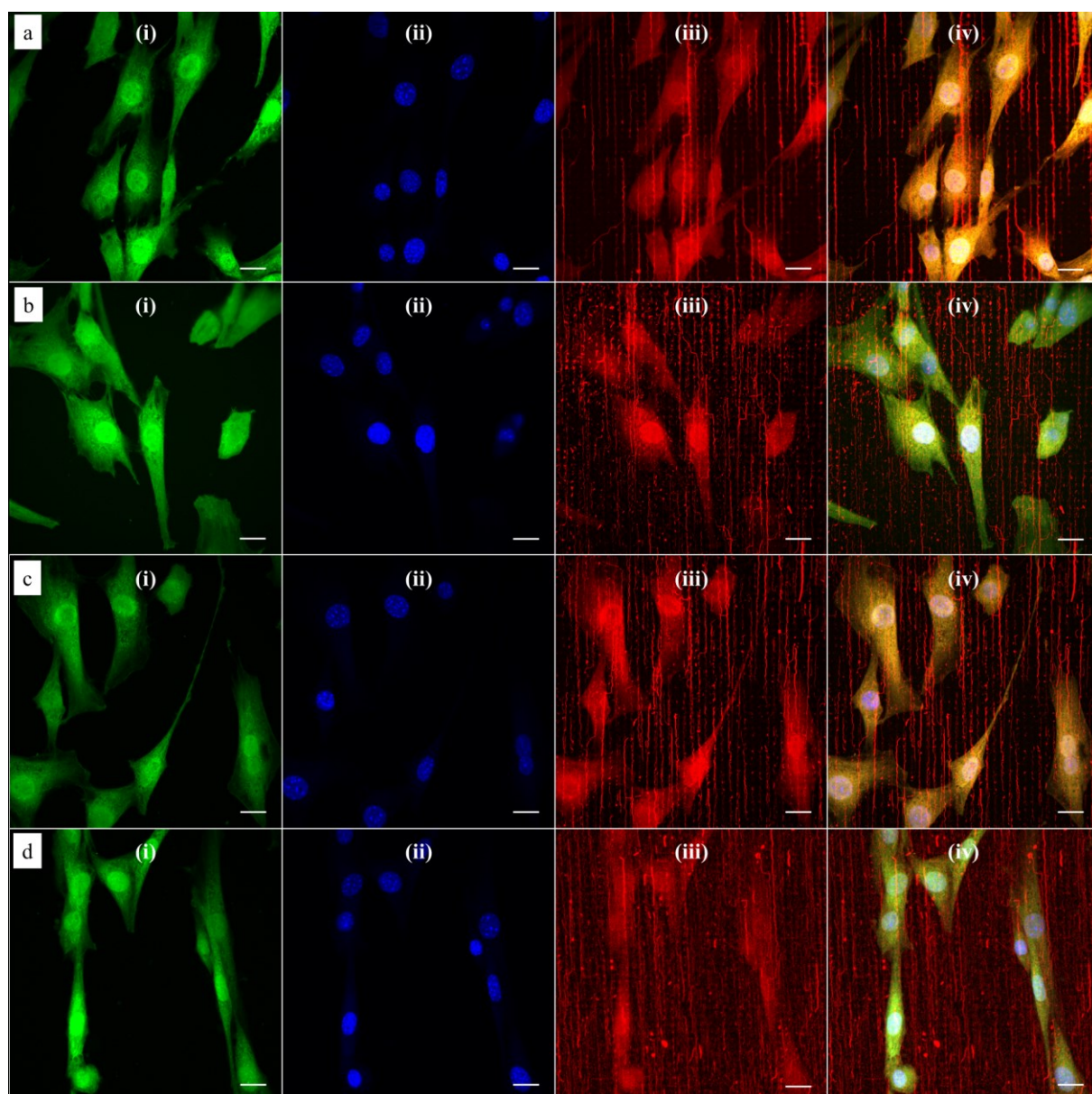


**Figure 4.3.** Confocal microscopy images of NIH/3T3 fibroblasts cultured on aligned and immobilized micelles after multiple printings: (a) 1; (b) 5; (c) 10 and (d) 20 printing times. Cells were labeled with the (i) CellTracker green probe (green channel) and the nucleus stained with (ii) DAPI (blue channel). Polymeric micelles were loaded with the (iii) hydrophobic dye DiI and imaged in the red channel. Simultaneous imaging of cells and polymeric micelles was performed by (iv) merging the three channels. Scale bar corresponds to 20  $\mu\text{m}$ .

Based on this strategy, we can control the density of micelles in the fibrous platform and study the fundamental understanding of topographic control of cell behaviour. After preparation of the nanofibrous platforms with different degrees of micelles densities, NIH/3T3 fibroblasts were seeded on the substrates and their response was analyzed after 24 hours (Figure 4.3). We observed that fibroblasts were able to grow on the surface with PS-b-

PEO micelles despite the fouling-resistant properties of PEG[29-32]. This can be attributed to the presence of methacrylate modified PEO terminal groups in the polymeric fibrous micelles, which may provide the cellular adhesion sites on the biologically inert PEG surface. Moreover, as shown in Figure 4.3, the cells seeded on the aligned micelles showed alignment tendency, while cells cultured on flat glass surface without micelles were randomly oriented (Figure 4.4). In the platform with the highest density of micelles, corresponding to 20 printing times and an coverage are of 31.4% (Figure 4.3d), we observed the highest tendency for cell alignment along the micelle direction and cells also acquired a stretched spindle shape (Figure 4.3d). In the substrate with the lower micelle density (1 printing time and 4.4% of coverage area), cells were preferentially oriented along the micelles directions but their morphology was less stretched (Figure 4.3a). This characteristic morphological change of cells on these modified substrates strongly suggests that densely aligned copolymer micelles have the ability to guide cell alignment, in consistent with that observed in the aligned electrospun fibers[24].

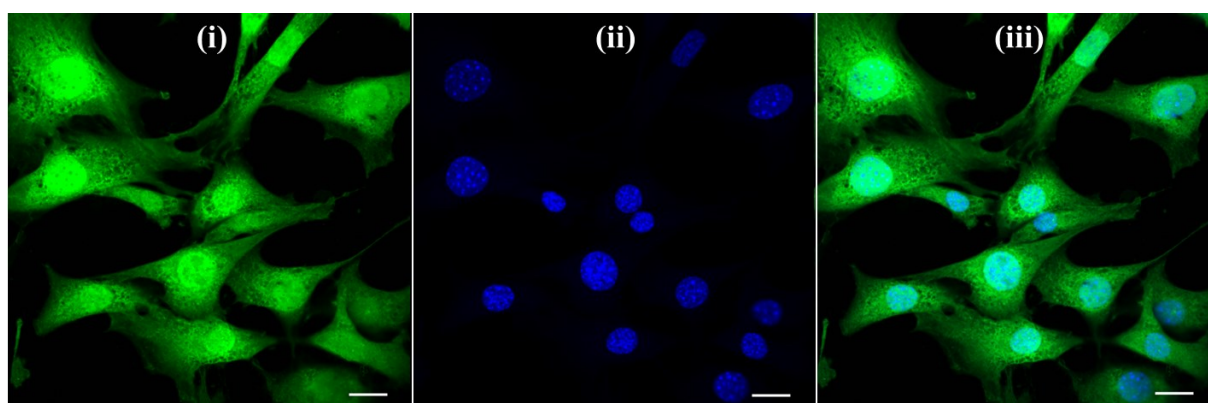


**Figure 4.4.** Confocal microscopy images of NIH/3T3 fibroblasts cultured on glass slide grafted with MA groups and used as control group. (i) CellTracker green probe (green channel), (ii) nuclear DAPI staining (blue channel), and (iii) merged the former two channels. Scale bar corresponds to 20  $\mu\text{m}$ .

To quantitatively analyze cellular behaviour on the substrates with different densities of micelles, the aspect ratio, i.e. ratio between long axis and short axis of ellipse, and orientation angle  $\theta$  of fibroblasts were measured using ellipse fitting method (Figure 4.5a). In the presence of aligned micelles, the aspect ratio (i.e. elongation) of the cells was not considerably different from the control group (Figure 4.5b). In contrast to our results, fibroblasts cultured on aligned electro-spun nanofibers were usually shown to elongate along the fiber direction[33]. Compared to that work, the density of nanofibrillar micelles used in this research is much lower. This suggests that elongation of fibroblasts may need a higher density of fibers. However, regarding the orientation degree of fibroblasts, we observed that increasing the density of aligned micelles dramatically increases the degree of cell alignment (Figure 4.5c). To compare the orientation degrees of cells cultured on



substrates with different micelle densities, we used the Gaussian curve to fit each histogram (blue curves) and calculate their full width at half maximum (FWHM). The degree of cell alignment is reflected by the height (apex) and shape (FWHM) of the peaks. As the covering area percentage of the micelles increased, the heights of the peaks increased as well while the shape became sharper, i.e., the FWHM decreased (Figure 4.6). It indicates that cells cultured on a platform with higher density of micelles show better orientation profile than the one with lower density of micelles, in agreement with our former observation (Figure 4.3 and Figure 4.4).

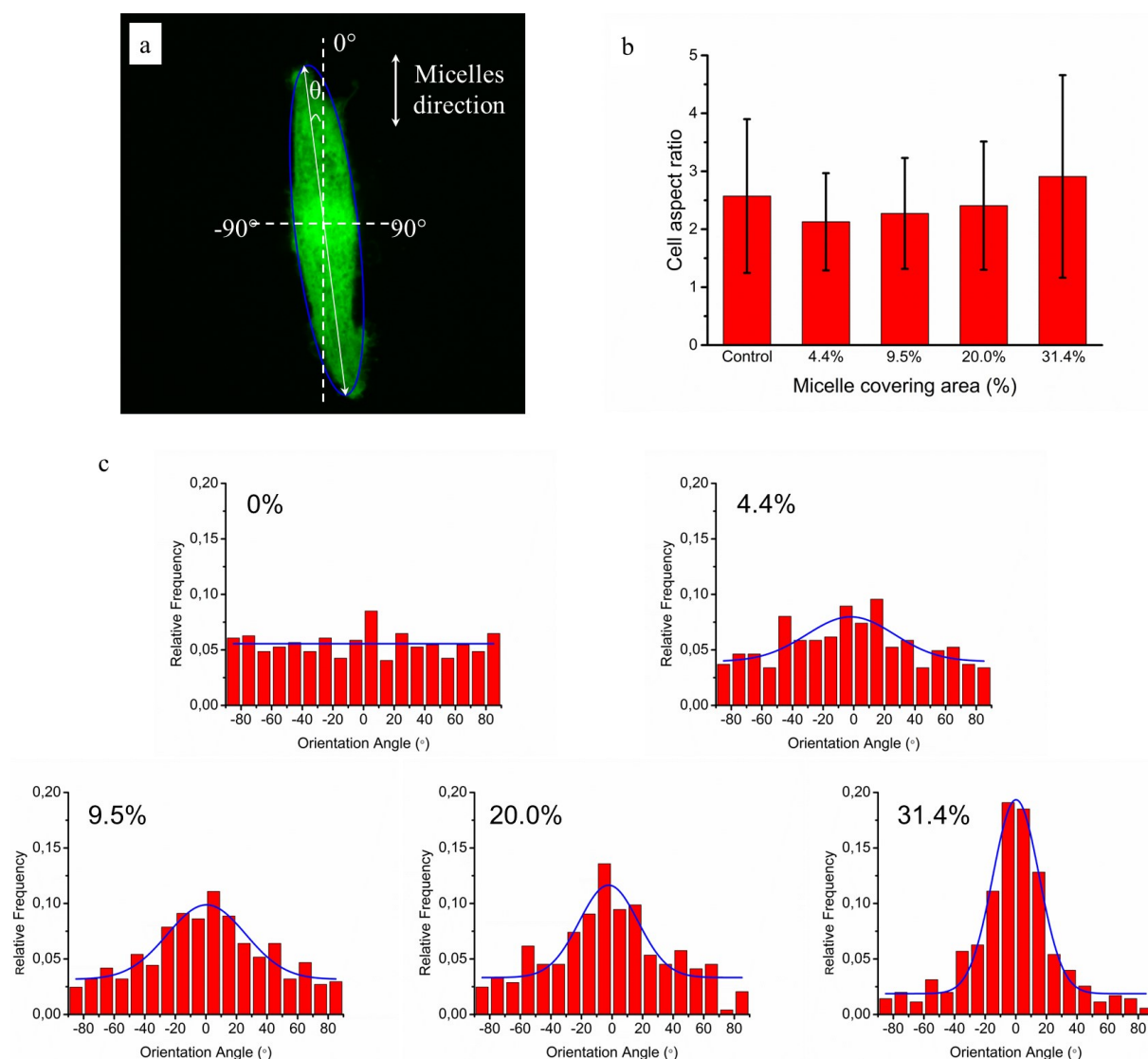


**Figure 4.5.** NIH/3T3 cellular elongation and orientation on the aligned micelles. (a) Representative confocal image of cell and fitting ellipse used to measure elongation (ratio of major axis/minor axis) and orientation (angle  $\theta$ ). (b) Cellular aspect ratio as a function of micelle covering percentage. (c) Distribution of NIH/3T3 cells orientation angle ( $\theta$ ) on glass substrates with various area percentages of micelle coverages: 0%, 4.4%, 9.5%, 20.0% and 31.4%. The blue lines are the corresponding Gaussian fitting curves.

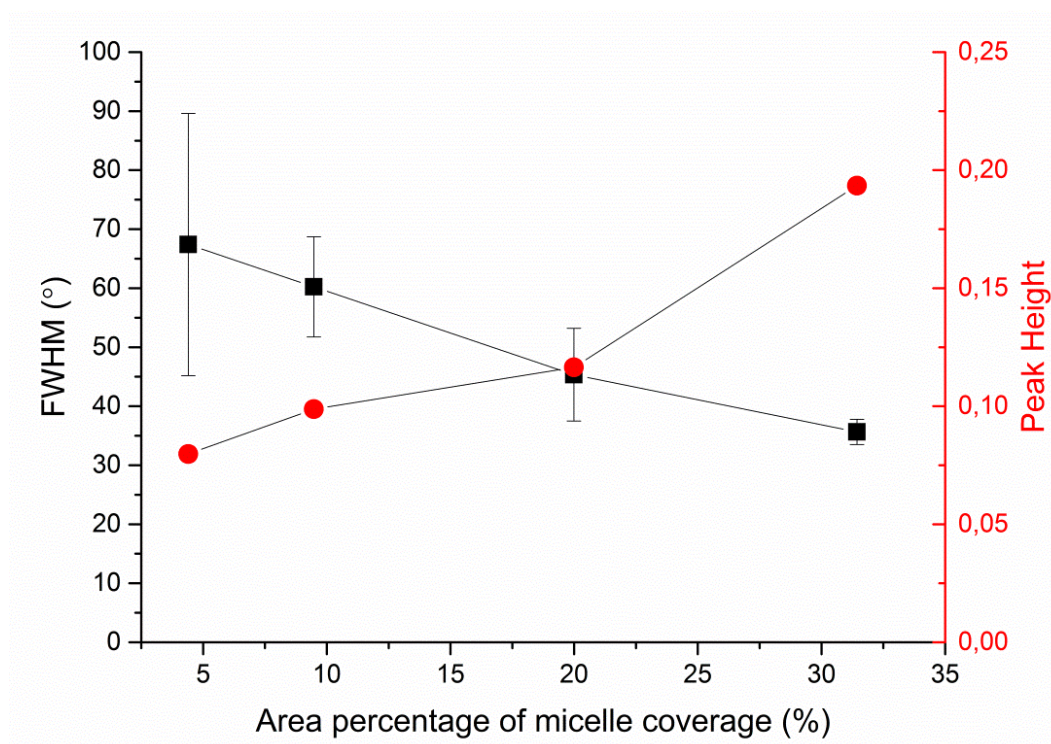


**Figure 4.6.** Relationship between area percentage of micelle coverage and characteristic parameters (full width at half maximum (FWHM) and peak height in Gaussian fitting curves) of cellular alignment.

Since cellular alignment and cell differentiation have been demonstrated to correlate with nuclear elongation[34, 35], herein we also investigated the nuclear aspect ratio dependence on the covering area percentage of aligned micelles using ellipse fitting method (Figure 4.7a). Similar to cellular elongation, no significant nuclear stretching was observed (Figure 4.7b). Nevertheless, as the nuclear aspect ratios are around 1.3 in the control group, indicating non-spherical nuclei, the nuclear orientation was still measured to quantitatively evaluate the effect of aligned micelles on the nuclear alignment. As shown in Figure 4.7c, the nuclear orientation increased with increasing micelle densities on the glass surface as previously observed in the cellular orientation. In contrast to cellular orientation, poor Gaussian fittings were observed here for platforms with a low micelle densities (curves not shown), limiting the use of the FWHM and apex of the peak to quantitatively reflect the relationship between the extent of nuclei orientation and micelle density.

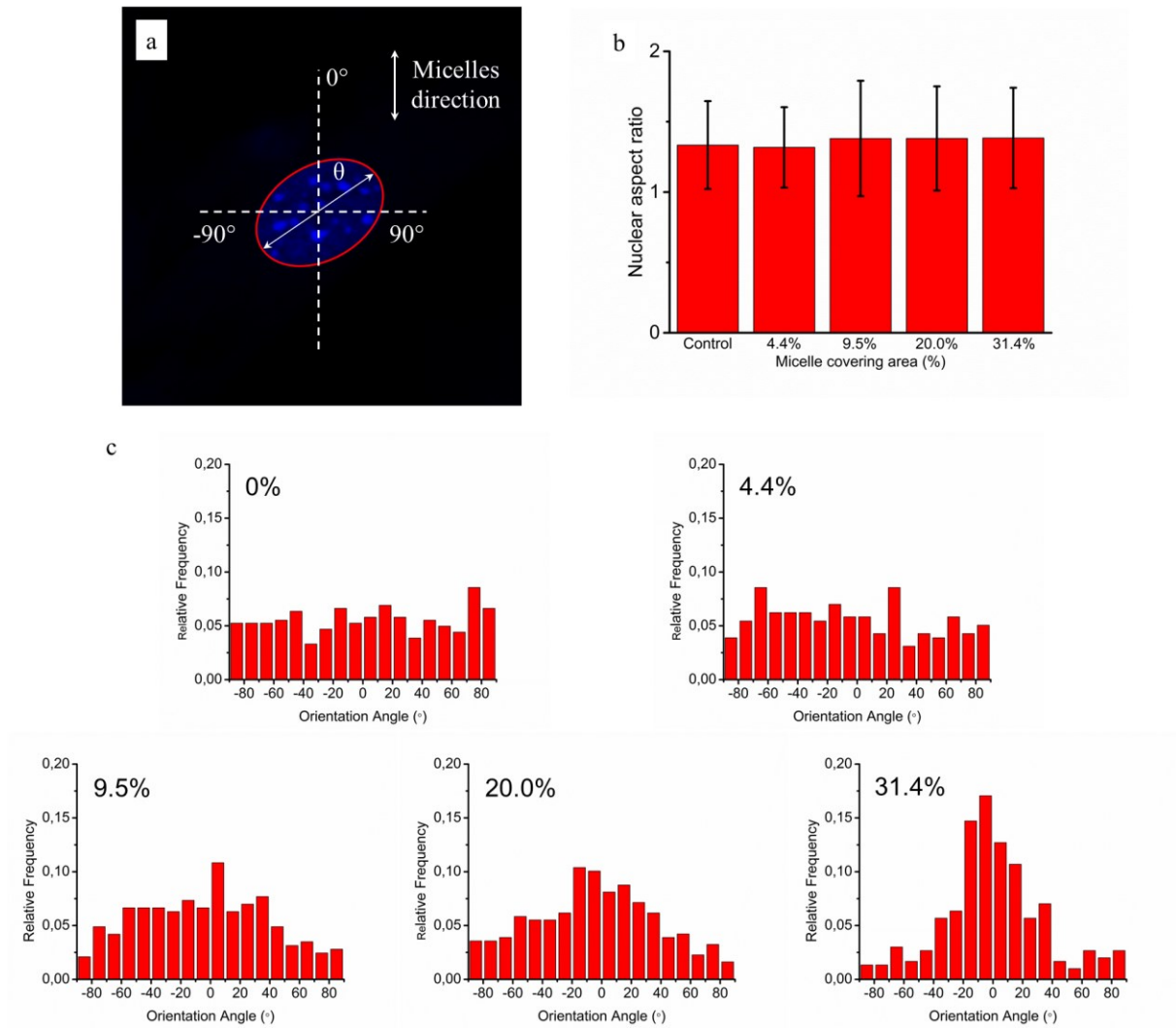


**Figure 4.7.** NIH/3T3 nuclear elongation and orientation on the aligned micelles. (a) Representative confocal image of nucleus and fitting ellipse used to measure elongation (ratio of long axis/short axis) and orientation (angle  $\theta$ ). (b) Nuclear aspect ratio as a function of micelle covering percentage. (c) Distribution of NIH/3T3 nuclei orientation on glass substrates with various area percentages of micelle coverages: 0%, 4.4%, 9.5%, 20.0% and 31.4%.

Based on the above results, we can conclude that coverage area percentage of micelles equal or below 31.4% have no significant effects on cellular and nuclear elongation. On the other hand, the orientation degrees of cells and nuclei increase proportionally to the coverage area of micelles, being maximal at the highest density of micelle coverage (31.4%). This may give a hint that, similarly to orientation, different fiber densities are required for cellular and nuclear stretching.

#### 4.2.3. Multidirectional micelles

Since the natural extracellular matrix (ECM) is not just one-dimensional topographic pattern, a simple method to fabricate a platform with more complex topographic features is a critical

component in tissue engineering. Our method combining self-assembly with soft lithography can provide a solution to build a synthetic platform with multi-direction cues by simply printing micelles in different directions. Based on this concept, we investigated cellular responses to orthogonally and tri-directionally aligned micelles. To ensure that the micelles in each direction have the same possibility to stimulate cells, we printed micelles alternately in different directions at the same density (5 printing times for each direction). Then, NIH/3T3 fibroblasts were cultured on these multi-direction cues for 24 hours. The morphology of cells on multiple aligned micelles is shown in Figure 4.8. In the case of orthogonal cues, cells appeared to align in two preferential directions, the same as those of the micelles (Figure 4.8a), indicating that micellar contact guidance in these two directions has the same impact. However, when a third direction with further micelle printing was introduced, cellular response became more complex (Figure 4.8b), and it is no longer possible to distinguish the three directional alignments.

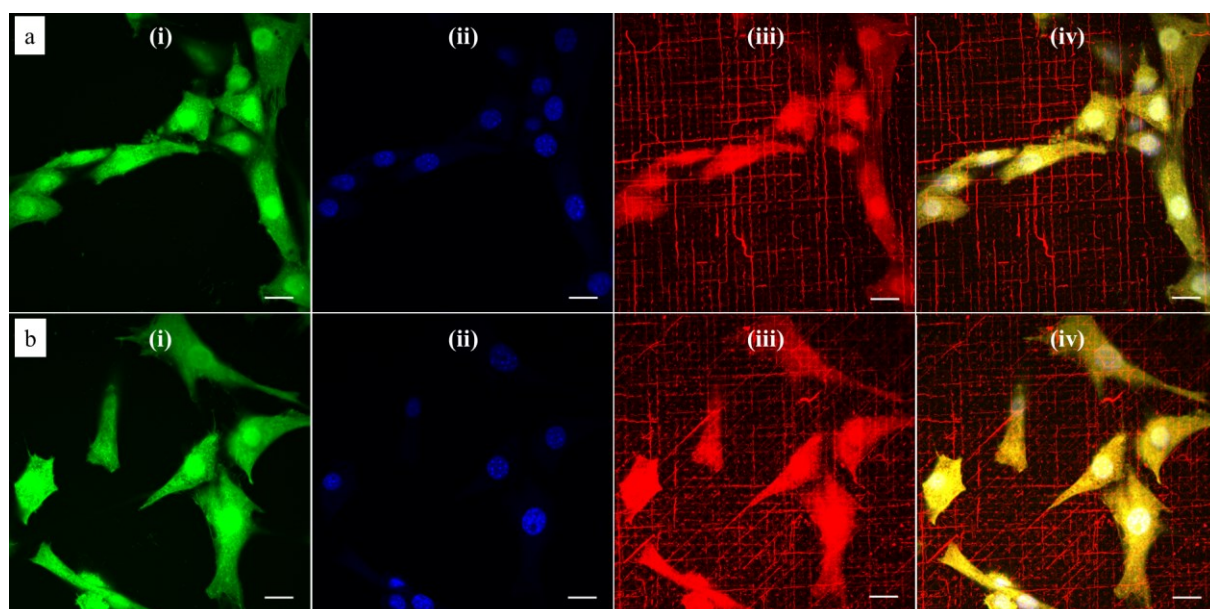


**Figure 4.8.** Representative confocal microscopy images of NIH/3T3 fibroblasts cultured on multi-directionally aligned micelles: (a) orthogonally and alternatively printed micelles at each direction for 5 times at each direction; (b) tri-directionally and alternatively printed micelles for 5 times at each direction. Cells were labeled with the (i) Cell Tracker green probe (green channel) and the nucleus stained with (ii) DAPI (blue channel). Polymeric micelles were labeled with the (iii) dye DiI and imaged in the red channel. (iv) Corresponds to merging of the three channels. Scale bar corresponds to 20  $\mu\text{m}$ .

To quantitatively analyze cellular alignment in these two cases, the distribution of orientation angle ( $\theta$ ) was investigated. Regarding the horizontally and vertically aligned micelles, three preferential angles of cell alignment were observed (Figure 9a), showing cells display a similar contact guidance in both directions. However, it becomes more complicated

in the substrate with tri-directionally aligned micelles (Figure 9b). A larger number of cells oriented towards 30 degrees, indicating that the micelles aligned in the third direction (45°) led to more deviation by their mutual contact guidance. It can, therefore, be suggested that cells could integrate multi-direction cues during determining the direction of cell orientation together with mutual interactions, which agrees with former reports[36, 37].

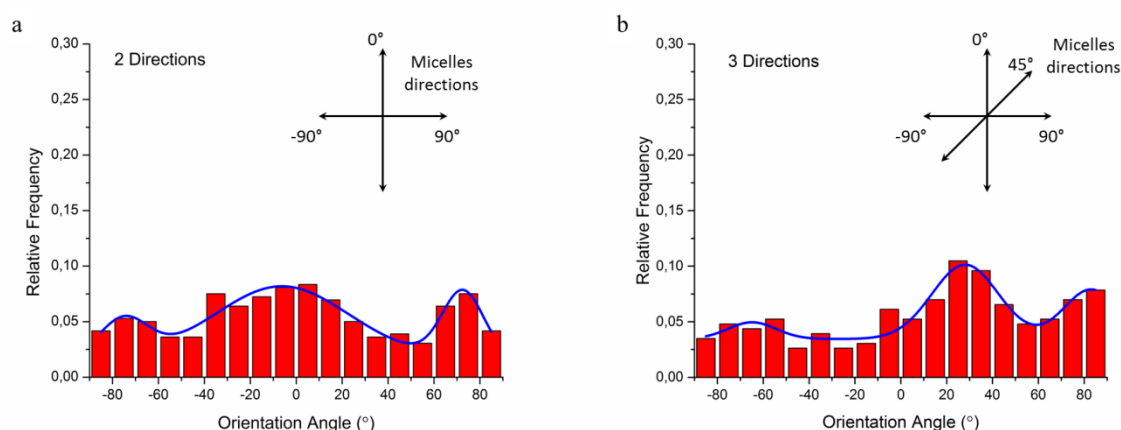


**Figure 4.9.** Histograms of the relative alignment of NIH/3T3 fibroblasts on multi-directionally aligned micelles: (a) orthogonal directions and (b) three directions. The insert drawing and the blue lines are the corresponding directions of aligned micelles and the multiple peak fit with Gaussian functions, respectively.

### 4.3. Conclusions

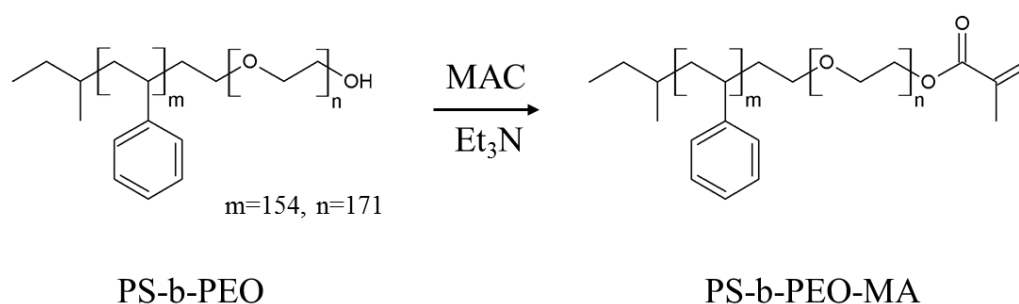
In summary, we have demonstrated that ultra-long block copolymer fibrous micelles are capable of regulating cell orientation on a surface. The degree of cell alignment increased with the area density of micelles. When the area percentage of micelle coverage increased to 31.4%, the cellular alignment became more significant even if no significant cell elongation was observed. For high enough micelle surface density, nuclear alignment was also observed although no considerable nuclear elongation was detected. Furthermore, the cells show a competitive response to the micelle networks with multi-directionally alignment. Our unique micellar platform suggests that fibrous micelles of block copolymers can be used to mimic the native fibrous networks surrounding cells. Considering the innumerable possibilities of biochemical modification of the micelle corona end-groups (like terminal methacrylate groups in our work), we believe this work provides a versatile approach to future studies mimicking cell interactions with native fibrous networks containing various chemical functionalities.



## 4.4. Experimental section

### 4.4.1. Synthesis and preparation of micelles

Pristine block copolymer, polystyrene-*b*-polyethylene oxide (PS-*b*-PEO), having an –OH terminal group in PEO block was purchased from Polymer Source, Inc. (Canada). Polydispersity index is 1.09 and the molecular weights of PS and PEO blocks are 16.0 kg/mol and 7.5 kg/mol, respectively. In order to fix the micelles onto the substrate after printing, we synthesized PS-*b*-PEO-MA by reaction of PS-*b*-PEO with methacryloyl chloride (MAC) as follows.



**Scheme 2.** Reaction of polystyrene-*b*-polyethylene oxide (PS-*b*-PEO) with methacryloyl chloride.

Briefly, 500 mg of PS-*b*-PEO (0.02 mmol) was first dissolved in 50 mL of tetrahydrofuran (THF) and then 13 mmol of triethylamine ( $\text{Et}_3\text{N}$ ) was added under vigorous stirring at room temperature. MAC (13 mmol) was slowly added to the reaction mixture while stirring and resulting mixture was allowed to react for 24h at 25°C to substitute terminal alcohol of PS-*b*-PEO with methacryloyl group. Then, the reaction mixture was centrifuged at 10000 rpm for 15 min, after which the supernatant was carefully removed from the precipitated triethylamine hydrochloride salts. This procedure was repeated 2-3 times, after which the remaining solution was concentrated with rotary evaporator to about 5 mL. The resulting solution was slowly added to 600 mL of hexane, and the precipitated PS-*b*-PEO-MA polymer was isolated by filtration, washed several times with ethanol thoroughly, and dried in a vacuum oven at 50°C and 50 mbar for 2 days. Following modification of PS-*b*-PEO,  $^1\text{H}$  nuclear magnetic resonance ( $^1\text{H}$ -NMR, Agilent-400 MR DD2) spectroscopy was used to verify the structure and substitution efficiency. As shown in Figure S1, the methacryloyl functionality was confirmed by  $^1\text{H}$ -NMR ( $\text{CDCl}_3$ ): PS-*b*-PEO-MA,  $\delta$  (ppm) 5.6 and 6.2 ( $\text{CH}_3\text{-C=CH}_2$ ), 1.9 ( $\text{CH}_3\text{-C=CH}_2$ ).

Functionalized filamentous micelles were prepared by the evaporation-induced self-assembly method, which has been reported elsewhere[17]. Typically, our modified method gives rise to a broad length distribution with a peak around 150-200  $\mu\text{m}$  and a very long tail of quenched ultra-long micelles[18]. Instead of using pure PS-*b*-PEO, stock solutions of 10

mg/mL copolymers were prepared with 10% of PS-b-PEO-MA/PS-b-PEO weight fractions. The fluorescent probe 1,1'-dioctadecyl-3,3,3',3'-tetramethylindocarbocyanine perchlorate (DiI) was added to the stock solutions before micelle preparation to facilitate micelle visualization by confocal microscopy.

#### **4.4.2. Fabrication of PDMS stamp**

The PDMS stamp with micropillars were produced by conventional soft lithography, which was reported in our previous work[18, 19]. Briefly, a master silicon template with a pattern (3.5×3.5  $\mu\text{m}$  squares with 2  $\mu\text{m}$  gaps) was first produced by deep reactive ion etching technique. Then, the silicon template was treated with a vapour of silanization agent (tridecafluoro-1,1,2,2-tetrahydrooctyl)trichlorosilane for 4h, following by curing the mixture of PDMS prepolymer (Sylgard 184, Dow Corning Co. Ltd.) and curing agent (weight ratio: 10: 1) with the template at 68°C for 24h. After peeling off the formed PDMS stamp from silicon mould, we immersed it into a bath of ethanol for 16h to remove unreacted compound and dried in the air before using.

#### **4.4.3. Alignment of micelles**

The micelles were aligned using a dewetting technique reported before[18, 19]. Briefly, 20  $\mu\text{L}$  of micelle solution was deposited on the edge of stamp pattern and then dragged in one direction by capillary force using lens tissue. As a result of controlled wetting process, micelles were well aligned and deposited on top of the micropillars.

#### **4.4.4. Printing and crosslinking micelles onto glass slides**

First, methacrylated glass slides (Glass-MA) were prepared by rinsing glass coverslides with ethanol and acetone several times, then cleaned with plasma for 140s, following by silanization with 3-(trichlorosilyl)propyl methacrylate for 4h. Second, a PDMS micropillar stamp with aligned micelles was prepared as described above, using 0.1 mg/mL of micelle solution containing 5 mg/mL of photo initiator, lithium phenyl-2,4,6-trimethylbenzoylphosphinate (LAP), which was synthesized as previously described[20]. Then, the PDMS micro-pillar stamp with the aligned micelles on top was brought into contact with Glass-MA slides under gentle force (around 40 g) for 30s and then slowly peeled off at low speed (around 1 mm/s) to transfer print the aligned micelle array. Finally, the Glass-MA with micelles was irradiated for 20 min to crosslink the micelles onto glass slides under UV light. For preparing substrates with different micelle coverages, the number of times for printing micelles were adjusted before UV irradiation. Note, to prevent degradation of LAP, aluminium foil was used to cover all glass vials and petri dishes during the whole aligning and printing process.

#### **4.4.5. Cell Culture**

The cell line used in this study (NIH/3T3 mouse embryonic fibroblasts) was obtained from the American Type Culture Collection (ATCC, USA) and cultured in Dulbecco's modified Eagle's medium (DMEM) supplemented with 10% newborn calf serum (NCS) and 0.5% (v/v) penicillin–streptomycin. Cell cultures were prepared from deep-frozen stock vials, seeded in 75 cm<sup>2</sup> culture bottles (Cellstar, Greiner Bio-One), incubated under standard cell culture conditions (37 °C, 5% CO<sub>2</sub> atmosphere and water-saturated 95% air) and maintained until sub-confluence was reached (70-80%). For the experimental studies, cells were trypsinized and seeded at a density of 2×10<sup>4</sup> cells/cm<sup>2</sup> in the modified nanofibrous glass substrates, which were placed in 6-well plates. Cells were allowed to interact with the substrates overnight. After this incubation period, the adherent cells were labelled with a CellTracker™ Green 5-chloromethylfluorescein diacetate solution (Molecular Probes, C7025) at a concentration of 10 μM in serum-free medium for 45 minutes at 37°C. Cells were then washed twice with Dulbecco's Phosphate-Buffered Saline (DPBS, Gibco) and fixed with pre-warmed 3.7% formaldehyde in PBS for 15 min. Cells were washed again thrice with DPBS and mounted with DAPI Vectashield (Vector Laboratories) for confocal microscopy. Images were captured with a Carl Zeiss LSM710 microscope and were superimposed to determine the localization of the CellTracker dye, the DAPI nuclear dye and the DiI micellar dye. Experiments were performed in duplicate.

#### **4.4.6. Characterization**

The micelles and NIH/3T3 fibroblasts were visualized using a laser scanning confocal microscopy (LSM 710, Carl Zeiss Microscopy GmbH, Germany) with a Fluor 40×/1.30 oil M27 objective lens. The nuclei were stained with DAPI for fluorescence imaging. Atomic force microscopy (AFM) was performed using an NT-MDT (NTEGRA) microscope and HA\_NA tips with resonance frequency around 240 kHz. All topography scans were obtained in tapping mode in the air and at room temperature. Then, the grain threshold method[21] was utilized to quantitatively analyse AFM results and investigate the coverage area of micelles.

#### **4.4.7. Micelle alignment analysis**

Micelle alignment was investigated by Fast Fourier Transform (FFT) image analysis as a function of printing times[22-24]. Since the “frequency” information of micelles in confocal images will be converted to a grayscale pattern by FFT function, the degree of micelle alignment can be easily reflected in the FFT output images. The confocal images with 1024×1024 pixels were first converted to 8-bit grayscale TIF files and then processed with ImageJ software (version 1.48v, National Institutes of Health, USA, <http://imagej.nih.gov/ij>).

#### 4.4.8. Cellular alignment analysis

To quantify orientation and elongation of cells and nuclei on substrates, an in-house program was developed with Matlab® using the image processing toolbox. Briefly, cell or nucleus was fitted with an ellipse shape using the moments algorithm[25, 26] and various elliptical parameters were obtained. The angle between the major axis of fitting ellipse and aligned direction of micelles was defined as orientation angle ( $\theta$ ) and used to quantify cellular alignment, while the aspect ratio between the length of major axis and minor axis was applied to evaluate the elongation behaviour. Around 300 data points were taken from confocal images for analysis of each sample.

#### 4.5. References

- [1] Langer R, Vacanti JP. Tissue Engineering. Science. 1993;260:920-6.
- [2] Mecham RP. Overview of extracellular matrix. Current protocols in cell biology. 2012;Chapter 10:Unit 10 1.
- [3] Mouw JK, Ou GQ, Weaver VM. Extracellular matrix assembly: a multiscale deconstruction. Nat Rev Mol Cell Bio. 2014;15:771-85.
- [4] Frantz C, Stewart KM, Weaver VM. The extracellular matrix at a glance. J Cell Sci. 2010;123:4195-200.
- [5] Engel E, Michiardi A, Navarro M, Lacroix D, Planell JA. Nanotechnology in regenerative medicine: the materials side. Trends Biotechnol. 2008;26:39-47.
- [6] Ma PX. Biomimetic materials for tissue engineering. Adv Drug Deliver Rev. 2008;60:184-98.
- [7] Sill TJ, von Recum HA. Electrospinning: applications in drug delivery and tissue engineering. Biomaterials. 2008;29:1989-2006.
- [8] Wang XF, Ding B, Li BY. Biomimetic electrospun nanofibrous structures for tissue engineering. Mater Today. 2013;16:229-41.
- [9] Liu XH, Ma PX. Phase separation, pore structure, and properties of nanofibrous gelatin scaffolds. Biomaterials. 2009;30:4094-103.
- [10] Yang F, Murugan R, Ramakrishna S, Wang X, Ma YX, Wang S. Fabrication of nano-structured porous PLLA scaffold intended for nerve tissue engineering. Biomaterials. 2004;25:1891-900.
- [11] Nam YS, Park TG. Porous biodegradable polymeric scaffolds prepared by thermally induced phase separation. J Biomed Mater Res. 1999;47:8-17.
- [12] Whitesides GM, Grzybowski B. Self-assembly at all scales. Science. 2002;295:2418-21.
- [13] O'Leary LER, Fallas JA, Bakota EL, Kang MK, Hartgerink JD. Multi-hierarchical self-assembly of a collagen mimetic peptide from triple helix to nanofibre and hydrogel. Nat Chem. 2011;3:821-8.
- [14] Mendes AC, Baran ET, Reis RL, Azevedo HS. Self-assembly in nature: using the principles of nature to create complex nanobiomaterials. Wires Nanomed Nanobi. 2013;5:582-612.
- [15] Harada A, Kataoka K. Supramolecular assemblies of block copolymers in aqueous media as nanocontainers relevant to biological applications. Prog Polym Sci. 2006;31:949-82.

- [16] Kataoka K, Harada A, Nagasaki Y. Block copolymer micelles for drug delivery: design, characterization and biological significance. *Adv Drug Deliver Rev.* 2001;47:113-31.
- [17] Zhu JT, Hayward RC. Spontaneous generation of amphiphilic block copolymer micelles with multiple morphologies through interfacial instabilities. *J Am Chem Soc.* 2008;130:7496-502.
- [18] Zhang K, Glazer PJ, Jennings L, Vedaraman S, Oldenhof S, Wang Y, et al. A facile approach for the fabrication of 2D supermicelle networks. *Chem Commun (Camb).* 2016;52:12360-3.
- [19] Glazer PJ, Bergen L, Jennings L, Houtepen AJ, Mendes E, Boukany PE. Generating Aligned Micellar Nanowire Arrays by Dewetting of Micropatterned Surfaces. *Small.* 2014;10:1729-34.
- [20] Fairbanks BD, Schwartz MP, Bowman CN, Anseth KS. Photoinitiated polymerization of PEG-diacrylate with lithium phenyl-2,4,6-trimethylbenzoylphosphinate: polymerization rate and cytocompatibility. *Biomaterials.* 2009;30:6702-7.
- [21] Guan QB, Norder B, Chug LY, Besseling NAM, Picken SJ, Dingemans TJ. All-Aromatic (AB)(n)-Multiblock Copolymers via Simple One-Step Melt Condensation Chemistry. *Macromolecules.* 2016;49:8549-62.
- [22] Ayres C, Bowlin GL, Henderson SC, Taylor L, Shultz J, Alexander J, et al. Modulation of anisotropy in electrospun tissue-engineering scaffolds: Analysis of fiber alignment by the fast Fourier transform. *Biomaterials.* 2006;27:5524-34.
- [23] Valente TAM, Silva DM, Gomes PS, Fernandes MH, Santos JD, Sencadas V. Effect of Sterilization Methods on Electrospun Poly(lactic acid) (PLA) Fiber Alignment for Biomedical Applications. *Acs Appl Mater Inter.* 2016;8:3241-9.
- [24] Orlova Y, Magome N, Liu L, Chen Y, Agladze K. Electrospun nanofibers as a tool for architecture control in engineered cardiac tissue. *Biomaterials.* 2011;32:5615-24.
- [25] Voss K, Suesse H. Invariant fitting of planar objects by primitives. *Ieee T Pattern Anal.* 1997;19:80-4.
- [26] Lenhert S, Meier MB, Meyer U, Chi LF, Wiesmann HP. Osteoblast alignment, elongation and migration on grooved polystyrene surfaces patterned by Langmuir-Blodgett lithography. *Biomaterials.* 2005;26:563-70.
- [27] Meijering E, Jacob M, Sarria JCF, Steiner P, Hirling H, Unser M. Design and validation of a tool for neurite tracing and analysis in fluorescence microscopy images. *Cytom Part A.* 2004;58a:167-76.
- [28] Loesberg WA, te Riet J, van Delft FCMJM, Schon P, Figdor CG, Speller S, et al. The threshold at which substrate nanogroove dimensions may influence fibroblast alignment and adhesion. *Biomaterials.* 2007;28:3944-51.
- [29] Gombotz WR, Wang GH, Horbett TA, Hoffman AS. Protein adsorption to poly(ethylene oxide) surfaces. *J Biomed Mater Res.* 1991;25:1547-62.
- [30] Sofia SJ, Premnath VV, Merrill EW. Poly(ethylene oxide) Grafted to Silicon Surfaces: Grafting Density and Protein Adsorption. *Macromolecules.* 1998;31:5059-70.
- [31] McPherson T, Kidane A, Szleifer I, Park K. Prevention of protein adsorption by tethered poly(ethylene oxide) layers: Experiments and single-chain mean-field analysis. *Langmuir.* 1998;14:176-86.
- [32] Jeon SI, Lee JH, Andrade JD, Degennes PG. Protein Surface Interactions in the Presence of Polyethylene Oxide .1. Simplified Theory. *J Colloid Interf Sci.* 1991;142:149-58.

- [33] Fee T, Surianarayanan S, Downs C, Zhou Y, Berry J. Nanofiber Alignment Regulates NIH3T3 Cell Orientation and Cytoskeletal Gene Expression on Electrospun PCL plus Gelatin Nanofibers. *Plos One*. 2016;11.
- [34] Brammer KS, Oh S, Cobb CJ, Bjursten LM, van der Heyde H, Jin S. Improved bone-forming functionality on diameter-controlled TiO<sub>2</sub> nanotube surface. *Acta Biomater*. 2009;5:3215-23.
- [35] Maniotis AJ, Chen CS, Ingber DE. Demonstration of mechanical connections between integrins cytoskeletal filaments, and nucleoplasm that stabilize nuclear structure. *P Natl Acad Sci USA*. 1997;94:849-54.
- [36] Zhou XT, Hu J, Li JJ, Shi J, Chen Y. Patterning of Two-Level Topographic Cues for Observation of Competitive Guidance of Cell Alignment. *Acs Appl Mater Inter*. 2012;4:3888-92.
- [37] Mi HY, Salick MR, Jing X, Crone WC, Peng XF, Turng LS. Electrospinning of unidirectionally and orthogonally aligned thermoplastic polyurethane nanofibers: Fiber orientation and cell migration. *Journal of Biomedical Materials Research Part A*. 2015;103:593-603.

## 4.6. Appendix

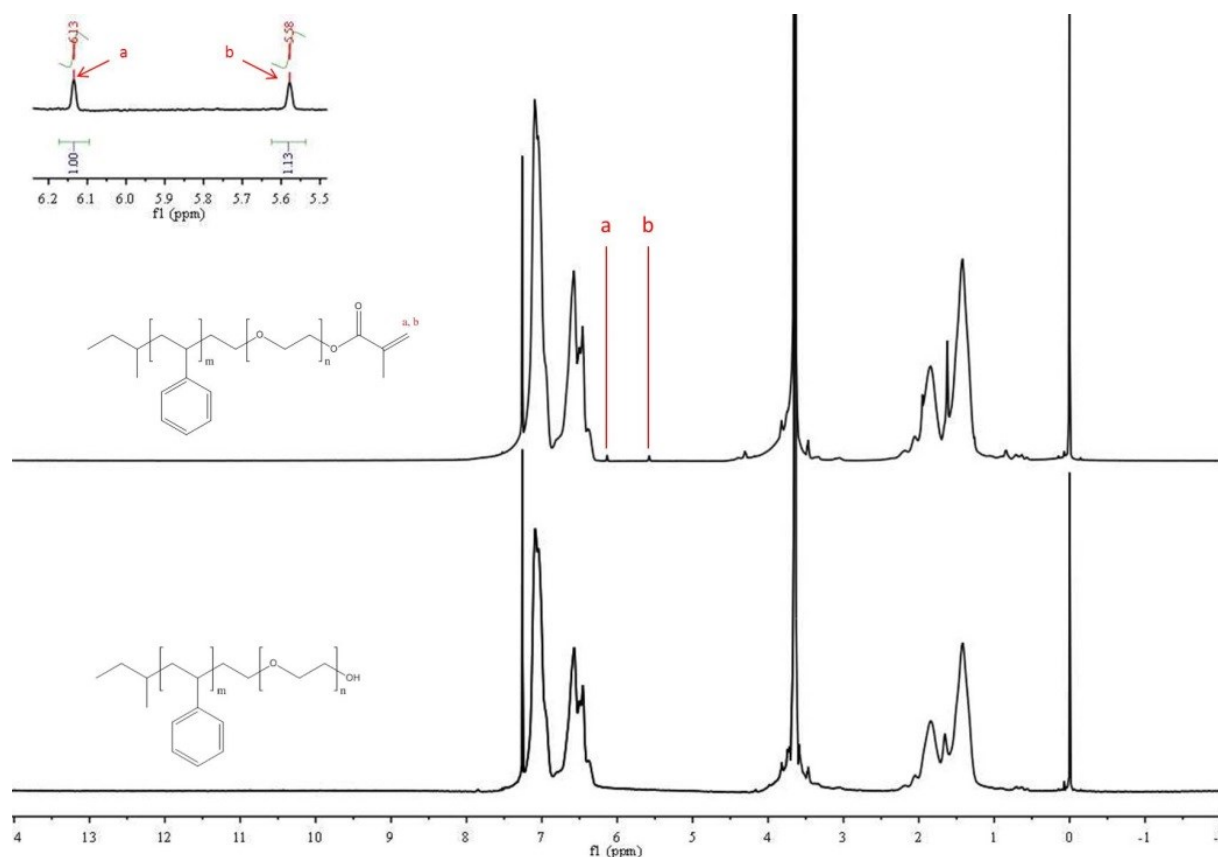


**Figure S1.** <sup>1</sup>H-NMR spectra of PS-b-PEO and PS-b-PEO-MA in CDCl<sub>3</sub>. The characteristic peaks of terminal methacryloyl group are assigned in the figure and magnified in insert figure.

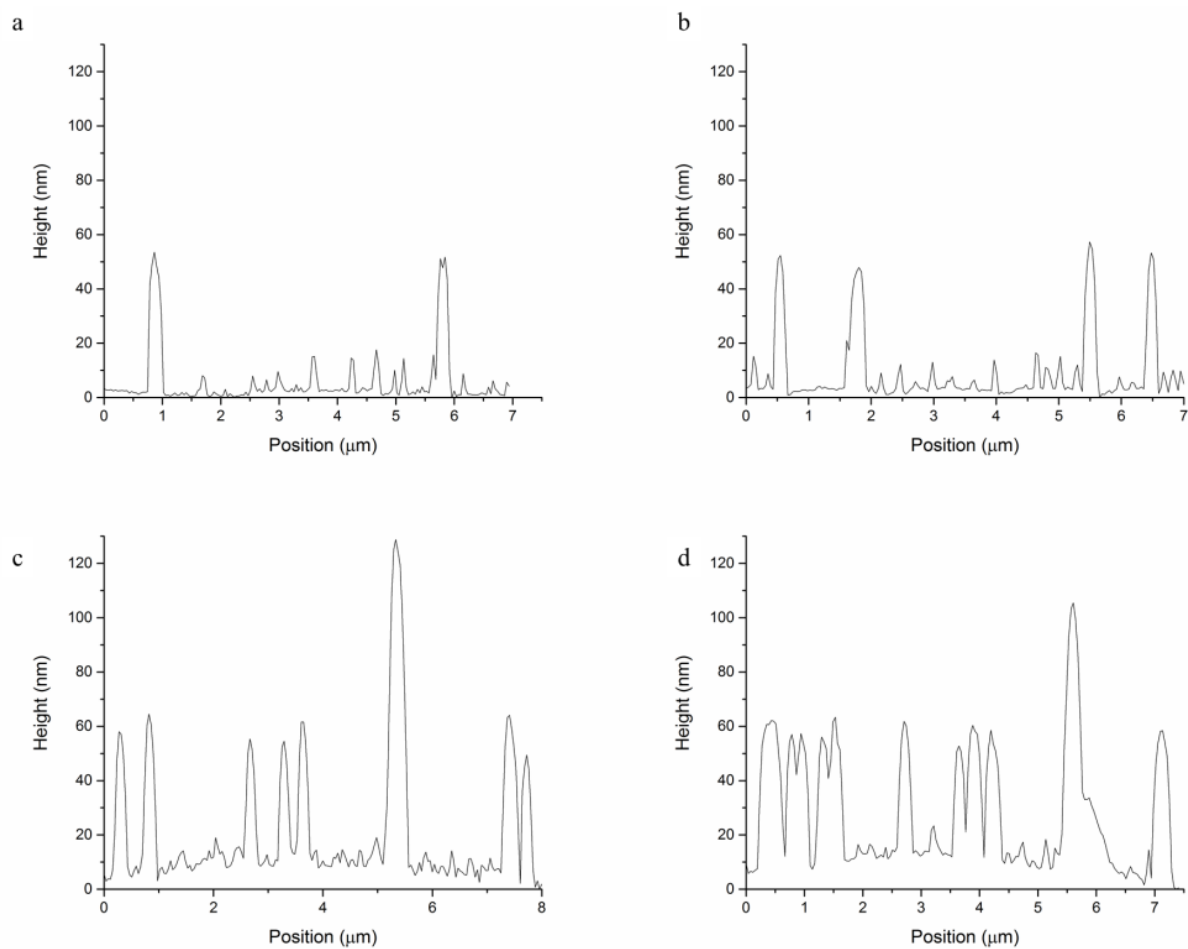


**Figure S2.** Line scan profiles of the micelles printed and cross-linked on the glass surface: (a) 1, (b) 5, (c) 10, (d) 20 printing times.

# Soft gel micro-devices from supramolecular assemblies of block copolymers

# 5

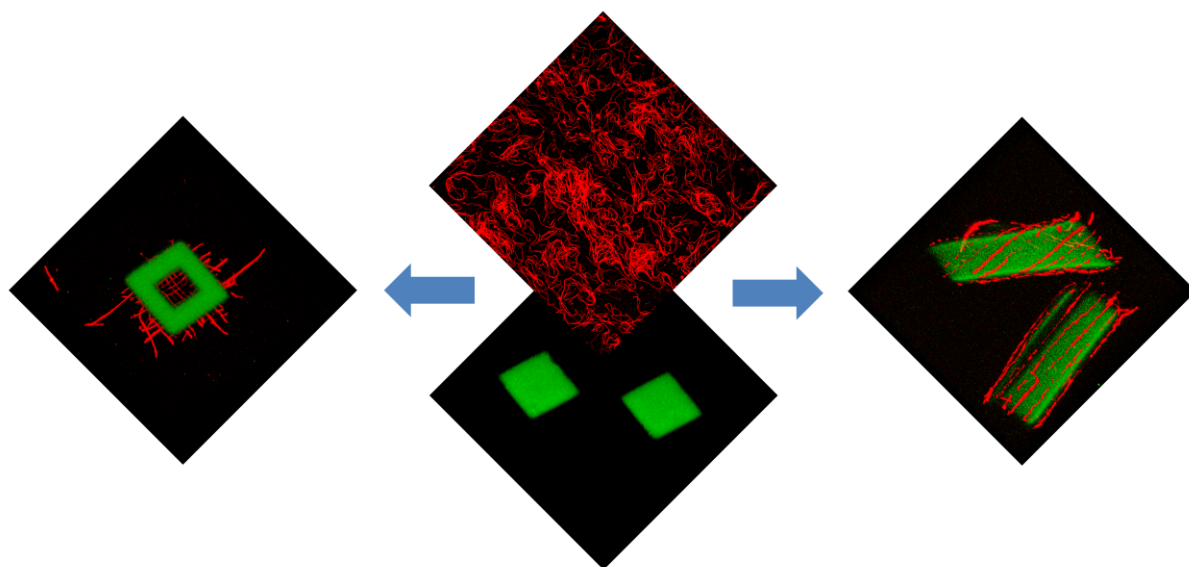
The content of this chapter is based on:

K. Zhang, S. Oldenhof, Y. Wang, H. Chen, J.H. van Esch and E. Mendes, *Manuscript in preparation*.



## Abstract

Supramolecular self-assembly represents a highly promising route for the creation of complex and functional devices at micro-/nano- scale, yet the precise manipulation and integration of supramolecular assemblies for construction of sophisticated devices with designed functionalities remains a challenge. Through a hybrid approach combining self-assembly of block copolymers and  $\mu$ -contact printing techniques, we have developed two different kinds of functional soft devices, including a soft nano-fishnet and a shape-morphing sheet. The former one can trap and release microparticles, while the later one exhibits a controlled rolling behaviour. Ultra-long, kinetically-trapped copolymer cylindrical micelles have been embedded in a hydrogel matrix in an ordered and aligned manner, leading to the mentioned functionalities of soft devices. Such control of the precise structure of the soft gel composite opens new doors in the development of soft functionalized devices with supramolecular assemblies.



## 5.1. Introduction

Over the past decades, studies on the self-assembly of supramolecules mainly focused on the principles regulating the assembly process to achieve desired nanostructures or properties[1-4]. Despite the fact that a wide variety of functional nanostructures[5, 6], including spheres, cylinders, vesicles and other more complex and impressive morphologies[7-15] have been developed, only few studies have focussed on the use of these assemblies for the creation of more complex and novel functional gel devices[16, 17]. The formidable challenge is precise spatiotemporal control of self-assembly process and subsequent manipulation of self-assembled structures, especially with respect to integration of the assemblies into more sophisticated systems across multiple length scales. Although recent advances in manipulation of the assemblies have been described with success such as flow-based[18], lithographic-templating[19, 20] or optical-tweezer-based[21] methods, no other construction of functional devices based on manipulation of already assembled polymer supramolecular structures have been investigated so far, nor have those methods been used to create a composite gel device. Herein, using de-wetting and printing techniques, we demonstrate that a single large 2D array of very long, ordered and aligned supramolecular cylindrical assemblies integrated within hydrogels enables modulation of macroscopic properties of the composite system.

The method proposed here through a combination of microfabrication, de-wetting and printing of quenched nano-structured systems, bridges the gap of simultaneous manipulation of gel structures at micro- and nano- scales. To demonstrate this principle, we build two different kinds of soft gel devices which are capable of either trapping/releasing microparticles or of rolling with controlled directionality, respectively. Our work opens the door not only to addressing fundamental questions surrounding supramolecular assemblies controlled shaping of hydrogels, but also it is a promising step in the development of soft functional devices tailored by supramolecular assemblies.

## 5.2. Results and Discussion

To develop the soft devices by manipulation and integration of supramolecular assemblies, we combined polymer chemistry, self-assembly of block copolymers and lithography techniques. First, methacrylated block copolymers of polystyrene-b-poly(ethylene oxide) (PS-b-PEO-MA) has been formulated and used to prepare supramolecular assemblies. Through an evaporation-induced self-assembly approach (Figure S1 and S4), the quenched, assembled copolymer nano-fibrils (i.e. filamentous micelles) that exhibit both a nanoscopic and micrometric dimension can be formed, offering an opportunity of subsequent manipulation at macro-scale. For the soft matrix part, methacrylated dextran (DexMA)

(Figure S2) has been synthesized and selected to form soft hydrogels using a laser-assisted photocrosslinking technique. Figure 5.1 illustrates the fabrication process and corresponding structures of hydrogels with controllable architectures of fibrillary assemblies. It begins by manipulation of filamentous micelles on a patterned poly(dimethylsiloxane) (PDMS) substrate. Using the guided de-wetting method as previously described (Figure S5), the cylinder micelles were aligned and suspended across micropillars of PDMS stamp. Subsequently, the organized micelle array has been transfer-printed onto a spin-coated DexMA film containing certain amount of photoinitiator, lithium phenyl-2,4,6-trimethylbenzoylphosphinate (LAP) (Figure S3). The “inked” PDMS stamp with organized micelles on top was lightly brought into contact with the spin-coated DexMA film for 30 s, followed by slowly peeling off stamp at rate of around 1 mm/s, yielding the DexMA film with aligned micelles printed on the surface. Ultimately, a laser-assisted photocrosslinking and patterning was performed to construct the desired shape of hydrogels and anchor block copolymer micelles. As the corona of formed ultra-long cylinder micelles contains the terminal groups of methacryloyl (MA), these micelles are capable of grafting onto DexMA hydrogels during photocrosslinking process. After washing away the unreacted DexMA and LAP, the soft devices consist of DexMA hydrogel and PS-*b*-PEO-MA micelles were formed.

As shown in Figure 5.1b-1 and 5.1c-1, one dimensional and two dimensional superstructures of micelles embedded on DexMA film were successfully achieved by a simple transfer-printing method. After illumination with confocal microscopy laser, the designed area of DexMA film and micelles were crosslinked, resulting in a darker region (Figure 5.1b-2 and 5.1c-2). Since the unreacted DexMA and micelles can be dissolved or dispersed into water again, only the formed DexMA hydrogels with organized micelles on surface will be left on the glass substrate. Figure 5.1b-1 and 5.1c-2 demonstrate the concept of fabrication of soft devices with supramolecular assemblies. By taking advantage of our laser-assisted patterning of hydrogels, facile and flexible shape design, we can easily fabricate a wide variety of architectures for our supramolecular devices. As an example, DexMA hydrogels with different shapes and sizes were prepared (Figure 5.1d). Notably, as the micelles were ultra-long (around 170  $\mu\text{m}$ ) capable of bridging the adjacent hydrogel regions, a free-standing superstructures of micelles can be obtained (as shown in the magnified regions of Figure 5.1d).

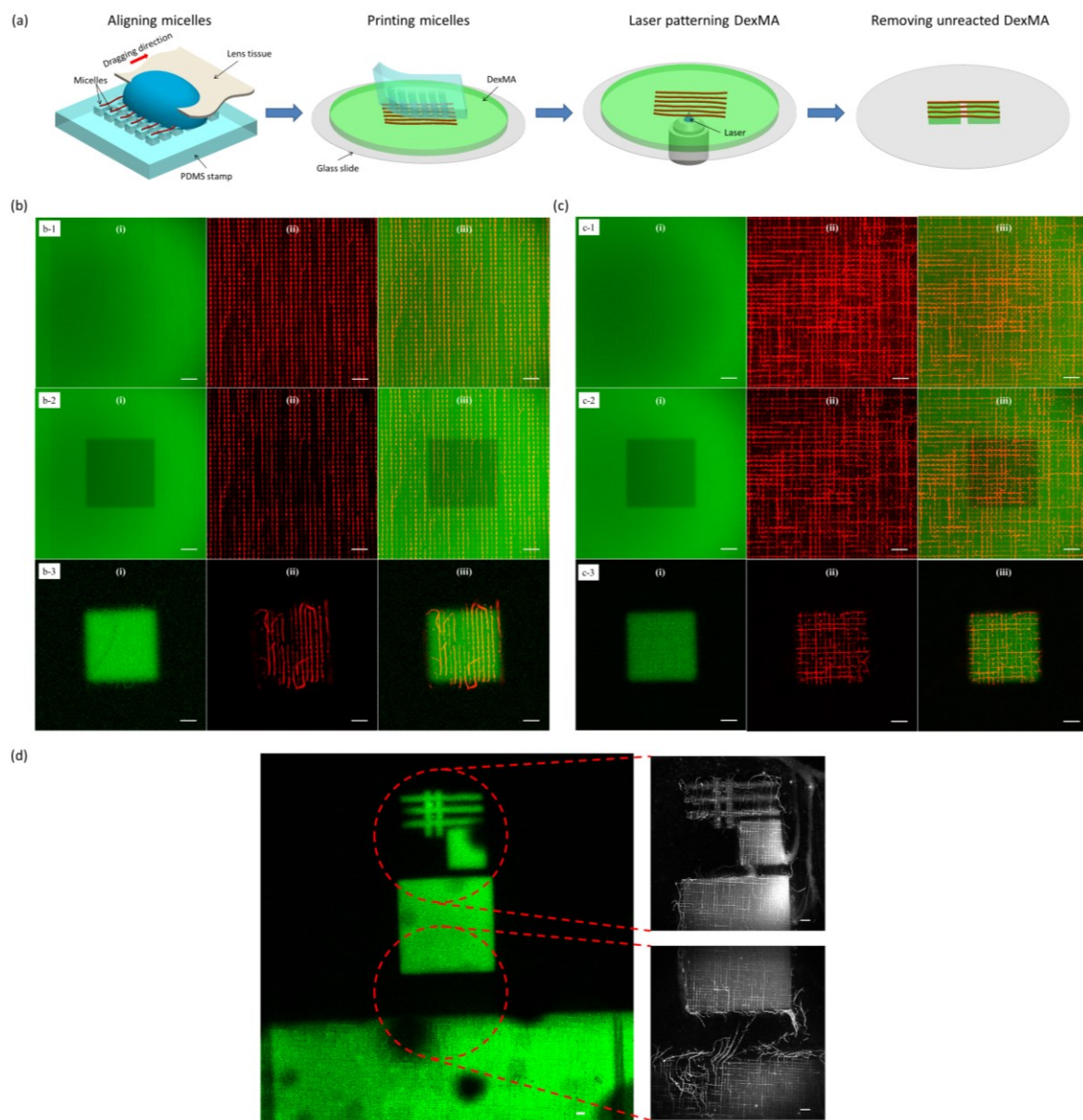


**Figure 5.1.** Formation of soft devices with organized supramolecular fibrillary assemblies. (a) Schematic illustration of method for embedding organized supramolecular fibrillary assemblies into hydrogels. PS-*b*-PEO-MA micelles are first aligned on PDMS stamp by guided dewetting technique, followed by transfer printing of micelles onto a spin coated DexMA film. Then, Localized laser crosslinking of DexMA and PS-*b*-PEO-MA micelles is performed by using confocal laser scanning microscope. After thoroughly washing with water, unreacted DexMA and micelles are removed, yielding organized superstructures of micelles on hydrogels. Confocal microscopy images of micro-fabrication process of DexMA hydrogels with printed (b) one directional and (c) two directional PS-*b*-PEO-MA micelles. (b-1) and (c-1) printed micelles on DexMA film, (b-2) and (c-2) localized laser crosslinking of DexMA and micelles, (b-3) and (c-3) formation of DexMA hydrogel sheet with aligned micelles. (i) Fluorescein dye (green channel) stained DexMA hydrogel. Polymeric micelles were loaded with (ii) hydrophobic dye Dil and imaged in the red channel. (iii) merged the former two channels. (d) Confocal microscopy images of artificially designed structures of hydrogels. Scale bars: 20  $\mu\text{m}$ .

Based on this unique characteristic, we envisioned a soft nano-fishnet device by using the DexMA hydrogels as a skeleton for micellar grids. As shown in Figure 5.2a, the irradiation area was designed as a hollow square to form the framework and 2D micelle network embedded on the hydrogel surface was suspended across this frame to make a soft fishnet structure. To prove the fishnet concept, we simply tested the ability of trapping/releasing microparticles. As shown in Figure 5.2b, when the microparticles ( $d=8\ \mu\text{m}$ ) deposited onto the supramolecular fishnet with grid size of  $5\times 5\ \mu\text{m}$ , the micelles can block the particles to penetrate through the network (Figure 5.2b-4). From the orthogonal view (Figure 5.2b-5), we observed that microparticles (green channel) were only contacting with micelles (red channel) not substrate surface (black edge), demonstrating the ability of blocking microparticles that larger than micellar grids. On the other hand, the concept can be proved by encapsulating the microparticles with two different sizes in micelle networks, one was larger ( $d=8\ \mu\text{m}$ ) and another one was smaller ( $d=1\ \mu\text{m}$ ) than grid size (Figure 5.2c-1, 5.2c-2). After immersing into a large amount of water, the small particles were released from the fishnet structure and dispersed into the solution, while the big ones were still trapped by micellar grids (Figure 5.2c-4, 5.2c-5). To gain greater insight into the relation between micellar grids and microparticles, we focused on the big particles encapsulated in DexMA film with micellar grids. As demonstrated in Figure S6, the criss-crossed micelles were paved on the top of microparticles, resulting in blocking the particles to release. Here, we demonstrate that novel functions, trapping/releasing microparticles, can be achieved by careful spatial design and fabrication of hybrid supramolecular covalent hydrogel devices, soft fishnet.

To demonstrate the scope of our approach, we also investigated to which extend controlled spatial deposition of supramolecular assemblies can be used to tune the mechanical properties of microgel devices. In nature, many plants are capable of withstanding multiform external forces or stimuli by performing desired shape transformation[22, 23]. This kind of shape adaption is controlled by the delicately organized microstructures, such as fibrils, within the biological systems[24-26]. The anisotropic swelling/shrinkage properties lead to a controlled shape-morphing behaviour[27-30]. Having taken inspiration from these natural systems, we extend our imagination to the soft devices controlled by supramolecular assemblies. First, in order to make this kind of ‘smart’ devices, charged monomers, sodium acrylate (SA), were polymerized onto the hybrid DexMA hydrogels by the second irradiation (Figure 5.3a). The unbound SA or poly(acrylic acid) (PAA) chains formed by photopolymerization were removed by a careful washing step, yielding pH responsive hydrogel actuators encoded with micelles. When the hybrid hydrogels were immersed in deionized water (pH 6.3) or a buffer solution (pH 7) that has a higher pH than  $pK_a$  value of PAA, 2D hydrogel sheets swelled and rolled up (Figure S7b). This process was completely

reversible, as the expanded and rolled up hydrogel returned to its original square shape when exposed to the solution with lower pH (Figure S7a).

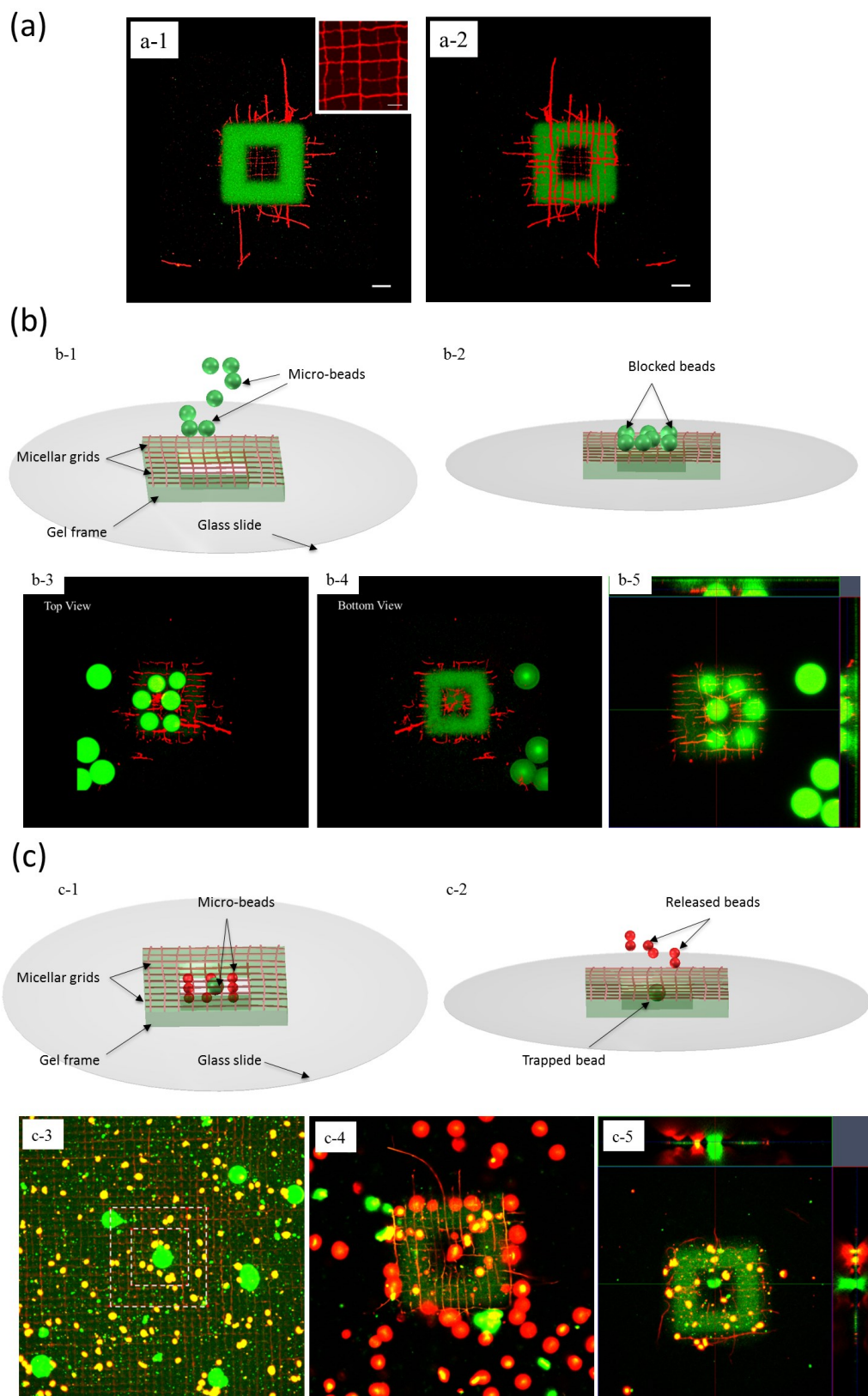


**Figure 5.2.** Soft fishnet constructed by supramolecular assemblies and hydrogels. (a) Confocal microscopy images of soft fishnet: (a-1) bottom view and magnified fishnet structure (inserted

image), (a-2) top view. (b) “Fishing” of microparticles: (b-1) scheme of microparticles dispersed above fishnet in solution, (b-2) scheme of microparticles deposited on top of fishnet, (b-3) top view, (b-4) bottom view and (b-5) orthogonal view of soft fishnet with microparticles. (c) Proof of trapping/releasing microparticles using soft fishnet: (c-1) scheme of microparticles encapsulated in fishnet, (c-2) scheme of microparticles trapped and released from fishnet, (c-3) confocal microscopy image of DexMA film containing many microparticles with two different sizes ( $d=1\ \mu\text{m}$  and  $8\ \mu\text{m}$ ), (c-4) bottom view and (c-5) orthogonal view of soft fishnet with microparticles. Scale bars:  $20\ \mu\text{m}$ .

Since the aspect ratio of hydrogel (length/width) can affect the response behaviour by introducing anisotropy[31], we, herein, chose the square pattern to eliminate the effect of shape for study. To investigate whether the organized supramolecular assemblies enable to manipulate actuation behaviour of hydrogels, the control, DexMA hydrogel without micelles, was prepared using the similar process for hybrid hydrogels. Only an additional bleaching step was performed before grafting of PAA to label the hydrogels with a black rectangle on the top right area (Figure 5.3c-1), which is useful for easily recognising the rolling behaviour of hydrogels without micelles. Here, we need to notice that to prevent from introducing supererogatory crosslinking by this bleaching step, the formed DexMA hydrogels without micelles were thoroughly washed to remove the LAP and unreacted DexMA left from prior step.

As shown in Figure 5.3b and 5.3c, the hydrogels with and without micelles were rolled up in various modes, such as transversal rolling (Figure 5.3b), longitudinal rolling (Figure 5.3c-2 ) and diagonal rolling (Figure 5.3c-3). To quantitatively analyse the rolling behaviour of hydrogels with and without micelles, the rolling angle  $\theta$  defined as the angle between rolling axis and y axis (Figure 5.3d) was measured in 3D confocal images. According to the relative positions to glass surface during gel formation process, we defined two surfaces (Figure 5.3d), top surface (TS) which is far away from the glass surface or the surface embedded with micelles and bottom surface (BS) which is contacted with glass. When the hydrogels rolled up to hide TS inside and expose BS outside, the value of rolling angle  $\theta$  we defined is positive. In contrary, the value is negative. Interestingly, we observed for all hydrogels with micelles a “negative” rolling way (negative  $\theta$ ), while all hydrogels without micelles show a “positive” rolling angle (Figure 5.3e). Meanwhile, we observed that in contrast to the relatively random curling motion of hydrogels without micelles, more than 90% of hybrid hydrogels rolled parallel with micelles (i.e.  $\theta$  is close to  $0^\circ$ ). All these results indicate that a single layer of organized micelle array within hydrogel surface is capable of modulating the response behaviour and control the rolling directionality. The observation agrees with the principle of actuation observed in natural plants, in which the oriented cellulose microfibrils control the motion[32, 33]. Since the aligned micelles on the top layer of hydrogels oriented in Y direction, the hydration-induced expansion along Y axis was restricted and the bottom



layer was unrestrained to swell. This anisotropy swelling directed the curling exclusively toward the bottom side and rolling parallel with micelles.

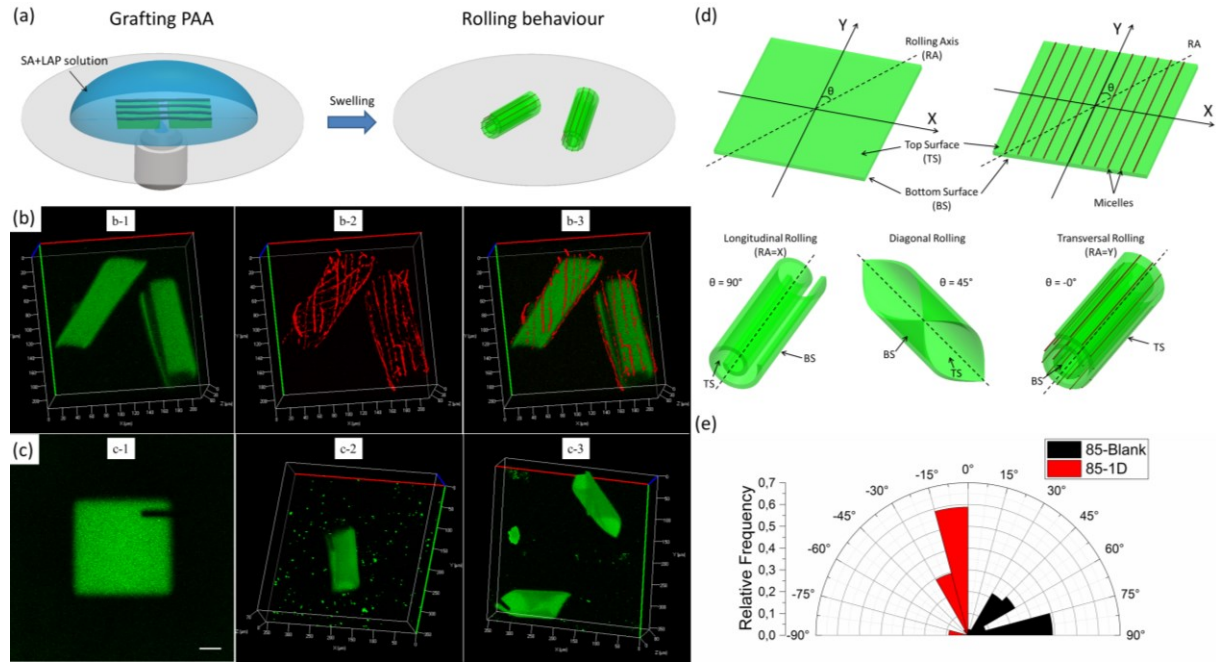


**Figure 5.3.** Tailoring stimuli-responsive behaviour of hydrogels with supramolecular assemblies; Proof of supramolecular assemblies capable of tailoring stimuli-responsive behaviour of hydrogels. (a) Scheme of endowing DexMA hydrogels with pH responsive properties. Laser assisted polymerization is utilized to graft poly(acrylic acid) chains on to DexMA hydrogels. (b) 3D confocal microscopy images of rolling-up behaviour of DexMA hydrogel with micelles: (b-1) Fluorescein dye channel (green); (b-2) polymeric micelles channel (red); (b-3) merged channel. (c) 3D confocal microscopy images of rolling-up behaviour of DexMA hydrogel without micelles: (c-1) labelling pure DexMA hydrogels by bleaching a rectangle area on the top right side; (c-2) and (c-3) representative rolling-up behaviour of DexMA hydrogels without micelles. (d) Definition of rolling angle  $\theta$  for analysis of rolling-up behaviour including longitudinal, diagonal and transversal rolling. (e) Distribution of rolling angles in DexMA hydrogel sheets ( $85 \times 85 \mu\text{m}$ ) with and without micelles.

Based on the classical Euler-Bernoulli bending theory, we know that the bending stress required to deform slender beams is inversely proportional to the length of beams.

$$\delta_x = \frac{M_z y}{I_x} \quad (1)$$

where  $\delta_x$  is the bending stress,  $M_z$  is the moment about the neutral axis and inversely proportional to length of beam,  $y$  is the perpendicular distance to the neutral axis,  $I_x$  is the second moment of area about the neutral axis  $x$ . We can recognize that the size of DexMA hydrogels could affect the extent of deformation and thus indirectly magnify or reduce the influence of micelles. Here, we also investigated the effect of aligned micelles on the deformation of hydrogel with different sizes (Figure 5.4). As expected, the small hydrogels



(45×45  $\mu\text{m}$ ) without micelles adopted the diagonal rolling mode more (i.e.  $\theta$  is close to 45°), while the larger blank hydrogels (125×125  $\mu\text{m}$ ) prefer transversal rolling mode (i.e.  $\theta$  is close to 90°). Because in the case of small hydrogels, the diagonal rolling has a larger bending length (diagonal line) than that of transversal rolling (side of square), resulting in a smaller bending stress required to deform. Consider the aligned micelles that restricted the expansion along micelles during swelling. We can envisage that the micelles will have smaller effect on the rolling behaviour of small hydrogels than that on larger hydrogels. This was proved by our results (Figure 5.4a and 5.4b), namely the larger hydrogels preferred to roll parallel with micelles while the smaller hydrogels rolled in diagonal mode, further demonstrating that a single layer of organized micelle array on the surface of hydrogels can tailor the responsive behaviour.

To further understand the role of aligned micelles in modulation of hydrogels rolling behaviour, we designed more complex architectures where an orthogonal network was printed on the surface of DexMA hydrogels (Figure 5.4c). In this regard, the swelling was restrained in two perpendicular directions. The hydrogels are rolling around the diagonal defined by the printed micellar square lattice where exclusively single rolling mode, diagonal, was observed for hydrogels with small (45×45  $\mu\text{m}$ ) gel size (Figure 5.4c-2). Since the bending stress required for larger hydrogels is smaller, the rolling direction of larger hydrogels is more unstable. For larger (85×85  $\mu\text{m}$ ) gels, except the main diagonal mode, transversal rolling mode was also observed (Figure 5.4c-4). Based on these results, we can conclude that the soft devices with controlled shape-morphing properties were constructed and tailored by supramolecular assemblies.

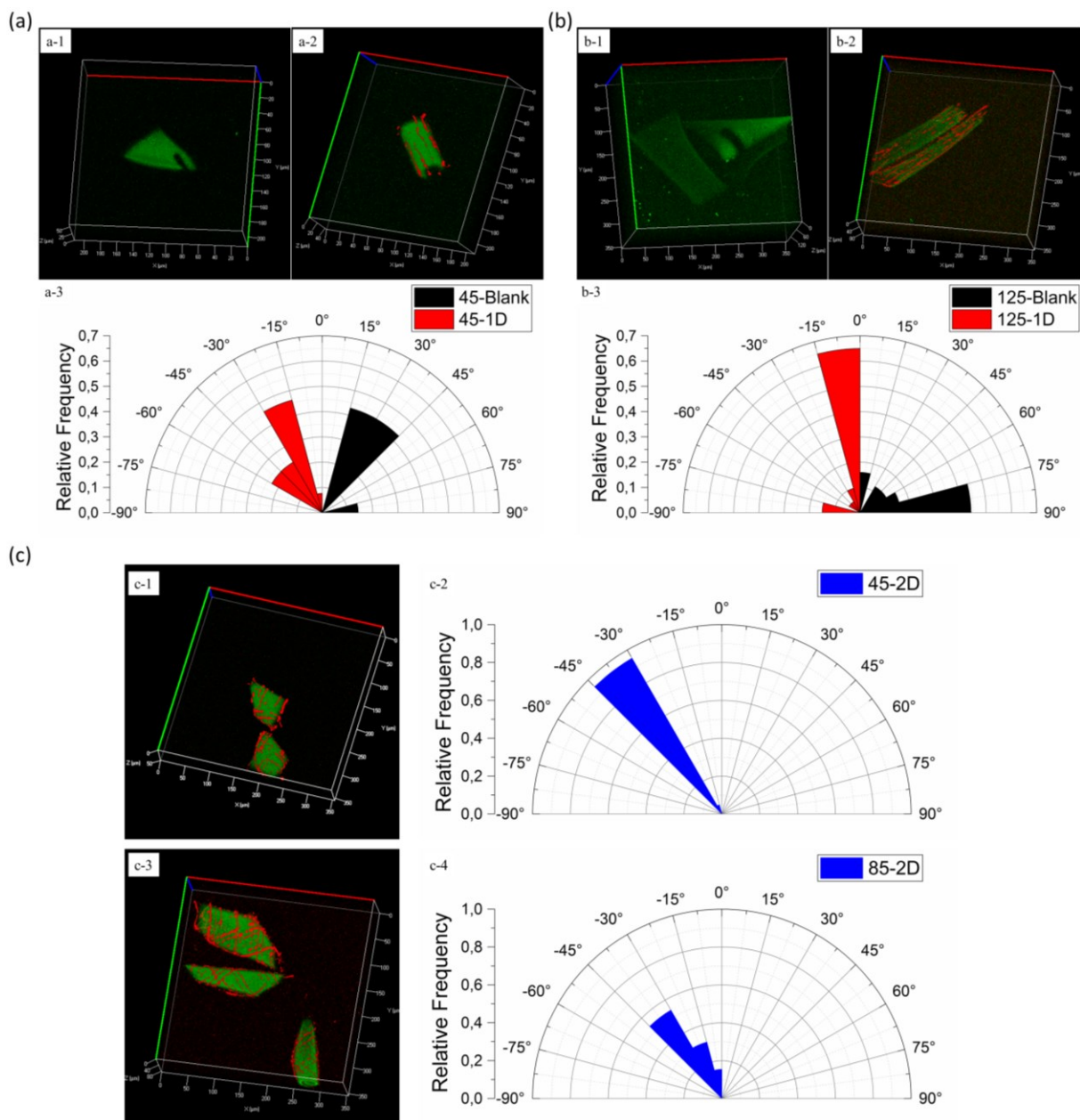


**Figure 5.4.** Evaluation of the effect of hydrogel size and multiple printed micelles on the rolling-up behaviour. (a) Rolling-up behaviour of small DexMA hydrogel sheets (45×45 μm) (a-1) without and (a-2) with micelles, (a-3) distribution of rolling angles, (b) Rolling-up behaviour of big DexMA hydrogel sheets (125×125 μm) (b-1) without and (b-2) with micelles, and (b-3) distribution of rolling angles. (c) Rolling-up behaviour of micellar grids embedded DexMA hydrogel sheets with different sizes: (c-1) (45×45 μm) and (c-3) (85×85 μm), and corresponding distribution of rolling angles (c-2) and (c-4), respectively.

## 5.3 Conclusions

Using a hybrid strategy, combination of ‘bottom-up’ and ‘top-down’ approaches, programmed and complex soft devices, such as nano-fishnet and actuators, can be built up. Our work demonstrates that a single layer of supramolecular assemblies enables to tailor the

responsive actuation of hydrogels. We envision that the strategy of supramolecular assembly programming hydrogels could serve as a powerful tool in construction of sophisticated devices and tissue engineering, and open a new view of designing intelligent biomaterials that could apply in many fields, such as responsive drug delivery and soft robots.

## **5.4. Experimental section**

### **5.4.1. Synthesis of methacrylated block copolymers**

Block copolymers of polystyrene-*b*-poly(ethylene oxide) (PS-*b*-PEO) with a terminal group of methacryloyl in PEO block (PS-*b*-PEO-MA) was synthesized following published protocols. Briefly, block copolymers of polystyrene-*b*-poly(ethylene oxide) (PS-*b*-PEO) having an -OH group in the end of PEO block reacted with methacryloyl chloride in a base, triethylamine, condition.

### **5.4.2. Preparation and alignment of functionalized block copolymer micelles**

The mixture of PS-*b*-PEO and PS-*b*-PEO-MA (weight ratio: 9:1) was used to prepare functionalized filamentous micelles by the evaporation-induced self-assembly method, which has been reported in our previous work (see Chapter 2). The fluorescent probe 1,1'-dioctadecyl-3,3,3',3'-tetramethylindocarbocyanine perchlorate (DiI) was used to stain the micelles for confocal microscopy imaging. Using a guided de-wetting technique as described previously, the fibrous micelles with methacryloyl groups in the end of corona part were aligned and deposited on top of poly(dimethylsiloxane) (PDMS) stamp with micropillar (length×width×height, 3.5×3.5×3.0 μm) arrays.

### **5.4.3. Synthesis of methacrylated dextran (DexMA)**

Dextran (Mw 500,000 g/mol) was methacrylated by reaction with glycidyl methacrylate, according to a modified, previously described procedure[34]. The preparation of DexMA was performed by the reaction with glycidyl methacrylate according to a modified, previously reported procedure. In short, 10 g of dextran (Mw=500,000 g/mol) and 2 g of 4-dimethylaminopyridine (DMAP) were dissolved in 100 mL of anhydrous dimethyl sulfoxide (DMSO) by vigorous stirring under nitrogen atmosphere. Subsequently, 0.01 mol of glycidyl methacrylate was added drop-wise under stirring, followed by coupling reaction at 30°C for 24 hours. The solution was cooled to room temperature and precipitated into 800 mL of ethanol. Then, the crude product was filtered out and washed thoroughly in ethanol for three times. In the end, the final product was dried in the vacuum oven at 45°C for 48 hours. The degree of substitution (the amount of methacrylate groups per 100 dextran glucopyranose residues) was determined by <sup>1</sup>H-NMR.

#### 5.4.4. Synthesis of photoinitiator LAP

To prepare dextran hydrogels, a water-soluble photoinitiator, lithium phenyl-2,4,6-trimethylbenzoyl-phosphinate (LAP), was synthesized according to procedure previously described[35] (Figure S3).. Briefly, 4.8 g of 2,4,6-trimethylbenzoyl-chloride was added drop by drop to react with 4.5 g of dimethyl phenylphosphonite under stirring and nitrogen atmosphere. After stirring at room temperature for 18 hours, a solution of lithium bromide (9.2 g) in 2-butanone (150 mL) was added to the reaction mixture, followed by heating up to 50°C. Subsequently, the mixture was left to react 1 hour and then cooled down to room temperature. After resting 4 hours, the precipitate was filtered and washed three times with 2-butanone to remove unreacted lithium bromide. The excess solvent was removed by vacuum, yielding a white powder of LAP.

#### 5.4.5. Lazer-assisted fabrication of hydrogels with supramolecular assemblies

**Table 1.** Setting parameters of confocal microscopy for photo patterning of DexMA hydrogels.

Setting Parameters	Vaules
Frame size	1024×1024
Pixel dwell	1.27 $\mu$ s
Average scanning No.	2
Laser power	50%
Zoom	1.0
Pin hole	1 AU
Laser wavelength	405 nm

DexMA was first fully dissolved at 10 wt% in deionized water and mixed with photoinitiator LAP (0.5 wt%) to prepare the stock solutions. Then, 150  $\mu$ l stock solution was spread onto cleaned coverslips (diameter: 30 mm) following spin coating at 2000 rpm for 2 min. PDMS stamp with aligned micelles on top was brought into contact with DexMA film on coverslips under gentle force (around 40 g) for 30s. After slowly peeling off stamp (around 1 mm/s), the aligned micelle array was successfully transferred on the DexMA film. For fabricating DexMA hydrogel with methyacrylated micelles, an upright point-scanning confocal microscope (LSM 710, Carl Zeiss Microscopy GmbH, Germany) equipped with a Fluar 40×/1.3 oil M27 objective and with 405 nm diode laser, 458/488 nm multiline Argon laser, 543 nm Helium/Neon (HeNe) and a 633 nm HeNe laser was employed. The bleaching mode and

user-defined scanning option of the microscope software (ZEN 2009) allowed precisely controlled arbitrary patterns and crosslinking time. To prepare DexMA hydrogels, the parameters used in microscope software were shown in Table 1. For labelling the DexMA hydrogels without micelles, we used longer irradiation time (pixel dwell : 12.61  $\mu$ s) and more scanning times (Average scanning No.: 4) with stronger laser power (100%).

#### **5.4.6. Fabrication of pH responsive actuators**

To fabricate the pH responsive actuators, DexMA hydrogels were functionalized with sodium acrylate. The DexMA hydrogels formed on the glass surface were first washed thoroughly with demineralised water, and then immersed in 60  $\mu$ l of 26.8 wt% sodium acrylate (SA) solution containing 0.5 wt% of LAP for 15 min. After second illumination of DexMA hydrogels in this solution, SA were successfully grafted onto the DexMA hydrogels, yielding pH responsive properties. Note that the laser power used for grafting SA was 5.0%, while the rest settings are the same.

#### **5.4.7. Fabrication of fishnet device and investigation of trapping/releasing particles.**

To fabricate the fishnet device, the aligned micelle arrays were printed twice in orthogonal directions to form fishnet structure on DexMA film. Then, the hollow square structures were formed using the same procedure of laser irradiation as described above. For encapsulating microparticles inside of fishnet device, DexMA solution containing microparticles with two different sizes ( $d=1\text{ }\mu\text{m}$  and  $8\text{ }\mu\text{m}$ ) was sprayed on the glass slide followed by spin coating to form DexMA film. Subsequently, the crosslinking step was the same as formation of hydrogels.

### **5.5. References**

- [1] Philp D, Stoddart JF. Self-assembly in natural and unnatural systems. *Angew Chem Int Edit.* 1996;35:1155-96.
- [2] Stupp SI, Palmer LC. Supramolecular Chemistry and Self-Assembly in Organic Materials Design. *Chem Mater.* 2014;26:507-18.
- [3] Whitesides GM, Grzybowski B. Self-assembly at all scales. *Science.* 2002;295:2418-21.
- [4] Riess G. Micellization of block copolymers. *Prog Polym Sci.* 2003;28:1107-70.
- [5] Mai YY, Eisenberg A. Self-assembly of block copolymers. *Chemical Society Reviews.* 2012;41:5969-85.
- [6] Schacher FH, Rupp PA, Manners I. Functional Block Copolymers: Nanostructured Materials with Emerging Applications. *Angew Chem Int Edit.* 2012;51:7898-921.

- [7] Qiu HB, Cambridge G, Winnik MA, Manners I. Multi-Armed Micelles and Block Co-micelles via Crystallization-Driven Self-Assembly with Homopolymer Nanocrystals as Initiators. *J Am Chem Soc.* 2013;135:12180-3.
- [8] Li X, Gao Y, Boott CE, Hayward DW, Harniman R, Whittell GR, et al. "Cross" Supramicelles via the Hierarchical Assembly of Amphiphilic Cylindrical Triblock Comicelles. *J Am Chem Soc.* 2016;138:4087-95.
- [9] Qiu HB, Hudson ZM, Winnik MA, Manners I. Multidimensional hierarchical self-assembly of amphiphilic cylindrical block comicelles. *Science.* 2015;347:1329-32.
- [10] Qiu H, Du VA, Winnik MA, Manners I. Branched cylindrical micelles via crystallization-driven self-assembly. *J Am Chem Soc.* 2013;135:17739-42.
- [11] He XM, Hsiao MS, Boott CE, Harniman RL, Nazemi A, Li XY, et al. Two-dimensional assemblies from crystallizable homopolymers with charged termini. *Nat Mater.* 2017;16:481-+.
- [12] Nazemi A, He XM, MacFarlane LR, Harniman RL, Hsiao MS, Winnik MA, et al. Uniform "Patchy" Platelets by Seeded Heteroepitaxial Growth of Crystallizable Polymer Blends in Two Dimensions. *J Am Chem Soc.* 2017;139:4409-17.
- [13] Qiu HB, Gao Y, Boott CE, Gould OEC, Harniman RL, Miles MJ, et al. Uniform patchy and hollow rectangular platelet micelles from crystallizable polymer blends. *Science.* 2016;352:697-701.
- [14] Dou H, Li M, Qiao Y, Harniman R, Li X, Boott CE, et al. Higher-order assembly of crystalline cylindrical micelles into membrane-extendable colloidosomes. *Nat Commun.* 2017;8:426.
- [15] Li XY, Gao Y, Boott CE, Winnik MA, Manners I. Non-covalent synthesis of supermicelles with complex architectures using spatially confined hydrogen-bonding interactions. *Nat Commun.* 2015;6:8127.
- [16] Li XY, Wolanin PJ, MacFarlane LR, Harniman RL, Qian JS, Gould OEC, et al. Uniform electroactive fibre-like micelle nanowires for organic electronics. *Nat Commun.* 2017;8.
- [17] Ren G, Wu PT, Jenekhe SA. Solar cells based on block copolymer semiconductor nanowires: effects of nanowire aspect ratio. *ACS Nano.* 2011;5:376-84.
- [18] Li B, Han W, Jiang BB, Lin ZQ. Crafting Threads of Diblock Copolymer Micelles via Flow-Enabled Self-Assembly. *Acs Nano.* 2014;8:2936-42.
- [19] Park S, Kim B, Yavuzcetin O, Tuominen MT, Russell TP. Ordering of PS-*b*-P4VP on patterned silicon surfaces. *Acs Nano.* 2008;2:1363-70.
- [20] Cao L, Massey JA, Winnik MA, Manners I, Riethmuller S, Banhart F, et al. Reactive ion etching of cylindrical polyferrocenylsilane block copolymer micelles: Fabrication of ceramic nanolines on semiconducting substrates. *Advanced Functional Materials.* 2003;13:271-6.
- [21] Gould OEC, Qiu HB, Lunn DJ, Rowden J, Harniman RL, Hudson ZM, et al. Transformation and patterning of supermicelles using dynamic holographic assembly. *Nat Commun.* 2015;6:10009.
- [22] Fratzl P, Barth FG. Biomaterial systems for mechanosensing and actuation. *Nature.* 2009;462:442-8.
- [23] Studart AR. Biologically Inspired Dynamic Material Systems. *Angew Chem Int Edit.* 2015;54:3400-16.
- [24] Forterre Y, Skotheim JM, Dumais J, Mahadevan L. How the Venus flytrap snaps. *Nature.* 2005;433:421-5.

- [25] Elbaum R, Zaltzman L, Burgert I, Fratzl P. The role of wheat awns in the seed dispersal unit. *Science*. 2007;316:884-6.
- [26] Egan P, Sinko R, LeDuc PR, Keten S. The role of mechanics in biological and bio-inspired systems. *Nat Commun*. 2015;6.
- [27] Dawson C, Vincent JFV, Rocca AM. How pine cones open. *Nature*. 1997;390:668-.
- [28] Foster R, Mattsson O, Mundy J. Plants flex their skeletons. *Trends Plant Sci*. 2003;8:202-4.
- [29] Armon S, Efrati E, Kupferman R, Sharon E. Geometry and Mechanics in the Opening of Chiral Seed Pods. *Science*. 2011;333:1726-30.
- [30] Studart AR, Erb RM. Bioinspired materials that self-shape through programmed microstructures. *Soft Matter*. 2014;10:1284-94.
- [31] Zhang LD, Chizhik S, Wen YZ, Naumov P. Directed Motility of Hygroresponsive Biomimetic Actuators. *Advanced Functional Materials*. 2016;26:1040-53.
- [32] Fratzl P, Elbaum R, Burgert I. Cellulose fibrils direct plant organ movements. *Faraday Discuss*. 2008;139:275-82; discussion 309-25, 419-20.
- [33] Erb RM, Sander JS, Grisch R, Studart AR. Self-shaping composites with programmable bioinspired microstructures. *Nature Communications*. 2013;4.
- [34] Baker BM, Trappmann B, Wang WY, Sakar MS, Kim IL, Shenoy VB, et al. Cell-mediated fibre recruitment drives extracellular matrix mechanosensing in engineered fibrillar microenvironments. *Nat Mater*. 2015;14:1262-8.
- [35] Fairbanks BD, Schwartz MP, Bowman CN, Anseth KS. Photoinitiated polymerization of PEG-diacrylate with lithium phenyl-2,4,6-trimethylbenzoylphosphinate: polymerization rate and cytocompatibility. *Biomaterials*. 2009;30:6702-7.

## 5.6. Appendix

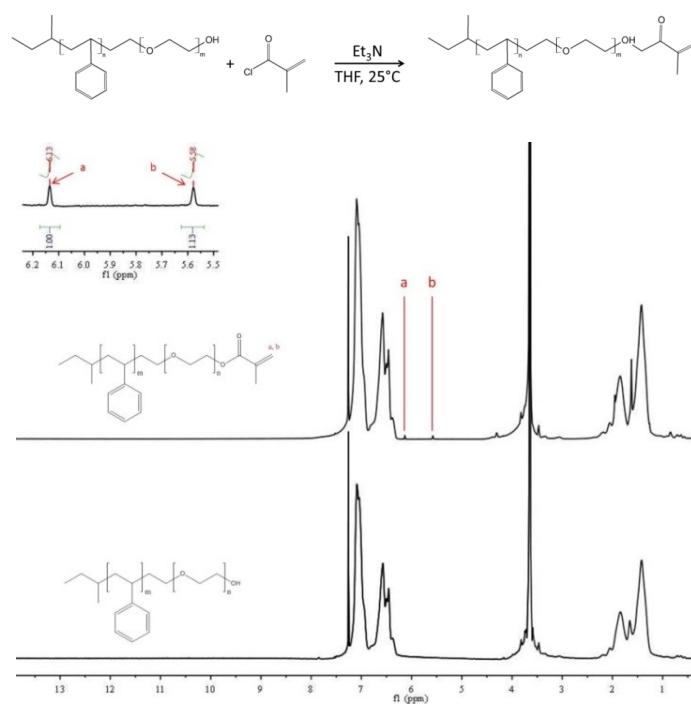


**Figure S1.** Reaction of PS-*b*-PEO with methacryloyl chloride and corresponding <sup>1</sup>H-NMR spectra of PS-*b*-PEO-MA and PS-*b*-PEO dissolved in chloroform. (same as Figure S1 in Section 4.6)

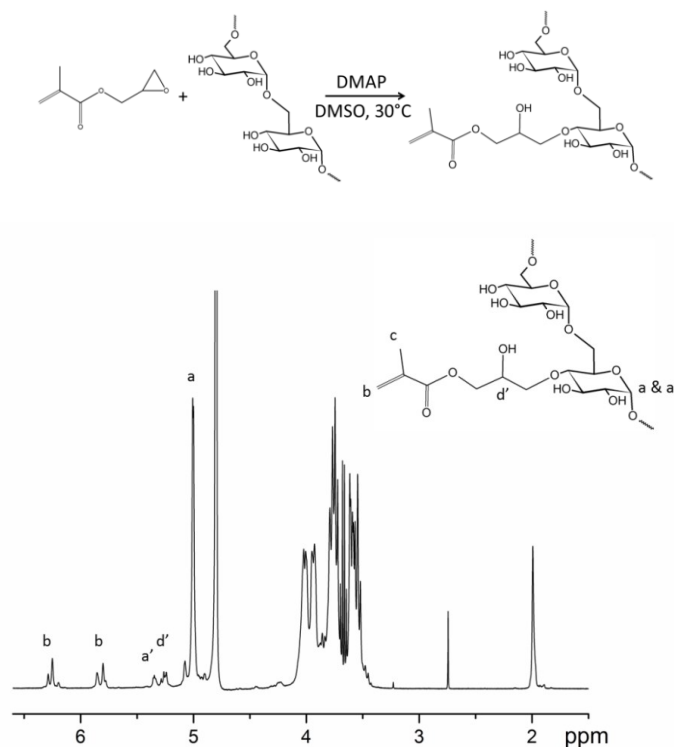


**Figure S2.** Reaction of dextran with glycidyl methacrylate and corresponding  $^1\text{H}$ -NMR spectra of DexMA dissolved in  $\text{D}_2\text{O}$ .



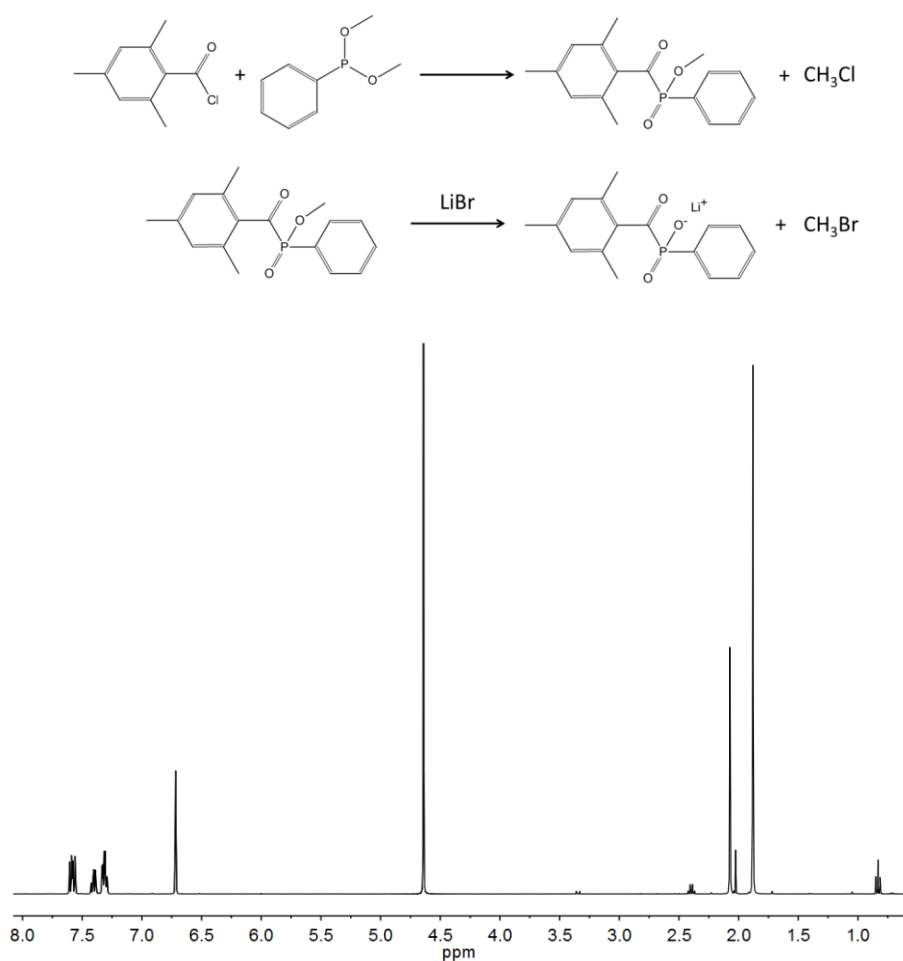


**Figure S3.** Synthesis of lithium phenyl-2,4,6-trimethylbenzoyl-phosphinate and corresponding  $^1\text{H}$ -NMR spectra in  $\text{D}_2\text{O}$ .

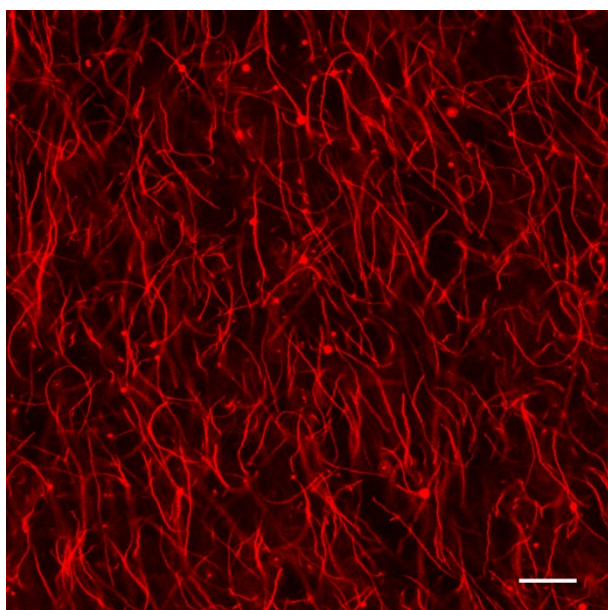


**Figure S4.** Confocal microscopy image of functionalized micelles formed by the evaporation-induced self-assembly method. Scale bar: 20  $\mu\text{m}$ .

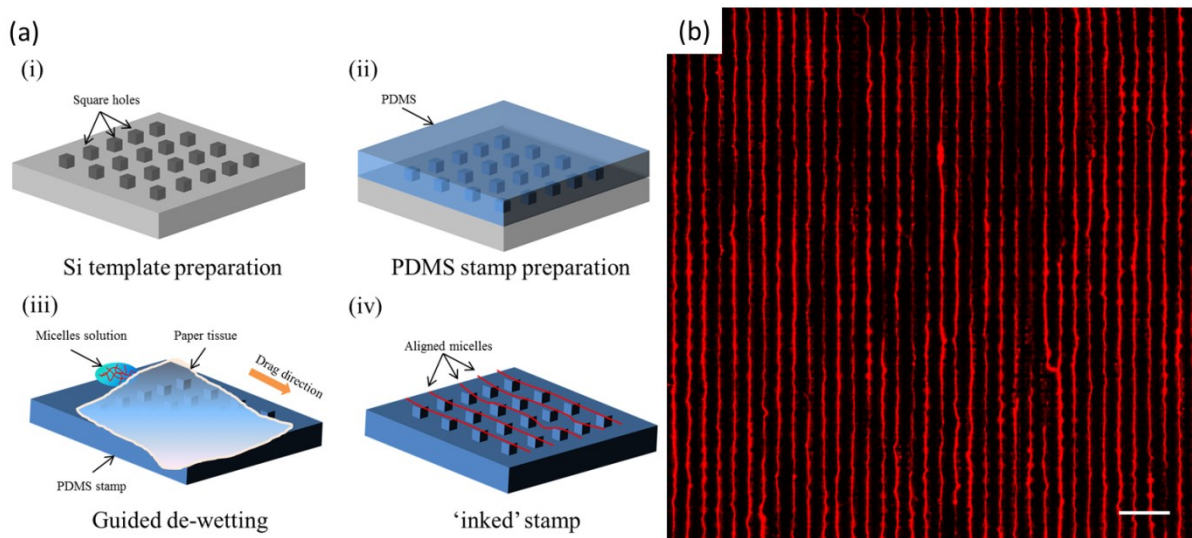


**Figure S5.** (a) Scheme of fabrication of PDMS stamp and alignment of methacrylated micelles: i) fabrication of silicon wafer template; ii) PDMS preparation; iii) guided de-wetting process; iv) aligned micelles on PDMS pillars. (b) Confocal microscopy image of aligned micelles. Scale bar: 20  $\mu\text{m}$ .

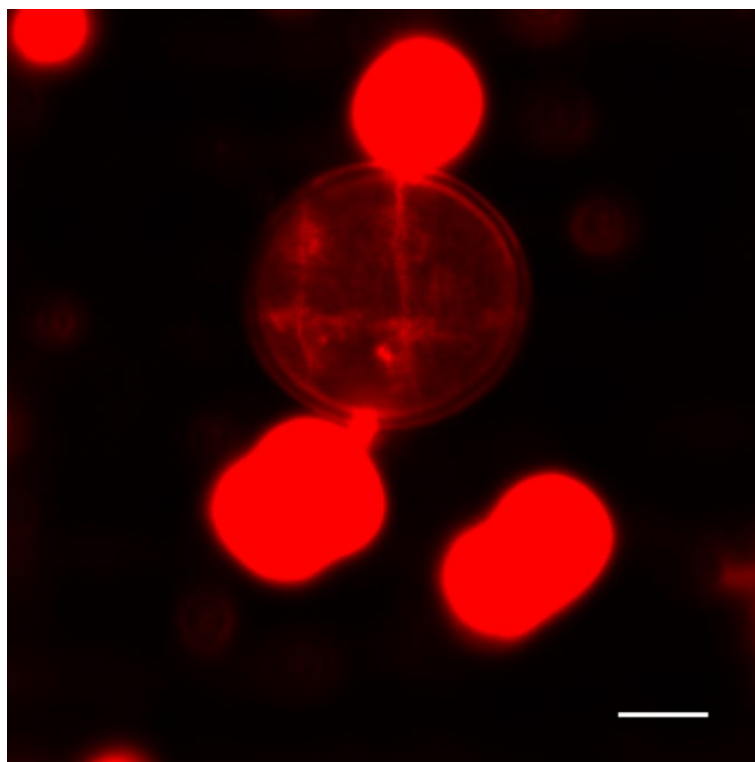


**Figure S6.** Confocal microscopy image of skew micelles on microparticle (red channel). Scale bar: 5  $\mu\text{m}$ .

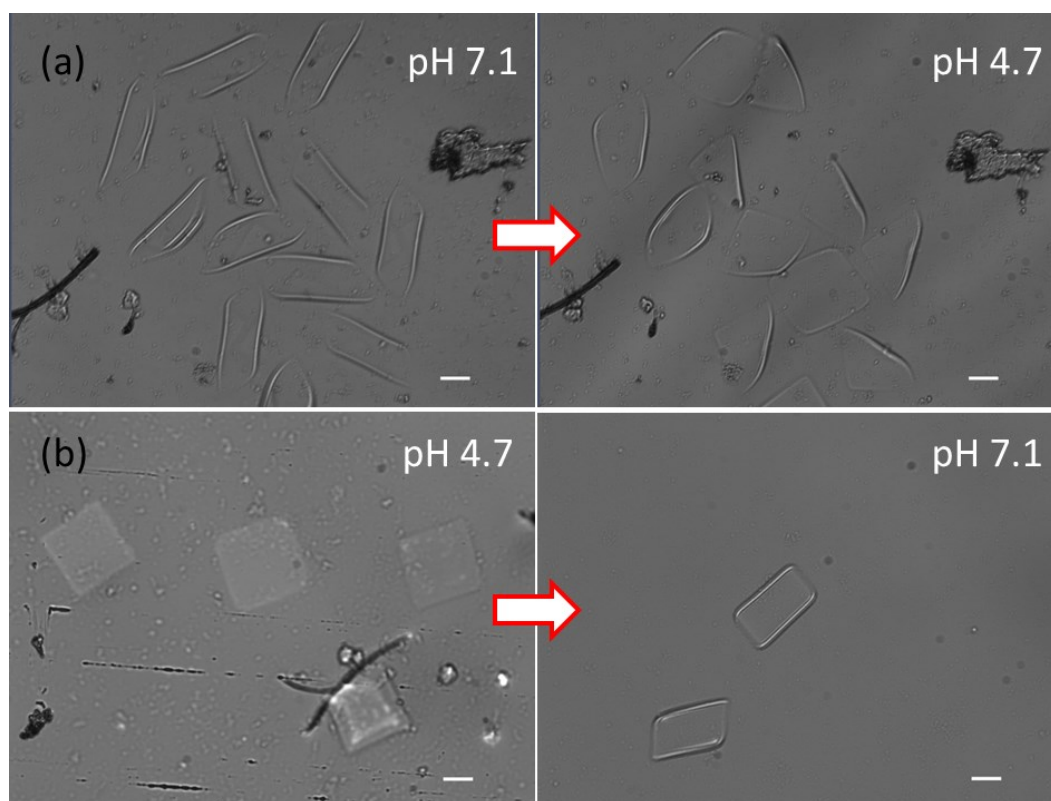


**Figure S7.** Optical microscopy images of DexMA hydrogels response to the changes of solution pH. (a) hydrogel structures before and after changing pH from 7.1 to 4.7; (b) hydrogel structures before and after changing pH from 4.7 to 7.1.

## Summary

Self-assembly of amphiphilic block copolymers in aqueous solution provides a versatile tool to create complex and functional micelles with various nanostructures, such as spherical, cylindrical and bilayer structures. As an important class in these structures, nanofibrillar micelles have attracted growing interest due to their unique properties that can potentially mimic biological analogues. For example, a great number of nanofibrillar structures, such as actin filaments and collagen gels with filamentous structures, were found in nature systems and have greatly motivated researchers to mimic these systems with synthetic materials. Besides, precise spatiotemporal control and integration of these nanofibrillar structures will offer a powerful strategy for construction of new soft devices in the future. Therefore, in this thesis, we explore the ultra-long, stiff and quenched micelles of diblock copolymers and develop a hybrid approach combining self-assembly of block copolymers and micro-fabrication methods to manipulate these micelles for building soft devices.

In Chapter 2, we investigated the possibilities of gelation of these ultra-long, stiff and quenched micelles. Three different mechanisms of forming micellar gels are discussed. First, the physical interaction between micelles is investigated as a possible mechanism for gel formation of a solution of ultralong quenched copolymer micelles. Second, a thermal fusion mechanism is proposed where after heating the micelles above the glass transition temperature of the polystyrene core blocks, micellar clusters and some fused junctions between adjacent micelles are formed, enabling crosslinking of the micelles and the formation of three dimension networks, namely micellar gels, after cooling down to room temperature. A third aspect on the formation of a network of ultralong micelles is based on a chemical crosslinking between the corona (PEO) parts of neighbouring micelles. The crosslinking process is studied in-situ by rheology and shows a three-region time dependence including (1) initiation, (2) sol-gel transition and (3) plateau region. Compared with the two former gelation mechanisms, the latter one exhibits the lowest critical gelation concentration.

Since the micelles in micellar gels are organized in a random way, we attempt to develop a method in Chapter 3 to manipulate the quenched and ultra-long micelles in order to build supermicellar array with a high level of order. By utilizing a guided dewetting method, we can align and deposit the nanofibrillar micelles onto the patterned PDMS surface. As PDMS is a popular candidate used for transfer printing, we can simply print these oriented micelles onto various flat substrates. Through controlling the printing times and printing directions of micelles, the designed 2D networks of cylindrical micelles can be formed. Ultimately, supermicellar structures are fixed by a thermal welding approach.

In Chapter 4, we describe how these organized micelles are used to take control over the cellular alignment behaviour. Here, we print and graft the functionalized cylinder micelles onto glass surface, yielding a new platform for cell alignment. We show that the area density

and orientation of fibrous micelles determine the alignment degree and directionality of cells, respectively. Furthermore, competitive guidance is found when cells are cultured on substrates with aligned micelles in various directions. We demonstrate for the first time that block copolymer nano-fibrous micelles are capable of regulating cellular response growing on a flat surface.

The last chapter, Chapter 5, is dedicated to further develop and application of these organized micelles in the construction of soft devices where we explore the possibilities of printing micelles onto soft surfaces, such as hydrogels. Through a hybrid approach combining the “bottom-up” method, self-assembly of block copolymers, with the “top-down” method, photo-lithography, we have developed two different kinds of soft devices. A first one, named “soft nano-fishnet”, enables us to trap and release microparticles while the second one, shape-morphing gel sheet, offers the ability of programmed spontaneous rolling behaviour. We demonstrate that a single layer of ordered, ultra-long nanofibrillar micelles embedded on the surface of hydrogel matrix can tailor the rolling responsive actuation of hydrogels. This strategy opens extensive opportunities for designing new soft devices, soft robots or soft surfaces.

## Samenvatting

Zelfassemblage van amfifiele blok co-polymeren in waterige oplossing is een universeel stuk gereedschap waarmee complexe en functionele micellen met verschillende nanostructuren, zoals sferische, cilindrische en bilaagstructuren gevormd kunnen worden. Als een belangrijke klasse in deze structuren groeien nanofibrillaire micellen in aandacht vanwege hun unieke eigenschappen die potentieel biologische analogieën kunnen imiteren. Een groot aantal nanofibrillaire structuren zoals actine filamenten en collageen gelen met een filamentstructuur worden bijvoorbeeld aangetroffen in natuurlijke systemen en hebben onderzoekers sterk gemotiveerd deze systemen na te maken met synthetische materialen. Daarnaast, precieze controle over de intramoleculaire afstand en integratie van deze nanofibrillaire structuren zullen een krachtige strategie bieden voor de constructie van nieuwe zachte systemen in de toekomst. Daarom verkennen we in deze dissertatie de ultralange, stijve en neergeslagen micellen van diblok copolymeren en ontwikkelen een hybride aanpak waarbij we zelfassemblage van blok copolymeren en micro-fabricage methoden combineren om deze micellen te manipuleren zodat er zachte systemen mee gemaakt kunnen worden.

In hoofdstuk 2 onderzoeken we de mogelijkheden van het geleren van deze ultralange, stijve en neergeslagen micellen. Drie verschillende mechanismen voor het vormen van micellaire gelen worden behandeld. Als eerste is de fysieke interactie tussen micellen onderzocht als mogelijk mechanisme voor gelvorming uit een oplossing van ultralange neergeslagen copolymere micellen. Daarna wordt een mechanisme van thermische fusie voorgesteld waarbij na verwarming tot boven de glastemperatuur van de polystyreen kern micellaire clusters en een aantal versmolten verbindingen tussen naastliggende micellen zijn gevormd, wat, na afkoeling tot kamertemperatuur, de mogelijkheid creëert tot het vormen van driedimensionale netwerken, namelijk micellaire gels. Een derde aspect van de vorming van een netwerk van ultralange micellen is gebaseerd op een chemische crosslinking tussen de corona (PEO) delen van naastliggende micellen. Het crosslinking proces is in-situ bestudeerd door middel van rheologie en laat een drie delen tijdafhankelijkheid zien, met een (1) initiatie, (2) sol-gel overgang en (3) plateau deel. Vergeleken met de twee eerstgenoemde geleermechanismes geeft de laatstgenoemde de laagste kritische geleringsconcentratie.

Daar de micellen in een micellaire gel op een willekeurige manier zijn geordend proberen we in hoofdstuk 3 een methode te ontwikkelen om neergeslagen en ultralange micellen te manipuleren zodat ze een supermicellair rooster vormen met een hoge mate van ordening. Door op een gecontroleerde manier water van een van een patroon voorzien PDMS-oppervlak te laten lopen kunnen we de nanofibrillaire micellen deponeren en uitlijnen. Daar PDMS een populaire kandidaat is om te gebruiken voor transferprinten kunnen we deze georiënteerde micellen gemakkelijk op verschillende vlakke substraten printen. Door de printtijden en printrichtingen te controleren kunnen de ontworpen 2D netwerken van

cilindrische micellen worden gevormd. Uiteindelijk worden de supermicellaire structuren gefixeerd door een thermische lasmethode.

In hoofdstuk 4 beschrijven we hoe deze georganiseerde micellen worden gebruikt voor het beïnvloeden van het uitlijningsgedrag van cellen. In dit geval brengen we de gefunctionaliseerde cilindrische micellen aan op een glasoppervlak, wat een platform oplevert voor de uitlijning van cellen. We laten zien dat de oppervlaktedichtheid en oriëntatie van vezelvormige micellen de mate van respectievelijk uitlijning en richting van cellen bepaalt. Verder is ontdekt dat als micellen in verschillende richtingen op een oppervlak zijn uitgelijnd er sprake is van competitieve geleiding. We laten voor de eerste keer zien dat blok copolymere nanovezelvormige micellen de cel respons kunnen beïnvloeden terwijl ze op een vlak oppervlak groeien.

Het laatste hoofdstuk, hoofdstuk 5, is gewijd aan het verder ontwikkelen van de toepassing van deze georganiseerde micellen bij de constructie van zachte systemen, waarbij we de mogelijkheden verkennen voor het printen van micellen op zachte structuren zoals hydrogelen. Door een hybride methode waarbij de “bottom-up” methode, zelfassemblage van blok copolymeren, en de “top-down” methode, fotolithografie, worden gecombineerd hebben we twee verschillende soorten zachte systemen ontwikkeld. De eerste, genaamd “zacht nanovisnet”, geeft ons de mogelijkheid microdeeltjes te vangen en weer vrijgeven, terwijl de tweede, “vormveranderende gelfilm”, ons de mogelijkheid geeft spontaan oprolgedrag te programmeren. We laten zien dat een enkele laag van geordende ultralange nanofibrillaire micellen, ingebed op het oppervlak van een hydrogelmatrix, de oprolrespons van hydrogels mogelijk kan maken. Deze strategie opent extensieve mogelijkheden voor het ontwerpen van nieuwe zachte systemen, zachte robots of zachte oppervlakken.

## Acknowledgements

The life of PhD study is like sailing on the sea, where you don't know what is waiting for you in the next second. It would be very hard to be survived without helps and supports from many great people in this journey. Here, I would like to express my sincere gratitude to all these people whom have contributed directly or indirectly to my PhD.

First of all, I would like to thank my promotor, Jan H. van Esch, who gave me a lot of help in this PhD journey. Thanks for all your efforts, insightful discussion and valuable comments on my research and manuscripts. Your broad knowledge and precise attitude in scientific research really set a great example for me. You can always quickly figure out the key points of problems in my research and inspired me to dig deeper into the data and questions. I have learnt a lot from you not only in the aspect of how to do research, but also in the writing skills. Thank you very much.

I would also like to particularly express my gratitude to my daily supervisor and co-promotor, Eduardo Mendes, who gave me this opportunity to pursue my PhD degree at TU/Delft. Thank you so much for your enthusiasm, motivation and support during these years. You always encourage me to be positive and optimistic when I have doubts about my research or when I am not confident in our papers. Your unlimited enthusiasm in science strongly encouraged me to keep passion in my research. Moreover, I really appreciate your comments and efforts on my manuscripts, from which I have learnt a lot. I still clearly remember the day when you showed me how to revise my first manuscript of chapter two in your office. Your patience and careful guidance are great help for me to pass through this struggling journey. I am also very happy to play football with you during these years. Thanks a lot.

I also want to thank Rienk Eelkema for his constructive suggestions on my experiments, and thank Stephen J. Picken for his help and discussion on microscopy. My appreciation also goes to Ger Koper for the talks about the culture and life in the Netherlands. Also thanks Antonia Denkova for her willingness help and valuable discussion on my PhD research. Here, I also would like to thank my postdoc supervisors, Dessi Koleva and Klaas van Breugel, who gave me a chance to work on the corrosion projects. I am also thankful to my new postdoc supervisors, Dimitra Dodou and Ivan Buijnsters, who introduced me to the field of biomimetic adhesives. Thank all of you for believing in me and supporting me before my PhD graduation.

For my thesis, I also thank all the committee members for their efforts and comments.

As a member of old NSM group and new ASM group, I sincerely acknowledge all the secretaries and technicians. I still remember that Wil and Karin tried to help me as much as possible on my first day at TU/Delft. Although my English is not very good, both of you are so nice and are always patient to give me help. I also want to thank Mieke who gave me many



help in the new ASM group. I am also thankful to our new secretary, Veby, who helped me through the last stage of my PhD study. Thanks to Marcel Bus for your assistance in AFM experiments. You are always patient to explain the rules in the lab and the details in the mechanism and operation of AFM to me. I really appreciate that you can help me translate the summary part. Thank you so much for your help and efforts. I also would like to express my gratitude to Ben Norder for helping me in so many experiments including rheology, TGA and DSC etc., and also thank you for your great advices in my research. I would like to thank Lars van der Mee for his assistance in the synthesis of nanoparticles, GPC experiments and ordering chemicals. Thank Louw for his help on TEM and surface tension measurements. I thank Duco for his help on SEM training and measurements.

Next, I would like to thank all my colleagues and friends, past and present, in the old NSM group (Haining, Piotr, Laurence, Zhen, Xiaoyan, Guanglin, Jicheng, Saida) and in the new ASM group (Kimi, Simge, Marta, Dainius, Emanuela, Alex, Chandan, Elena, Roman, Wouter, Wei, Sander, Alexandra, Frank, Karolis, Jos, Matija, Serhii, Emma, Vincent, Vasu, Fanny, Susan, Cansel, Tomasz, Angie, Yiming, Qian, Bowen, Katarzyna, Tobias, Michelle, Benjamin, Hendrik, Zhenyu and Fan) who made my life in these groups enjoyable. I am so happy that I can work together with all of you. Since we had so many fun and great moments, I cannot easily list them and cannot thank you enough in few sentences. I also would like to thank Robin and Tiantian from RID for their help in TEM and gamma irradiation experiments. My appreciation also goes to my master students, Dharani, Sitara and Aaditya, who have helped me in this work.

PhD study is not only about research, but also about life. I would like to convey my appreciation to all my Chinese friends that I met in the Netherlands. Thanks to Anping, Quan, Bobo, Clement, Yiming, Qian, Bowen, Zhen, Wuyuan, Jicheng, Yunlong, Zeng, Liangyong, Xiaohui, Kai Liu, Meixia, Ming Ma, Min Wang, Yujie, Xinlei, Xuerui, Kai Li, Shulan, Xiaowei, Cui, Jiayi, Wenqin, Zilong, Yan, Tao, Hongli, Guangliang, Shasha, Yu Xin, Peiyao, Ming Li, Hua, Tianshi, Zhipai etc. My life here has been enriched by all of you. Thank you very much. I also want to thank my best friend in US, Hongyu Chen, who gave me a lot of help and encouragements during my PhD study. Wish you all the best and succeed in your PhD study.

最后，我想感谢我亲爱的父母，感谢您们这么多年含辛茹苦地抚养和照顾，对我总是无条件的支持和理解。也十分感谢我亲爱的岳父岳母，谢谢您们一直以来对我的支持和帮助。在此，我要特别感谢我的爱人朱丽，感谢你在这风雨路上，不论前方如何曲折坎坷，都一直伴我左右，默默地支持和鼓励我。也谢谢你为我生了一个如此可爱暖心的闺女，让我们这个小家庭更加幸福甜蜜。爱你尽在不言中！

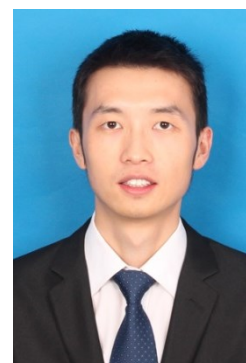
Kai Zhang (张凯)

## Curriculum Vitae

### Kai Zhang

Date of Birth: 12-Nov.-1986

Place of Birth: Huangshi, Hubei province, China



### Education

---

2017.10 to Present	Postdoc	Department of Biomechanical Engineering Delft University of Technology
2016.09 to 2017.08	Postdoc	Department of Structure Engineering Delft University of Technology
2012.11 to Present	Ph.D.	Department of Chemical Engineering Delft University of Technology
2009.09 to 2012.07	M.Sc.	College of Polymer Science & Engineering Sichuan University
2005.09 to 2009.07	B.Sc.	College of Polymer Science & Engineering Sichuan University

### Project Experiences

---

1. A new class of hierarchical biomimetic adhesives
2. Bioinspired coating and pulse technology for preventing MIC corrosion
3. Nanomaterial with tailored property for self-healing and corrosion control in reinforced concrete
4. Block copolymer micelles and hydrogels: synthesis, properties, manipulation and applications
5. Sub-micron magneto-responsive, hydrogel system
6. Crystallization behaviour of polyolefin in Multi-fluid multi-injection molding (MFMIM)
7. Stress relaxation behavior of HDPE molded by gas-assisted injection molding (GAIM)
8. Design and modelling of thermal plastic products and injection mold
9. Paraffin/poly(vinyl alcohol) phase change fibers for energy storage

## List of Publications

---

**K. Zhang**, P.J. Glazer, L. Jennings, S. Vedaraman, S. Oldenhof, Y. Wang, F. Schosseler, J.H. van Esch, E. Mendes. A facile approach for the fabrication of 2D supermicelle networks. **Chemical Communications**, 2016, 52, 12360-12363.

**K. Zhang**, L. Jeneings, P.J. Glazer, S. Vedataman, V. Lakshminarayanan, J.H. van Esch and E. Mendes. Two robust strategies towards hydrogels from quenched block copolymer nanofibrillar micelles. *Under revision*.

**K. Zhang**, A. Arranja, H. Chen, S. Mytnyk, Y. Wang, S. Oldenhof, J.H. van Esch, E. Mendes. Patterned nano-fibrous micelles of block copolymers for controlled cell alignment. *Under review*.

**K. Zhang**, S. Oldenhof, Y. Wang, J.H. van Esch and E. Mendes. Soft gel micro-devices from supramolecular assemblies of block copolymers. *In preparation*.

**K. Zhang**, Z. Liu, B. Yang, W. Yang, Y. Lu, N. Sun, M. Yang. Cylindritic structures of high-density polyethylene molded by multi-melt multi-injection molding. **Polymer**, 2011, 52, 3871-3887.

**K. Zhang**, Z. Liu, N. Sun, Y. Lu, B. Yang, L. Wang, M. Yang. Crystal morphology of HDPE molded by multi-fluid multi-injection molding. **Acta Polymerica Sinica**, 2011, (3), 235-239.

N. Singh, **K. Zhang**, C.A. Angulo-Pachón, E. Mendes, J.H. van Esch and B. Escuder. Tandem reactions in self-sorted catalytic molecular hydrogels. **Chemical Science**, 2016, 7, 5568-5572.

H. Mahmoud, **K. Zhang**, R.M. de Kruijff, A.G. Denkova and D.A. Koleva. Global performance of cement-based materials in the presence of N-doped mesoporous carbon spheres. **Cement and Concrete Research**, Manuscript submitted.

N. Singh, C. Maity, **K. Zhang**, C.A. Angulo-Pachón, J.H. van Esch, R. Eelkema and B. Escuder. Synthesis of double-network supramolecular hydrogel by having one network catalyse the formation of the second. **Chemistry A European Journal**, 2017, 23, 1-5.

Y. Wang, F. Versluis, S. Oldenhof, V. Lakshminarayanan, **K. Zhang**, Y. Wang, J. Wang, R. Eelkema, X. Guo and J.H. van Esch. Directed nanoscale self-assembly of low molecular weight hydrogelators using catalytic nanoparticles. **Advanced Materials**, 2018, Accepted.

R. Zhang, W. Yang, **K. Zhang**, J. Feng, C. Zhu, X. Xia, S. He, J. Feng, M. Yang. An unusual transition from point-like to fibrillar crystals in injection-molded polyethylene articles induced by lightly cross-linking and melt penetration. **RSC Advances**, 2015, 5, 21640-21650.

J. Wu, W. Yang, **K. Zhang**, R. Zhang, J. Feng, Z. Liu, B. Xie, C. Zhang, M. Yang. Shear field in the mold cavity of multi-melt multi-injection molding revealed by the morphology distribution of a model polymer blend. **Polymer Engineering & Science**, 2014, 54, 2345-2353.

L. Wang, B. Yang, N. Sun, **K. Zhang**, J. Feng, M. Yang. Role of gas delay time on hierarchical crystalline structure and mechanical property of HDPE molded by gas-assisted injection molding. ***Colloid and Polymer Science***, 2012, 290, 1133-1144.

K. Ke, Y. Wang, **K. Zhang**, Y. Luo, W. Yang, B. Xie, M. Yang. Melt viscoelasticity, electrical conductivity, and crystallization of PVDF/MWCNT composites: Effect of the dispersion of MWCNTs. ***Journal of Applied Polymer Science***, 2012, 125, E49–E57.

Z. Kan, Z. Liu, **K. Zhang**, H. Chen, J.Y. Hu, M. Hou, M. Yang. Polymerization System and Properties of Anionic Polyamide-6 for Vacuum Infusion Process. ***Chemical Journal of Chinese Universities***, 2012, 33(08): 1866-1871.

N. Sun, B. Yang, L. Wang, W. Yang, **K. Zhang**, M. Yang. Morphological study of linear low-density polyethylene molded by gas-assisted injection molding. ***Polymer-Plastics Technology and Engineering***, 2011, 50, 804-809.

Y. Lu, W. Yang, **K. Zhang**, M. Yang. Stress relaxation behavior of high density polyethylene (HDPE) articles molded by gas-assisted injection molding. ***Polymer Testing***, 2010, 29, 866-871.